Dissertation

Submitted to the

Combined Faculties for the Natural Sciences and for Mathematics
of the Ruperto Carola University of Heidelberg, Germany

for the degree of

Doctor of Natural Sciences

Presented by

Swarnima Joshi, MSc.

Born in: Kotdwara, India

Oral examination: 01.10.2019

Investigation of genes involved in muscle function using zebrafish

Referees: Prof. Dr. Uwe Strähle
Dr. Thomas Dickmeis

Table of Contents

Dedicated to my family

Summary

The genetic basis of many muscle diseases is known but an understanding of the mechanism underlying muscle weakness is often missing hence a gap remains for the development of effective treatments of these pathologies. Since the process of muscle development as well as function is highly conserved throughout evolution, the skeletal muscles of zebrafish (*Danio rerio*) show remarkable structural and molecular similarities to those of humans. At the same time, they also make up a considerable portion of its body. Therefore, investigating the developmentally relevant motility genes in zebrafish could help to decipher essential but poorly understood aspects of myogenesis.

In this project, I adopted two distinct experimental approaches. The first part of the thesis deals with creating a genetic knockout model to understand the molecular function of the genes *apobec2a* and *2b* which were shown to be relevant for muscle development by our lab. In the course of creating knockouts, we applied a novel, efficient and cost-effective method to predict guide RNA efficiency in zebrafish. The quantitative assessment of gRNAs was provided by the web tool, PCR-F-SEQ which was developed and optimized by us especially for the zebrafish model system. This tool represents a simple but powerful method to screen injected batches of embryos before sending them for raising. Although *apobec2a/2b* morphants show a dystrophic phenotype, the genetic knockouts do not exhibit any muscle phenotype indicating a possible genetic compensation.

In addition, an unbiased approach of investigating the motility mutants isolated from Tübingen screens was used. The rate of retrieval of mutant couples from sperm samples of the Ist and IIIrd Tübingen screens were around 66% and 40% respectively. Following the revival and phenotypic characterization of these lines, we developed a pipeline using next generation sequencing to accurately identify the disease-causing alleles. Mapping of mutations and validation of candidate genes were successfully done for all the six revived lines. Amongst which, we reported a missense mutation in *choline-O-acetyltransferase a* (*chata*) gene, encoding an enzyme essential for the synthesis of a major neurotransmitter, acetylcholine (ACh). The *in-silico* analysis showed that the substitution of serine to arginine might affect the protein stability disrupting the catalysis of acetyl CoA and choline to form ACh.

In conclusion, this thesis showcases the challenges and strengths of both reverse and forward genetic approaches to study vertebrate development and also highlights the importance of strategies and tools now available for making genetic models.

Zusammenfassung

Die genetische Grundlage vieler Muskelerkrankungen ist zwar bekannt, aber oft fehlt die Kenntnis des Mechanismus, der der Muskelschwäche zugrundeliegt, so daß eine Lücke für die Entwicklung effektiver Behandlungen dieser Pathologien verbleibt. Da der Prozess der Muskelentwicklung wie auch der Muskelfunktion in der Evolution hochgradig konserviert ist, zeigen die Skelettmuskeln des Zebrafischs (*Danio rerio*) bemerkenswerte strukturelle und molekulare Ähnlichkeiten mit denen des Menschen. Zugleich machen sie auch einen erheblichen Teil seines Körpers aus. Daher könnte die Untersuchung von entwickungsbiologisch relevanten Motilitätsgenen im Zebrafisch helfen, essentielle, aber wenig verstandene Aspekte der Myogenese zu entschlüsseln.

In diesem Projekt habe ich zwei unterschiedliche experimentelle Ansätze verfolgt. Der erste Teil der Dissertation befaßt sich mit der Erzeugung eines genetischen Knockout-Modells, um die molekulare Funktion der Gene *apobec2a* und *2b* zu verstehen, von denen unsere Arbeitsgruppe gezeigt hatte, daß sie relevant für die Muskelentwicklung sind. Bei der Erzeugung von Knockouts wandten wir eine neuartige, effiziente und kostengünstige Methode zur Vorhersage der Guide-RNA-Effizienz im Zebrafisch an. Die quantitative Bewertung von gRNAs erfolgte durch das Online-Werkzeug PCR-F-SEQ, das von uns entwickelt und speziell für das Zebrafisch-Modellsystem optimiert wurde. Dieses Werkzeug stellt eine einfache, aber mächtige Methode dar, um injizierte Chargen von Embryonen zu screenen, bevor sie in die Aufzucht gegeben werden. Obwohl *apobec2a/2b*-Morphanten eine dystrophen Phänotyp zeigen, weisen die genetischen Knockouts keinen Muskelphänotyp auf, was auf eine mögliche genetische Kompensation hinweist.

Des weiteren wurde ein unvoreingenommer Ansatz zur Untersuchung von Motilitätsmutanten aus den Tübinger Screens benutzt. Die Rate der Wiedergewinnung von mutanten Paaren aus Spermienproben des I. und III. Tübinger Screens lag bei 66% bzw. 40%. Nach der Rekonstitution und phänotypischen Charakterisierung dieser Linien führten wir eine Next-Generation-Sequenzierung durch, um die krankheitsverursachenden Allele exakt zu identifizieren. Kartierung der Mutationen und Validierung von Kandidatengenen wurden erfolgreich für alle sechs rekonstituierten Linien durchgeführt. Von diesen publizierten wir eine Missense-Mutation im *choline-O-acetyltransferase a* (*chata*)-Gen, das ein für die Synthese des wichtigen Neurotransmitters Acetylcholin (ACh) essentielles Enzym kodiert. Die *in silico*-Analyse zeigte, daß die Substitution von Serin durch Arginin die Proteinstabilität beeinträchtigen und damit die Katalyse der Reaktion von Acetyl-CoA und Cholin zu ACh behindern könnte.

Insgesamt demonstriert diese Doktorarbeit die Schwierigkeiten und Stärken von revers-genetischen wie auch von vorwärts-genetischen Ansätzen zur Untersuchung der Wirbeltierentwicklung, sowie die Wichtigkeit der Wahl der richtigen Strategie und Werkzeuge für die Herstellung genetischer Knockout-Modelle.

Acknowledgements

This dissertation would have not been possible without the support of numerous people I have come across. First and foremost, I want to express my gratitude to my supervisor Prof. Uwe Strähle for his insights in navigating through this long journey. I will be forever grateful to him for providing me this opportunity.

I would like to sincerely thank Sepand for always accompanying us to the Zencode meetings and for guiding us. Without his effort, it would have been impossible to understand the value of teamwork.

I would like to acknowledge some other important people whose contribution to my research work has an outstanding importance: I would like to thank Christelle for introducing me to the topic and dealing with my research problems. She has always been there for me, kept me in check and over the years I have come to regard her as one of my supervisors. Thank you again for putting faith in me. Our invaluable aura of friendship will never fade. I am also very grateful to Robert for not just providing an immense help in correcting my paper and thesis but also for the patient guidance he has provided. His kind nature and vast knowledge provided insightful discussions about the research work. I would like to acknowledge other members of my thesis advisory committee, Dr. Kassel and Dr. Davidson for their encouragement and thought-provoking comments during annual progress seminars.

The members of Strähle group have contributed immensely to my personal and professional time at KIT. I am especially grateful for the people of the group who stuck it out in grad school with me: Sanamjeet and Vanessa, without whom this journey would have no colors.

For this research work, NGS data generation and analysis was crucial and for that I would like to wholeheartedly thank our sequencing facility and Sanamjeet for his efforts as well as continuous support. Without him this piece of work would be just incomplete. Apart from the research cooperation, I also would like to thank him for tolerating all the arguments we had and for maintaining such a friendly relationship. I am gladly taking our friendship along!

I am particularly indebted to Vanessa for being a great colleague and a lovely friend. Her blend of straightforward criticism combined with heart-warming support was utmost required during tough times. I would also like to thank her for introducing me to many protocols.

Masa and Volker shared some of their expert microscopy and muscle knowledge with me. It was a pleasure working alongside these great PostDocs. The joy and enthusiasm Volker have for his research was contagious and motivational for me, even during tough times in the PhD pursuit. In regards to making this journey even more joyous, I would also like to thank rest of the Strähle group members: Gao, Hendrik, Ariane, Luisa, Tanja, Sabrina, Angel, Dimitra. A special thanks to Anne and Gao for their excellent support for few of my experiments.

It was my pleasure meeting and having friendly discussions with members of Dickmeis group: Melanie, Andrea, Oksana, Mojtaba. Their presence made it even more lovely.

For behavioral analysis, I am very much thankful to Ravi and his screening platform. I would also like to thank Prof. Ralf Mikut and Johannes Stegmaier for collaborating with us on making the guide efficiency webtool. They have been extremely patient with our queries and have contributed a lot in shaping things. I am also grateful for Marco, Nadine, Sonja, Thomas and whole fish facility members for taking very good care of my fish lines. I very much appreciate their continuous efforts and willingness to do frequent changes as requested.

This thesis would definitely not take its shape without the major help of Rene for providing me with his extraordinary IT support. I am truly very grateful to him. Apart from that, I am thankful to my funding sources; Marie Curie association that made my PhD work and stay in Germany possible. Also, loved being a part of Zencode- ITN which provided an excellent platform to learn and grow altogether. I am also very thankful to Prof. Carsten Daub for hosting me for a secondment in his group at Karolinska Institute, Sweden.

Lastly, I would like to thank my family and friends for all their love and encouragement. For my parents, brother and his wife who supported me in all my pursuits. For the presence of my best friend Sonali here in Europe. She has provided immense support and motivation which kept me moving forward.

And most of all for an encouraging, loving and patient person *Aniruddha* whose support throughout my studies is the source of my sanity.

List of figures

List of tables

Publications

1. "Tracking of Indels by DEcomposition is a Simple and Effective Method to Assess Efficiency of Guide RNAs in Zebrafish."
   Etard C±, Joshi S±, Stegmaier J, Mikut R, Strähle U*.
   Published: Zebrafish, 2017.

2. "Mutation of a serine near the catalytic site of the *choline acetyltransferase a* gene almost completely abolishes motility of the zebrafish embryo."
   Joshi S±, Virdi S±, Etard C, Geisler R*, Strähle U*.
   Published: PLoSOne, 2018

± Authors contributed equally
* Corresponding author

1 Introduction

1.1 General introduction

The skeletal muscle system is a crucial component of vertebrate anatomy having a fundamental role in locomotion and equally important in metabolic homeostasis (Jackson and Ingham, 2013; Manabe and Fujii, 2016). In a healthy state, it possesses an extraordinary ability to regenerate the small-scale injuries which are a result of extensive daily usage. This repair capacity is however compromised with age, genetic diseases and with large accidental abrasions (Khodabukus et al., 2018).

Muscle diseases such as muscular dystrophies and myopathies are a heterogenous group of diseases, sharing patterns of clinical symptoms like muscle wasting, weakness and impaired locomotion due to muscle fiber dysfunction (Goody et al., 2017; Sevy et al., 2016). Due to phenotypic heterogeneity, it remains very challenging to make a timely and accurate diagnosis in order to develop a therapy. In a subset of muscular dystrophies called dystroglycanopathies, clinical phenotypes span from severe, in case of congenital muscular dystrophy-dystroglycanopathy affecting eye and brain, to mild cases seen in adults as limb-girdle muscular dystrophy-dystroglycanopathy. A classical diagnostic approach involving laboratory evaluation, imaging studies, multidisciplinary consultations and histologic examination are still insufficient for many cases. Recently, another very successful, rapid and patient-specific approach called next-generation sequencing (NGS), has been used to accurately analyze the genetic cause. Thus, many of these myopathies have now been identified and linked to one or several genes.

To determine the molecular and cellular causes of phenotypic variability for designing therapies and to comprehend the relation between muscle development and disease, zebrafish serve as an excellent disease model. There are several reasons for zebrafish embryos in particular being the best suited model to study muscle development. Apart from their high number of offsprings, *ex-utero* development, transparent embryos and low maintenance costs; evolutionarily conserved muscle functions, somitic muscle accessibility and development of motility shortly after gastrulation make them superior to other model systems. Additionally, targeted gene inactivation using CRISPR/Cas9 in zebrafish has become quite successful in creating genetic knockouts. The techniques are rather cost efficient and rapid. On the other hand, large-scale random mutagenesis screens performed in zebrafish to

investigate developmentally relevant genes (Liu et al., 2017) have been quite successful. The mutants generated in these screens were classified according to the observed traits and around 1163 mutant lines were noted to display specific traits (Nüsslein-Volhard, 2012). Due to the large number, mutant sperm stocks were established without fully investigating the molecular causes. These samples were later brought to the European Zebrafish Resource Center (EZRC) at KIT. Due to our utmost interest in investigating novel players of muscle development, we took advantage of this large pool of uncharacterized lines; serving as a black box for studying developmentally relevant genes without any bias.

1.1.1 Types of muscles

Classification of vertebrate muscles is essential to understand their structure and function. The best and widely recognized classification categorizes it into three distinct groups, striated voluntary muscles (skeletal muscles), striated involuntary muscles (cardiac) and non-striated involuntary muscles (smooth) (Kisia and Onyango, 2005).

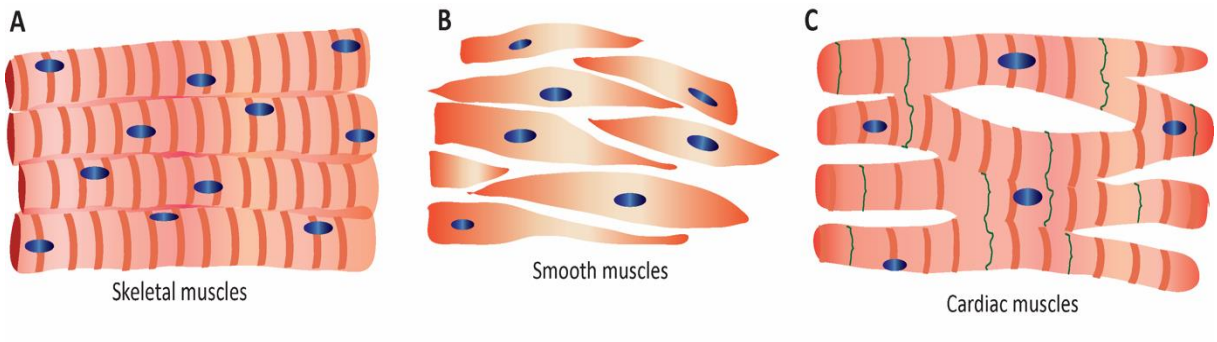

Figure 1. Schematic representation of different types of muscles.
(A) Skeletal muscle is composed of myofibers, formed by the fusion of myoblast cells into a syncytium (multi-nucleated structure) with the nucleus being peripherally localized (blue). They appear striated (orange lines) i.e. arranged into repetitive functional units called sarcomeres. (B) Smooth muscles are non-striated muscles, made up of mononuclear cells which in most of the cases contract as a sheet. (C) Cardiac muscles are striated heart muscles, made up of cardiomyocytes joined together by intercalated discs (green). Nuclei are centrally localized (blue) and fibers interlinked by branches.

Skeletal muscles are voluntary muscles, attached to the skeleton for the purpose of movement. They are composed of myofibers which have numerous peripherally located nuclei and organized striations (Figure 1A). Smooth muscles are composed of spindle-shaped cells with centrally located nuclei, arranged in a `dovetail´ pattern (thin ends of cells are adjacent to the thick middle portion of the next cell) (Figure 1B). They are non-striated, involuntary muscles located in the walls of visceral organs. Cardiac muscles are located in the walls of heart and are made up of myogenic fibers having centrally located nuclei (Figure 1C). They are involuntary striated muscles which contract rhythmically from early embryonic stages (DiFrancesco and Noble, 1985). Myogenic fibers are connected via branched

interlocking and have a distinct junctional specialization, called intercalated discs. These discs help in spreading electrical impulses from one cell to the other.

1.1.2 Skeletal muscle architecture

Skeletal muscles are characterized by a well-described arrangement of muscle fibers (myofibers or muscle cells) and connective tissue (Frontera and Ochala, 2015). Individual muscle is surrounded by a layer of connective tissue called Epimysium which provides strength to the muscle (Figure 2). Myofibers within the muscle are packaged into bundles, also called fascicle and are enveloped by a connective tissue layer called perimysium. Each individual myofiber of the bundle is also enwrapped with a layer of connective tissue called endomysium. Each muscle fiber is surrounded by a cell membrane called sarcolemma and is made up of several thousand myofibrils (MacIntosh et al., 2006). Myofibrils have a highly organized internal structure made up of myofilaments, the muscle proteins which form the

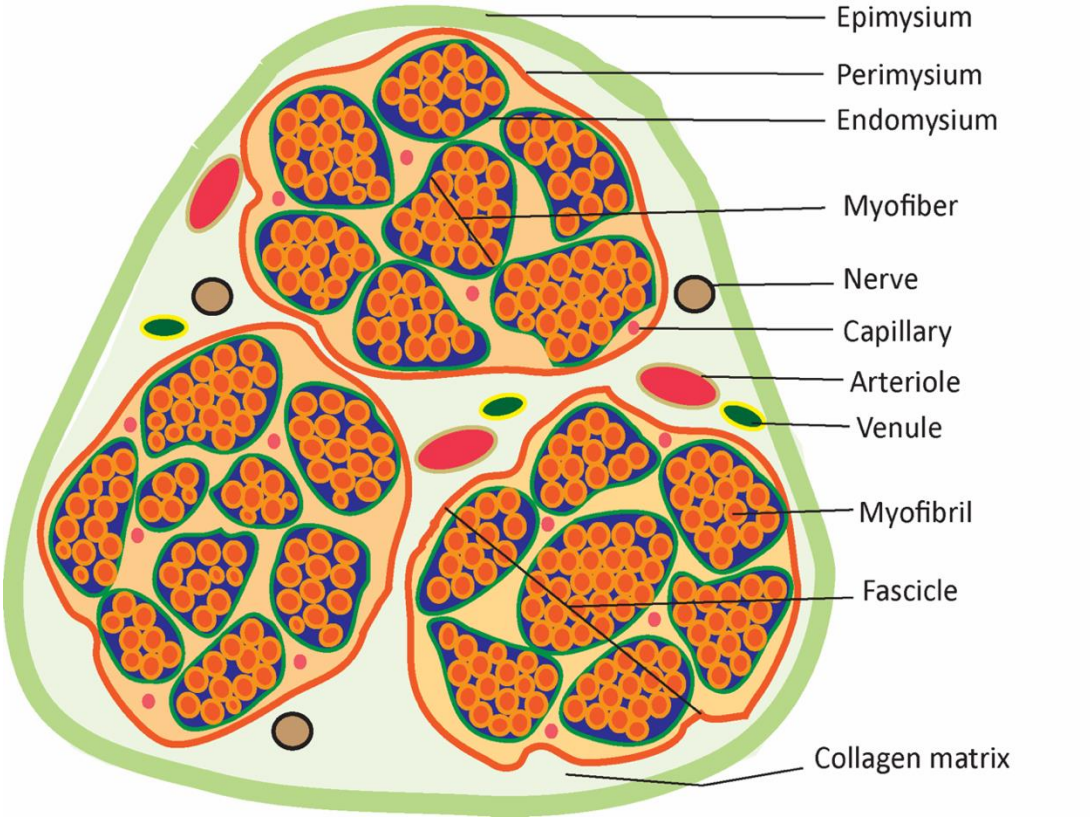

Figure 2. Schematic representation of a cross section through vertebrate muscle.
The overall muscle tissue is covered by an outer layer of connective tissue, epimysium covering fascicles, venules, arterioles and nerves. Myofibers are bundled together to form a fascicle together with narrow capillaries and surrounded by perimysium. Myofibers are coated with a thin layer of endomysium and are made up of thousands of myofibrils.

contractile units called sarcomeres.

It is composed of distinct types of fibers that are functionally adapted through differences in their physiological and metabolic properties (Jackson and Ingham, 2013; Schiaffino and

Reggiani, 2011). They are classified using many different criteria and according to the most frequently used classification there are two fiber subtypes: type I and type II. Type II fibers are subdivided into IIa and IIx (Frontera and Ochala, 2015; Galpin et al., 2012). Type I fibers are also called slow-twitch fibers as they possess lower contraction velocity but are rich in mitochondria which makes them aerobic in nature (Chemello et al., 2011; Pette and Staron, 1997). They are more efficient at using oxygen for ATP generation giving them ability to contract over long durations. These fibers are also called red muscles as they contain more myoglobin. On the contrary, Type II or fast muscle fibers inherit less mitochondria and myoglobin, therefore are anaerobic in nature and white in color. They are adapted to generate short speedy bursts of contractions but are fatigable unlike slow-twitch fibers which provide more endurance and are fatigue resistant. The type of fiber proportions therefore varies according to usage, slow fibers are numerous in marathon runners as they need long term endurance whereas, weightlifters require fast muscles for quick and enormous force generation for a short interval. Behavioral adaptations of fiber type are also seen in animals where most of the fishes need to be capable of quick movement away from predators and therefore have a high proportion of fast-twitch fibers. On the other hand, herbivorous mammals require more slow-twitch fibers, enabling sustained muscle action required for grazing.

Skeletal muscles in zebrafish

The musculo-skeletal system of zebrafish is simpler compared to that of tetrapods. The muscles are aligned into sequential chevron shaped myotomes separated by a thin connective tissue layer called vertical or transverse myosepta (Figure 3A). During early stages of development, the myotomes are clearly visible as V-shaped structures which fold and overlap to form a W shape in adults. The transverse myoseptum serves as a boundary for somites which anchors the myofibrils whereas the horizontal myoseptum runs along the length of the trunk and helps in pathfinding of cells during development.

Myosepta are functionally equivalent to myotendinous junctions in mammals; connecting skeletal muscles to the axial skeleton, enabling contractions. They are composed of matrix proteins mainly, dense collagen in the form of arrays and are required for adhesion of the sarcolemma to ECM. Upon muscle contraction, the force is transmitted to the collagen cones of the myosepta and to the vertebral column through the horizontal myosepta. The myosepta, being elastic in nature, help in absorbing the tension and prevent it from being transmitted to neighboring myomeres. Vertical/transverse myosepta being connected to the skin is a requirement for movement.

The extracellular matrix (ECM) proteins such as type 1, 4, 6 collagen, tenascin C, periostin, thrombospondin, laminin, DGC (dystrophin-glycoprotein complex consisting of dystrophin, dystroglycan and sarcoglycan) and integrins are expressed in somite boundaries. Mutations that prevent muscle fiber adhesion to their surrounding basement membrane make fibers vulnerable to damage during repeated contractions and relaxations.

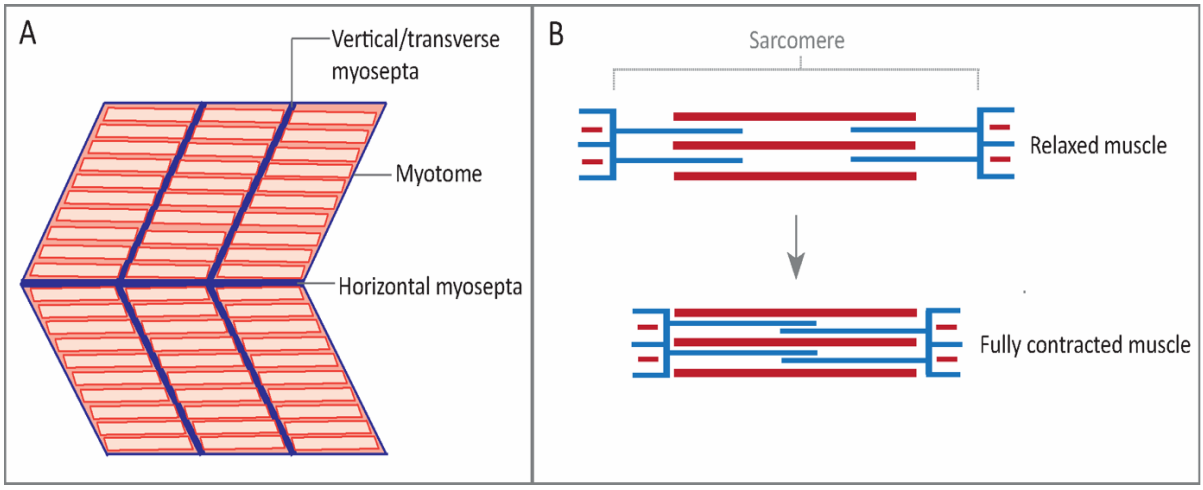

Figure 3. Zebrafish myotome and model of muscle contraction.
(A) Schematic drawing of developing zebrafish skeletal muscle myotome. Vertical myosepta separates chevron shaped (V-shaped) myotomes and exhibit an ordered arrangement. The horizontal myosepta is placed right in the middle, dividing the myotome in two halves. (B) Schematic view of sliding filaments for muscular contraction. Upon contraction, the thin filaments (blue) slide along the thick filaments (red) without changing the overall length of filaments. Such an arrangement causes the Z-lines to move closer together shrinking the overall sarcomeric structure.

Skeletal muscle cells are amongst the largest cells found in an organism, ranging to more than 100 µm in diameter and centimeters in length. The size of the muscle is mostly determined by the number and size of individual muscle fibers except during pathological conditions (Frontera and Ochala, 2015). Myoblast/ skeletal muscle cells fuse together to create a multinucleated structure (syncytium) called a myofiber. Each nucleus within the myofiber is responsible for controlling the type of protein synthesized in that specific region of the cell, which is called a nuclear domain. The protein expression is coordinated across adjacent domains of a single fiber which ensures similarity of proteins across the length of the fiber. Myofibers are composed of numerous myofibrils and are mainly composed of proteins (80%) and sarcoplasm (8%) where proteins are categorized in three distinct classes according to their function; contractile, regulatory and cytoskeletal proteins. Myofibrils take most of the space squeezing other components like mitochondria, nuclei and granules to the periphery (Rosen and Baylies, 2017). Myofibrils are made up of myofilaments which are composed of the two most abundant contractile proteins, actin and myosin. The striated appearance of skeletal muscle is because of the arrangement of these proteins in such a way that they create a repetitive pattern of stripes in the myofibril. This pattern is visible under a light microscope and is called a sarcomere, the fundamental unit of the muscle. During muscle contraction, thin filaments slide along thick filaments, shortening the overall sarcomere length as shown in Figure 3B.

1.1.3 Sarcomere structure and muscle contraction

The sarcomere is the region between two Z-lines, which are dark and narrow lines clearly visible in an electron micrograph. Z- lines are composed of a dense protein scaffold which anchors actin or thin filaments. Myosin or thick filaments are attached to the Z-line with the help of a large elastic protein called Titin (shown as blue springs in Figure 4). Titin not just holds myosin filaments but has also been reported to contribute to force generation during muscle actions. Light bands surrounding the Z-lines contain only thin filaments and together are called an I-band (Figure 4). The A-band is the dark zone of the myofibril where myosin filaments interact through myosin heads with actin filaments. The M-line is located right in the middle of the sarcomere in the A-band where myosin filaments are held. The H-zone is the zone in A-band, situated around the M-line and mainly composed of myosin filaments. During contraction this zone disappears completely due to sliding of myosin over actin filaments which shortens the distance between two Z-lines. Actin or thin filaments are also linked to other proteins like Nebulin. These filaments are connected across sarcomeres by α-actinin which provides rigidity to the overall structure. The regulatory proteins like Calcium-dependent troponin complex and tropomyosin play important roles in the process of activation that leads to sliding of myofilaments and generation of force.

The sarcoplasm of the muscle fiber also includes a transverse tubular system called T-tubules (Figure 4, shown in yellow) which are repetitive invaginations of sarcolemma or plasma membrane. The signal for muscle contraction is relayed through the axons of the motor neurons to muscle cells. At neuromuscular junction, the electrical signal from the motor neuron gets transformed into a chemical signal via release of a neurotransmitter molecule (acetylcholine) from the presynaptic membrane to the synaptic cleft by the process of exocytosis (MacIntosh et al., 2006). The released acetylcholine then diffuses across the synaptic cleft and binds to complementary receptors (nicotinic acetylcholine receptors) on ion channel proteins, present on the post synaptic membrane (Wang et al., 2018). The binding of the neurotransmitter to the receptors causes opening of sodium potassium-channels, creating a sodium potassium gradient. Increased levels of sodium ions cause positive charge across the post synaptic membrane, creating a membrane potential. T-tubules conduct this action potential to the interior of the cell uniformly (Jayasinghe and Launikonis, 2013). Activation of Voltage-dependent L-type calcium channels present on the membrane of T-tubules, triggers the activation of ryanodine receptors to open the calcium channels located on the membrane of sarcoplasmic reticulum (Lamboley et al., 2014). The calcium is reserved in the ends of the sarcoplasmic reticulum called terminal cisternae, that are in close contact with the transverse tubule system is then released into the cytoplasmic fluid. During the resting stage, the regulatory proteins like tropomyosin (light green) and troponin (dark green) makes the myosin binding sites on the actin molecules inaccessible as the two strands of tropomyosin wrap around the thin filaments covering the binding sites as shown in Figure 4. In the excitatory phase, the released calcium (in green) binds to the troponin displacing tropomyosin from the binding sites of myosin. The myosin heads bind to ATP and upon hydrolysis into ADP and P_i

attains a high energy state where the myosin heads extend to the binding sites on actin. The two filaments are then connected (cross-bridge). The byproducts ADP and P_i are then released causing myosin to return to a low energy state called a power stroke where thin filaments are pulled towards the center of the sarcomere. As the action potentials terminate, calcium gets pumped back into the ER, allowing the inhibition of the direct interaction of myosin and actin by retraction of troponin back to its state.

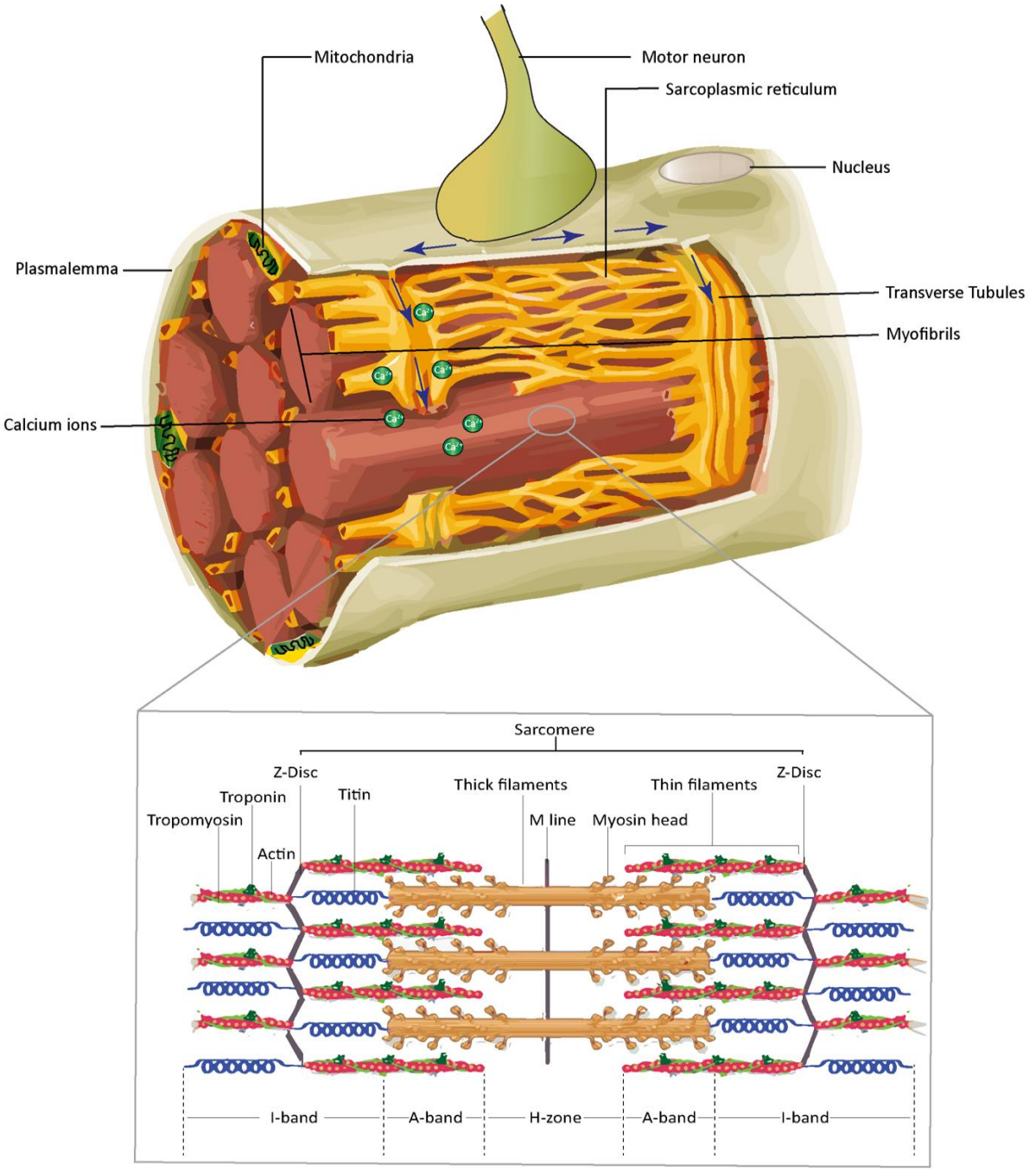

Figure 4. Conduction of nerve action potential for sarcomeric contraction.
Nerve action potential is transferred via a network of T-tubules (yellow). The ends of the sarcoplasmic reticulum present in close proximity of T tubules release stored calcium causing topological changes in the sarcomere allowing myosin heads to bind to the actin filaments which causes pulling of actin filaments towards the M-line, causing the contraction of the sarcomere. Image adapted and modified from Frontera and Ochala, 2015.

1.1.4 Sensory-motor coordination in zebrafish larvae

Motility of an animal is adapted to the environment it perceives. It is achieved by the coordination of sensory and motor components. When zebrafish sense vibrations in water from a threat, they follow a particular escape trajectory by turning to the contralateral side, forming a C-Shaped body curvature (Drapeau et al., 2002; Pietri et al., 2009; Umeda et al., 2016). This fast startle response of the embryo is called `C-bend´. Such an embryonic response to touch is observed at around 21 hpf, where a twist in the body occurs due to trunk muscle contraction. With age, this response becomes faster and a contralateral movement associated with alternate tail flips is seen. In larvae, the tactile stimuli on the head and trunk are detected by mechanosensory neurons, trigeminal (TG) and Rohon-Beard (RB) respectively. RB neurons are pseudo-unipolar neurons, having central and peripheral axons (Bernhardt et al., 1990; Metcalfe et al., 1990). These neurons are transient neuronal populations as most of them are replaced by dorsal root ganglion neurons (DRG) within 5 days post fertilization (Reyes et al., 2004). RB neurons cover the entire epidermis through their well-interconnected peripheral arbors (Figure 5A). RB cell bodies reside as longitudinal columns within the dorsal spinal cord. The central axon extends in the rostral-caudal direction, where the ascending branch reaches the hindbrain whereas, the peripheral axons undergo multiple bifurcations, forming a highly branched structure that innervates the skin. The longitudinally present central axons on the ipsilateral side altogether form a tract called dorsolateral fasciculus (DLF) (Liu, 2005; Ogino K., 2018; Umeda et al., 2016). Additionally, the central axons form synaptic contacts with commissure primary ascendance neurons (CoPA), from which the post-commissural axons merge with DLF on the contralateral side, enabling extension beyond the spinal cord.

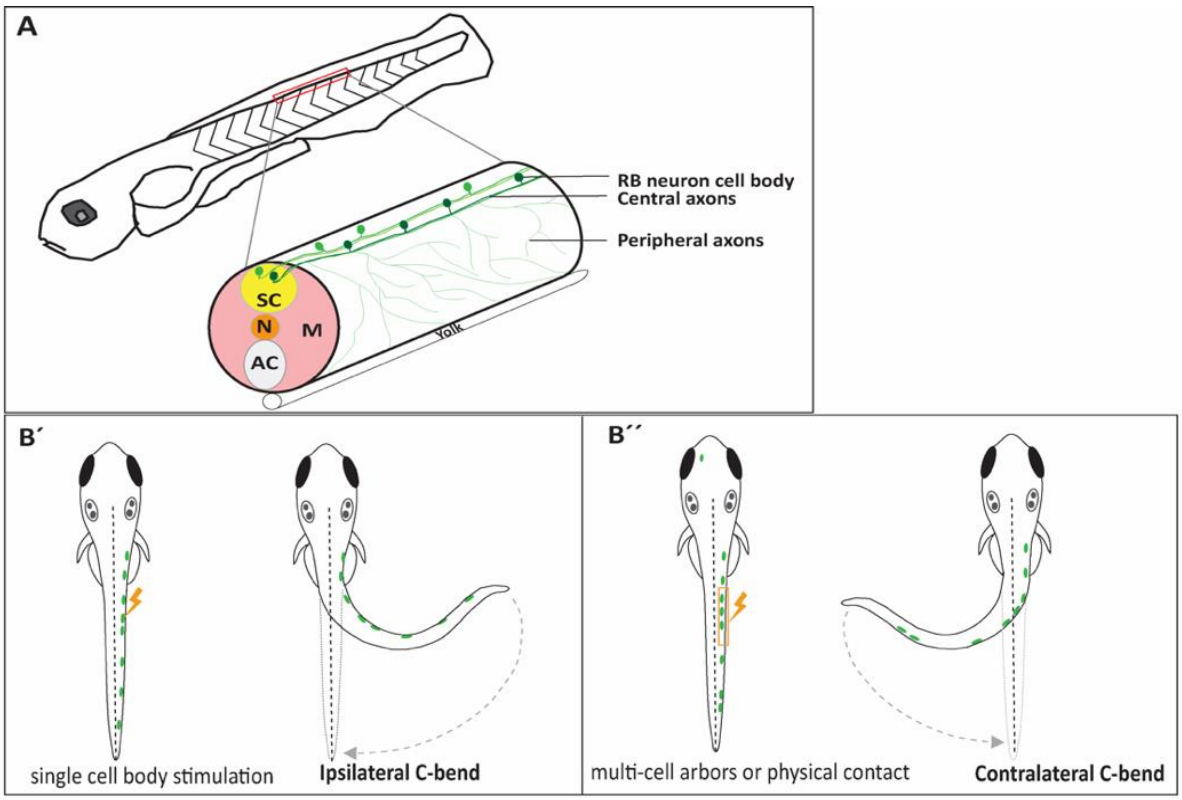

Figure 5. Larval response to types of stimulation.
(A) Schematic view of RB neuron morphology. Cell bodies of RB neurons are dorsally located in the spinal cord and are arranged in two longitudinal columns. They exhibit two types of ipsilateral axons, central and peripheral, differing in their morphology. Central axons bifurcate and extend their branches in rostral and caudal directions whereas, peripheral axons are highly branched and innervate epidermis. (B´) Turning response of zebrafish larvae upon photo stimulation of a single RB neuron. Single neuron stimulation causes ipsilateral turning whereas (B´´) photostimulation of peripheral arbors (multicell or touch evoked) causes contralateral turning of the larvae. Figure adopted and modified from Umeda et al. 2016.

It has been shown that robust, contralateral turning from the stimuli requires multicell stimulation on RB neurons like that of touch (Figure 5B´´) whereas, lower grades of stimulations (Photo-stimulation of single RB neuron) cause ipsilateral turning (Figure 5B´) (Umeda et al., 2016) which might be a common capturing response to minimal vibrations made by planktonic animals in water. Additionally, touch sensitivity studies done in mouse and cells proposed *Piezo1* and *Piezo2* being the mechanically activated channels expressed in many tissues (Coste et al., 2010). *Piezo* homologs (*piezo1*, *piezo2a*, and *piezo2b*) were also found in zebrafish of which only *piezo2b* is expressed specifically in TG and RB neurons in larvae at 24 hpf (Faucherre et al., 2013). These channels could potentially regulate calcium influx in neurons in response to touch (Bhattacharya et al., 2008).

1.2 Myogenesis in zebrafish

Skeletal muscle development begins with mesodermal cell commitment to the muscle lineage by the expression of members of the basic helix loop helix family of transcription factors called Myogenic Regulatory Factors (MRFs). *myod* and *myf5* are the first transcribed MRFs. Loss of function of *myod* or *myf5* does not affect trunk and tail muscles in the embryo but double mutants show problems with muscle differentiation, indicating a functional redundancy of these genes.

The skeletal muscles in zebrafish originate from the paraxial mesoderm, a tissue that forms in the blastopore during gastrulation and during embryonic axis elongation it is found in the tail bud (Chal and Pourquié, 2017). At the shield stage, skeletal muscle occupies the marginal zone as shown by fate mapping-studies and the muscle fiber progenitors occupy distinct locations within this zone (Devoto et al., 1996; Stickney et al., 2000). Slow muscle precursors are located close to the shield (future dorsal side) and fast muscle precursors around the margin, farther away (ventral side). These precursor cells then undergo defined movements such as involution, convergence and extension to arrange themselves in the segmental plate by the end of gastrulation (Ochi and Westerfield, 2007). The slow muscles differentiate earlier from a subset of cells which express *myod* and are located medially, close to the notochord (Figure 6A). These cells are called adaxial cells (epithelial like cells). These cells upon somite segmentation differentiate and elongate to form slow muscle fibers which

migrate radially to the surface of the myotome, forming a monolayer (Daggett et al., 2007) as shown in Figure 6B, C. These fibers are known as mononucleated superficial slow fibers (SSFs).

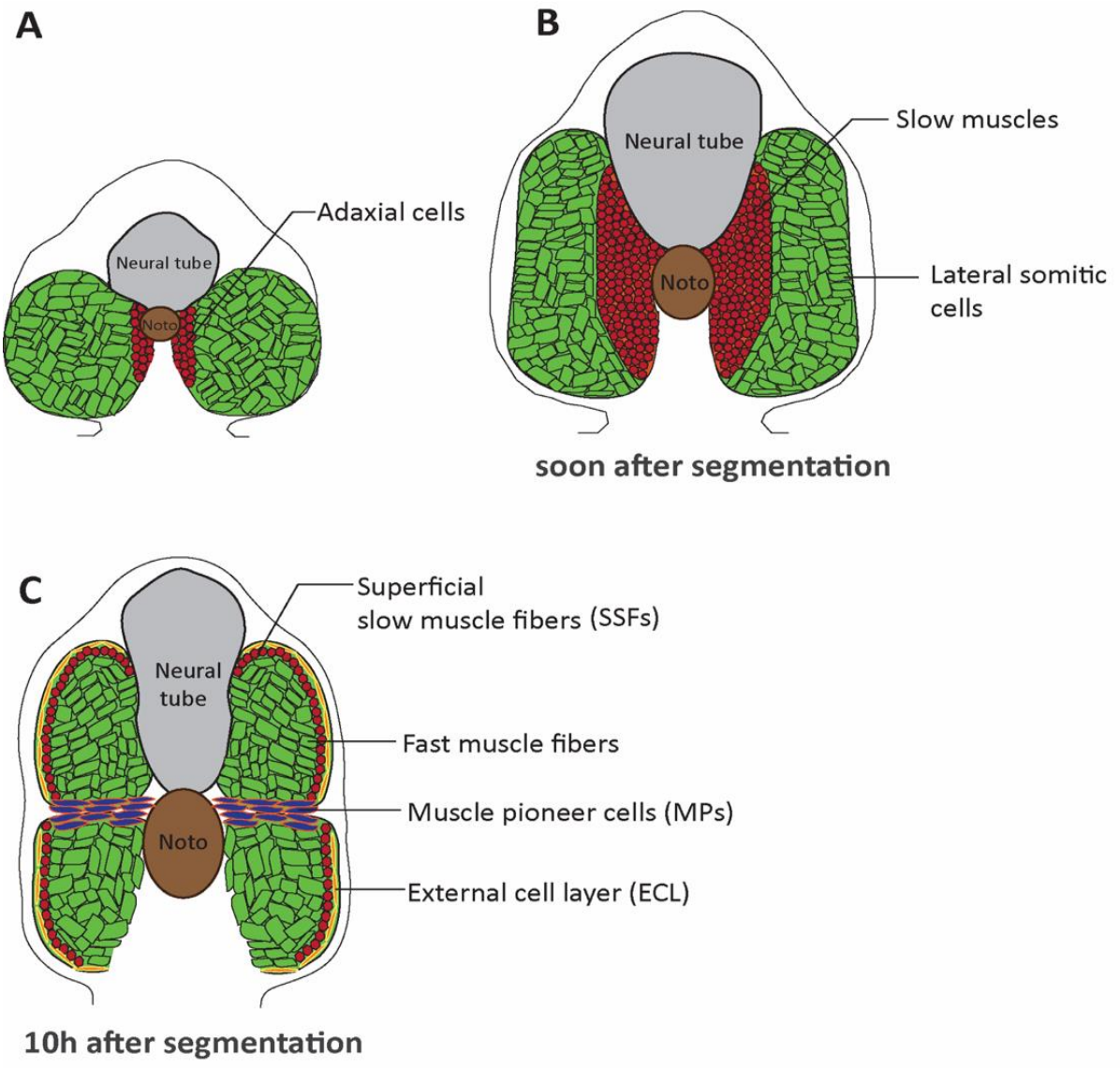

Figure 6. Somitic cell differentiation and migration.
Schematic representation of distinct localization of muscle precursor cells. (A) Transverse view of the arrangement of precursor cells at the end of gastrulation, red indicates the precursors of slow muscle cells (adaxial cells) and muscle pioneer cells; arranged around the presumptive notochord (Noto) in the center and surrounded by peripherally located fast muscle precursors in green. (B) During segmentation, adaxial cells differentiate along the dorso-ventral axis to form slow muscle cells (red), (C) Lateral migration of most of the slow twitch fibers forms a superficial layer of slow muscle fibers (SSFs in red). Some of the remaining, centrally localized adaxial cells form muscle pioneer cells (MPs in blue-red). At the same time, lateral somitic cells differentiate and fuse to form fast muscle fibers (green). The external cell layer (ECL in orange) appears in late segmentation stages. Figure modified from Yin et al. 2018 and Ochi and Westerfield, 2007.

The majority of the differentiating cells migrate but a small number remain medially localized at the horizontal myosepta, close to the notochord and are called the muscle pioneer cells (MPs) or satellite cells. At the same time another wave of FGF8-driven *myod* expression differentiates the more laterally placed somitic cells into a multinucleated array of syncytial fast muscle fibers (green) and to an external cell layer (ECL) (yellow in Figure 6C) (Stellabotte et al., 2007). ECL is equivalent to dermomyotome. By 24 hpf, chevron-shaped blocks of muscle are clearly visible in the embryos. In zebrafish, the spatio-temporal specification and localization along the medial-lateral axis (ML) is under the influence of sonic hedgehog (SHH) (Blagden et al., 1997; Wolff et al., 2003) whereas, along the dorso-ventral (DV) and anterior-posterior (AP) axis, inputs are given by bone morphogenetic protein (BMP) and fibroblast growth factor (FGF) respectively (Maurya et al., 2012; Nguyen-Chi et al., 2012).

1.3 Understanding gene function

1.3.1 Forward genetics: from phenotype to genotype:

Forward genetics is an unbiased approach towards understanding the genetic basis of a particular disease by identifying genes essential in a defined biological process. The inventory of genes known to be expressed in skeletal muscles does not provide a complete understanding of genetics underlying the muscular function or complex phenotypes seen in humans, suggesting a need for identifying novel players. Forward genetic approaches were carried out to get fundamental insights about vertebrate development utilizing zebrafish as a model system (Driever et al., 1996; Mullins et al., 1994a). Mutagenizing the whole genome randomly is an exhaustive approach to identify genes involved in development as several mutations are generated depending on the number and size of genes. In this approach screening of the population of animals that accommodate random modifications throughout the genome is performed. The modifications which alter the gene functions of interest are expected to exhibit a particular phenotype (Lawson and Wolfe, 2011). Carriers of modified alleles are then identified by subsequent examination of their progeny. Once an abnormal phenotype is seen, the mutated gene can be detected by linkage mapping of the allele within the genome, revealing genes that correlate with the observed biological process (Lawson and Wolfe, 2011; Mullins et al., 1994b; Solnica-Krezel et al., 1994).

<u>Mutagenesis approaches</u>

In order to create mutagenic lesions various physical agents like X-rays or gamma rays can be employed (Chakrabarti et al., 1983; Gridley et al., 1987). For insertional mutagenesis approaches both DNA and retroviruses have been successfully used. (Gridley et al., 1987; Ting et al., 1992). The exogenous DNA sequence can serve as a mutagen and also as a tag for

cloning the mutated gene upon integration into the genome. However, these techniques are inefficient and generate large deletions, translocations or chromosomal aberrations which make it challenging to accurately pinpoint the gene responsible for a mutant phenotype (Lawson and Wolfe, 2011). Research over several years in this field found out that chemical mutagens such as alkylating agents are far more efficient than other techniques. One of the favored mutagens, N-ethyl-N-nitrosourea (ENU), can achieve high mutagenic loads in zebrafish germ cells, where the induced phenotypes can be linked to lesions in one gene (Mullins et al., 1994b). It creates DNA adducts by ethylating oxygen or nitrogen atoms in DNA bases, which upon DNA replication results in errors (Noveroske et al., 2000). The mutation, a single nucleotide base change, is induced prior to meiosis and is fixed by DNA replication before developing into mature sperm cells. This reduces chances of mosaicism in the next generation. ENU can therefore result in nonsense mutations, splice variants and missense mutations. In zebrafish, adult males are subjected to mutagenesis by simply bathing the fish in ENU solution (Mullins et al., 1994a; Solnica-Krezel et al., 1994). To eliminate affected post-meiotic germ cells, several treatments at weekly intervals followed by a waiting period is adopted. Since there are many mutations generated in adult males, they are bred to homozygosity in F3 generations where mutations are segregated and interesting phenotypes can be screened. The genes associated with the observed phenotype are revealed by subsequent mapping of the responsible loci to chromosomal locations. The first large scale genetic screens in zebrafish were carried out in Boston and Tübingen where identification of the embryonic phenotypes was done in the F3 generations.

1.3.2 Reverse genetics: from genotype to phenotype:

Human disease modelling gives more insights about the mechanism and paves a way for drug discovery. Zebrafish has become an impressive model to investigate such questions and also for studying vertebrate development since 70% of human genes have orthologues in the fish. Following genome sequencing, most of the transcripts of protein-coding genes and non-coding genes within zebrafish genomes were annotated. Knowledge of the gene sequence made genetic manipulations much more specific since specific mutations can be made to evaluate the function of the gene. This kind of gene manipulation approach is called reverse genetics. A comprehensive collection of reverse genetics tools has been developed to study gene function in zebrafish.

<u>Tools for genetic modifications</u>

Morpholinos

One of the best-established and until recently, most widely used approaches is to knockdown the target gene expression post-transcriptionally by the use of antisense morpholino oligonucleotide analogs (morpholinos or MOs) which are artificially synthesized. They contain

morpholine rings as a replacement to the ribose backbone of nucleic acids which makes them resistant to nuclease digestion and also increases their binding to complementary RNA sequences (Summerton, 1999; Summerton and Weller, 1997). MOs exerts their effects either by attenuating protein translation or by disrupting RNA splicing. To study early development, MOs are directly injected into zebrafish one celled stage embryos. Other delivery methods like electroporation and injection into yolk have also been done (Amack and Yost, 2004; Thummel et al., 2006). Morpholinos labelled with fluorescein have been used to examine targeted inhibition and even photo-MOs which are under UV control have been used for localized conditional knock-downs (Hyde et al., 2012; Shestopalov et al., 2012; Tallafuss et al., 2012). Injected embryos are then analyzed for a phenotype and the effect is detectable up to five days after injection (Eisen and Smith, 2008; Yen et al., 2006). Although MOs are very convenient tools they also have some limitations. The phenocopy by MOs is non-heritable, with continuous cell divisions during development resulting in gradual dilution of MOs, activation of the p53 pathway leading to non-specific phenotypes, and `pseudo-phenotypes´ due to off-target effects being a few of the major limitations of this tool. Additionally, there is the possibility of incomplete gene silencing and the requirement for highly elaborate testing of the knock-down efficiency for each morpholino. Continuous efforts to develop better alternatives have resulted in the use of programmable nucleases like zinc finger nucleases (ZFNs), transcription activator-like nucleases (TALENs) and recently, the CRISPR/Cas9 system.

ZFNs

ZFNs were the first successful example of a nucleases that can be used to create target specific DNA double strand breaks (Doyon et al., 2008; Urnov et al., 2010). ZFN is a chimeric protein, engineered synthetically by combining a series of Cys_2His_2 zinc-finger DNA binding domains called a zinc finger array (ZFA) with the cleavage domain derived from FokI (a bacterial non-specific endonuclease). Each zinc finger with its alpha helix domain, recognizes and binds to a 3 bp DNA sequence which is specific and each ZFA usually contains three to six zinc finger motifs, recognizing a 9-18 bp target DNA sequence (Liu et al., 1997). Since FokI requires dimerization to be fully functional, ZFNs function in pairs with specificity to opposing DNA strands. They induce double strand breaks (DSBs) at the targeted locus which are repaired through error prone non-homologous end joining (NHEJ) generating small insertions and deletions in the genome. ZFNs can also induce large deletions when used together at a distant location in order to generate two DSBs to delete region in between (Lee et al., 2010). With all the other qualities of this tool, selection of efficient and specific ZFNs remains a challenge, limiting its broad application. The complexity of assembling zinc fingers for target specificity and need for laborious optimization made it less efficient. Commercially available screening and assembly was very expensive. Furthermore, unexpected cleavage effects have been shown to take place in a considerable frequency.

TALENs

Another promising reverse genetic tool for introducing targeted cleavage, TALENs were introduced in 2011. Transcription activator like effector proteins (TALEs) are derived from plant pathogenic bacteria called *Xanthomonas.* They contain a DNA-binding domain which is composed of several tandem repeat units, each responsible for recognize and binding to a single nucleotide in the target site (Boch et al., 2009; Moscou and Bogdanove, 2009). Classically, TALE repeat units contain 34 amino acid residues containing a repeat variable di-residue (RVD) at the 12^{th} and 13^{th} position, determining the specificity of the repeat unit. Compared to zinc finger proteins the principle and development of TALENs is simpler, making it an alternative promising tool. Golden Gate cloning strategy is the most widely used method employed to construct TALENs (Cermak et al., 2011). In this method multiple DNA fragments are assembled in a single reaction. More recent advancements brought forward much more faster, cost effective and high-throughput methods like the fast ligation-based automatable solid-phase high-throughput platform (FLASH), iterative capped assembly (ICA) and ligation-independent cloning (LIC) for TALE repeat assembling (Briggs et al., 2012; Reyon et al., 2012; Schmid-Burgk et al., 2013).

CRISPR/Cas9

It is now possible to target multiple genes in a highly efficient manner with a transformative CRISPR/Cas9 approach (Gagnon et al., 2014; Varshney et al., 2015a). The zebrafish genome being duplicated, targeting both of the paralogs to avoid functional redundancy is possible by this technique (Jao et al., 2013). This approach of genome editing is not only being used to generate knockouts but also for other purposes like allelic repair, epigenomic modulations, *in vivo* chromatic imaging and lineage tracings (Demarest and Brooks-Kayal, 2018; Li et al., 2016; Varshney et al., 2015b). Clustered Regularly Interspaced Short Palindromic repeats (CRISPR) are DNA stretches found in the genome of bacteria and other microorganisms. These innocuous sequences are a crucial part of their immune system. This tool has been adopted from the observation of the adaptive defense mechanism in bacteria and archaea against bacteriophages. They integrate snippets of foreign nucleic acids called spacers in their genome (Barrangou et al., 2007) which form a CRISPR array, holding the memory of the former invaders. If the invader attacks again, the bacteria produce RNA segments from these arrays to target the invaders' DNA. Since bacteria also have an endonuclease, Cas9, it cuts the DNA of the invader apart, disabling the prey. The Cas9 recognizes a sequence in CRISPR which is called the protospacer adjacent motif (PAM). This motif guides the Cas9 after a double strand is formed.

A ground breaking application of this mechanism for targeted mutation was in zebrafish, where CRISPR RNA is guided to the target site resulting in a double-strand break (DSB) by Cas9 endonuclease (Hwang et al., 2013). For genome editing purposes a CRISPR is simulated by generating a small guide RNA (20-22 bp) generated synthetically, specific to the target (Cong et al., 2013; Mali et al., 2013). This customized single guide RNA (sgRNA) recapitulates the function of CRISPR RNA. This RNA, being complementary to the DNA target when injected along with Cas9 protein causes DSBs and an error prone repair creates indels

which interferes with the function of the gene. Synthesizing single guide RNA (sgRNA) by annealing two oligonucleotides, serving as templates for *in vitro* transcription made the process cost effective, easy and rapid (Gagnon et al., 2014). The high target efficiency and germ line transmission made it one of the best techniques known so far. In the last few years, the technique has been employed for many model systems and targeted mutagenesis has enabled screening of large-number of genes. Several candidate genes have been associated with diseases and many disease models have come forth.

1.4 Genetic knockout model of *apobec2*

The chaperone Unc45 is required for proper folding and assembly of myosin into thick filaments. Zebrafish *unc45b* mutant embryos exhibit paralysis as they fail to form myofibrils in skeletal and cardiac muscles (Comyn and Pilgrim, 2012; Etard et al., 2007; Hawkins et al., 2008). A study in our group identified Apobec2, a putative C to U deaminase, as a novel Unc45b interaction partner (Etard et al., 2010). In contrast to mammals, zebrafish only express two members of this family, Apobec2 and Aicda (activation induced cytidine deaminase). Due to teleost genome duplication, zebrafish has paralogues of the former gene, *apobec2a* and *2b*. Characterization of zebrafish morphant for *apobec2a* and *2b* showed a possible requirement for integrity of the myosepta and myofiber attachment (Etard et al., 2010). This result was surprising since Apobec2 was classified as a deaminase, thus was not expected to be an interaction partner of a chaperone protein. It was also shown that Apobec2 deficient mice did not exhibit any major defect in health, fertility or survival up to 1 year (Mikl et al., 2005a). Histological examination also revealed no abnormalities. Although another study in mice showed that the deficiency of Apobec2 leads to increased ratio of slow to fast fibers leading to overall reduction of body mass up to 20% from birth (Sato et al., 2010a). Due to this non-conclusive research work, the role of Apobec2 had to be further investigated. For this purpose, I created genetic knockouts using CRISPR/Cas9 genome editing. I adopted a deletion strategy where two guides when injected together removed a big fragment of the gene, hoping to completely disrupt transcription.

1.5 Aim of this thesis

Skeletal muscles represent the largest tissue mass of the body and their development as well as function is a precondition for an active lifestyle. Any skeletal muscle disorder thus hinders basic chores of life. An acute need to better understand muscle disease pathology and the developmental basis of skeletal muscle formation is important for selecting the proper treatment strategies for patients.

To study the critical players for muscle development, zebrafish has long been used as a model organism. Previous studies in our research group found putative RNA editing proteins, Apobec2a/2b both being exorbitantly expressed in skeletal muscles and knock-down of the paralogues leading to muscular dystrophy. This indicated that they play a role in maintaining muscle integrity. The molecular role of this gene was yet to be elucidated and therefore, the first aim of my thesis was to create a genetic knockout model. With the commencement of a cleaner and targeted approach like CRISPR/Cas9, the project was based on employing this technique to knock out both the paralogues and establish stable lines in order to analyze single as well as double knockout lines.

In the quest of finding novel genes to better understand muscle development, another approach was used where existing mobility mutants from Tübingen screens were selected for the study. During the time of this large-scale mutagenesis screen, thousands of mutants were generated but were not characterized. These lines were brought to EZRC and stored as precious frozen sperm stocks. We chose to investigate samples from these stocks. The major tasks were to retrieve the lines from these frozen sperm samples, assess their phenotypes and most importantly to explore whether this type of analysis is a good approach to find novel genes. An additional aim was to discover the causal mutations by genome sequencing.

2 Material and Methods

2.1 Materials

Bacterial Strains

Cloning was done using competent cells, i.e., E. coli strains: XL1-blue obtained from Promega or TOP10 from Thermo fisher. Bacteria were grown in 100 ml LB medium overnight shaking at 37°C. The next day 100 ml LB medium was inoculated with about 10 ml of the bacterial culture. Cells were then grown until they reached an OD600 between 0.48 and 0.6. In this exponential growth phase cells were centrifuged for 10 minutes at 3,200 x g at 4°C. Afterwards supernatant was discarded and pellet was resuspended in TFB1. The suspension was then incubated for 1 hour on ice and centrifuged at 4,000 for 10 minutes at 4°C. This pellet was finally resuspended in TFB2. Aliquots of ~50 µl were snap frozen in liquid nitrogen and stored at -80°C.

Oligonucleotides

Oligonucleotides used in the experiments were designed using Primer3 web version 4.1.0 software and ordered from Metabion International AG in soluble form at 100 µM concentration which were diluted in a ratio of 1:10 for a PCR reaction.

Table 1. Oligonucleotides and Crispr guide sequences used in this project

Name	Sequence	Usage
Apobec2a gene		
*apobec2a*_sgRNA_Ex1	taatacgactcactataGGAGAAAAGCCCAACAGAAGgttttagagctagaaa	Guide were used in combinations:

*apobec2a*_sgRNA_int1	taatacgactcactataGGCGCACTGGTGATAGGGTGgttttagagctagaaa	-Ex1+Int -Int+Ex2 -Ex1+Ex2
*apobec2a*_sgRNA_Ex2	taatacgactcactataGTCGCGGCTGTTCGAGTGGGgttttagagctagaaa	
*apobec2a*_ex1fw	GTGTTTAGTTTCAGAGATGGCCGAT	Used to genotype: amplifies the leftover sequence (320 bp) after deleting part of Ex1 and intron
*apobec2a*_intrv	CATAGATTGGGTCTTTCCCGAGG	
*apobec2a*_int5'	AGGAGCCGTAATGCTACCGCT	Used to genotype: amplifies the leftover sequence (330 bp) after deleting part of Ex2 and intron
*apobec2a*_ex2rv	CAGGGTGTGAACTGCTGTTCG	
*apobec2a*_ex1fw + *apobec2a*_ex2rv	Used to genotype: amplifies the leftover sequence (250 bp) after using Ex1 to Ex2 guides together deleting almost the whole gene sequence	
*apobec2a*_intana_fw	CCAACATTAGTCCCGCCCTA	Used to differentiate homozygous to heterozygous fish. 500 bp fragment amplified only in heterozygous or wild type cases.
*apobec2a*_intana_rv	GTGTGTGTGTGTTTCCCGAA	
Apobec2b gene		
apobec2b_sgRNA_Ex1	taatacgactcactataAGAGATGCCTCAAGGGAATGgttttagagctagaaa	Guide were used in combinations: -Ex1+Int -Int+Ex2 -Ex1+Ex2
apobec2b_sgRNA_int1	taatacgactcactataGTTCAGCTAGCACATGGGTGgttttagagctagaaa	
apobec2b_sgRNA_Ex2	taatacgactcactataGGCGTTCGTGGTTACCTGGgttttagagctagaaa	
apobec2b_ex1fw	TGGCAGACAAAAAGGACAGC	Used to genotype: amplifies the leftover sequence (497 bp) after deleting part of Ex1 and intron
apobec2b_intrv	CAACTTACCCAGACTGCAAATCTG	
apobec2b_int5'	AGTCCCATCCAGACCTGCA	Used to genotype: amplifies the leftover sequence
apobec2b_ex2rv	GCTTTCAAGATCTCCACAAGC	

		(325 bp) after deleting part of Ex2 and intron
apobec2b_ex1fw + apobec2b_ex2rv	Used to genotype: amplifies the leftover sequence (360 bp) after using Ex1 and Ex2 guides together deleting almost the whole gene.	
apobec2b_intana_fw	ACAGCTCAGTACTTGGACCA	Used to differentiate homozygous to heterozygous fish. 670 bp fragment amplified only in heterozygous or wild type cases.
apobec2b_intana_rv	GGACCAAATGAACCGAACCA	
ChaT gene		
Primerbajan_fw	CAAAAGGCCAATTGGGTAAG	To check for bajan allele
Primerbajan_rv	CCTTGCTGTTTCTCTAGACTCTCA	
Chat-ageI5'	CTGGACCGGTCCGATGCCAGTTTCAAAAAGGGAAC	To amplify chat in fragments in combination with chat_rvpaper
Chat_fwpaper	TCTTCAACTTTGAGGATGCCAGTTTC	To amplify chat in fragments
Chat_rvpaper	TCCTGCGTCTTATGACTTGCTTCC	
Chat_EcoRI5'	CTGGGAATTCCCGATGCCAGTTTCAAAAAGGGAAC	To amplify chat in fragments also in combination with chat_rvpaper

Plasmids

The plasmids used in this study were bought from different sources and for ligation, 1:3 or 1:5 Plasmid: Insert ratios were used.

Table 2. Plasmids

Name	Source
pCS2+	NovoPro
pGEM-T easy	Promega

TOPO vector	Invitrogen

BACs

Bacterial artificial chromosomes as vectors to deliver large pieces of DNA to zebrafish embryo were used in this thesis for the purpose of rescuing mutant phenotypes.

Table 3. BACs used in this project.

Name	Source	Genes
1. *CH73-41E3*	BACPAC Resources, Oakland, USA.	*cenpq, jam2a, txnl4b, ercc5, mrpl16, trmt10c, atp5pf, mrpl39, blzf1, LOC101885604, si:ch73-41e3.7*
2. *CH73-244F7*		*tpp2, LOC100149425, ercc5, trmt10c, zgc:92518*
3. *CH211-129C2*		*LOC108187164, tmem255b, rasa3, pros1, cenpe, grk1a, tfdp1b, gas6*
4. *CH73-367P20*		*tmco3, adprhl1, dcun1d2b, grtp1a, tfdp1b*

Zebrafish lines

The mutant lines were stored as a sperm sample at EZRC and were revived by IVF. Post-fertilization embryos were cleaned and bleached for raising. Embryos were raised according to the Zebrafish book (Westerfield, 2007). Initially 50 embryos were raised per mouse cage, which were transferred 1 month later to a 10 l tank. After attaining sexual maturity, around 3 months they were screened for heterozygosity.

Table 4. Zebrafish lines revived from Tübingen and Sanger screens

ENU mutant lines	Internal allele name	Description
tk64	K64A	1st Tübingen screen
frozen (fro^{to27c})	O27C	
duesentrieb (dus^{tq250})	AQ50A	
slumber (slm^{tt208})	AT08B	
t31198	NS078SA	3rd Tübingen screen
t30064	LH005QAV	

bajan (chata^{tf247})	*Chata*	Revived for complementation
ryr1b^{sa14191}	*Ryr1b (sanger line)*	Revived for complementation
dusp27^{y241Et}	*Dusp27*	From ZIRC for complementation

2.2 Methods

2.2.1 Embryonic Methods and Fish handling

Zebrafish maintenance and husbandry

All the lines used were maintained and raised as described by Westerfield (2007). The lines were a priori registered and approved by local Animal protection committee (Regierungspräsidium Karlsruhe). European Zebrafish Resource Center (EZRC) guidelines were followed for bleaching and raising of the embryos to avoid disease manifestation. The lines brought from other fish facilities were first kept at the quarantine facility of KIT and the subsequent bleached generations were introduced in the fish facility for use. Wild type zebrafish were descendants of the AB line (University of Oregon, Eugene, USA). Fishes were maintained at 28.5°C on a 14h/10h light-dark cycle in system with recirculating water (Aqua Schwarz, Müller and Pfleger Ltd Germany). They were fed differently according to their age with granulate or flakes along with freshly hatched Artemia. Snails were added to the tanks to remove excess food and fungus. Embryos can be obtained by pairwise mating. Crossing was performed in smaller plastic cages containing a mesh and system water. The mesh contains holes larger than the diameter of eggs so that the eggs fall through it to the bottom of the compartment and cannot be reached by parents. The eggs can be collected as soon as they are laid with the help of sieve and transferred to Petri dishes. The embryos were bleached at the 24-hour stage (except microinjected eggs) before raising. Staging was based on the morphological changes as described by Kimmel et al., 1995. **Note**: The Tübingen background is much more aggressive than AB and hence a green fiber ball was added to the crossing cage for giving hiding space to the fish. Immediately after mating, the couples were separated.

Escape response assay

To check the motility defect, embryos at 48 hours post fertilization were subjected to a touch stimulus near the yolk extension. Wild type embryos at this stage responded with a strong bend of the body axis away from the stimulus and continued to swim. This assay was carried out for the motility mutant lines to identify the mutants and also to check the rescue after mRNA injection. Embryos were touched with forceps, were observed under a stereo

microscope and around 25% of the off-springs of heterozygous couples showed either diminished or complete loss of motility.

Birefringence assay

This assay was used to assess muscle integrity of the embryos and is well explained by Berger et al., 2012. Since muscle is an organized structure containing an anisotropic (A-) band, they shine when a bright, plane polarized light is passed through them. Defects in organization of sarcomeric repeats are read out in the form of reduced brightness.

Microinjection of zebrafish embryos

Microinjections were performed using a gas-driven microinjector system (Tritech) and a SMZ645 Nikon stereomicroscope on a Petri dish with the help of needles. They were performed as described by Müller et al., 1999. The microinjection needles were prepared from borosilicate glass capillaries with filament which were heated and pulled to form needles by Flaming-Brown needle puller. As per the experimental setup, the needles were filled with 1-5 μl injection solution containing 0.1% phenol red (tracemarker) using Eppendorf microloader pipette tips. The eggs were collected shortly after being laid and about 2-6 nl injection solution was injected through the chorion either into the cell itself or closer to the cell into the yolk at one-cell stage. After the injection, the embryos were transferred to a Petri dish with embryo water and incubated at 28°C. The injection mix depends on the experimental setup, can be DNA/RNA or both co-injected into the embryos. For gene knockout studies, about 120 ng/μl of each guide RNA along with 300 ng/μl of Cas9 protein was used as an injection mix. For BAC injection, about 30-50 ng/μl was used and for gene knockdown studies, morpholino (Gene Tools, LLC) at 0.2 mM concentration was injected.

In vitro fertilization

Mutant lines from ENU screens were kept in the form of frozen sperm stocks at EZRC. The chosen lines were then revived by in vitro fertilization (IVF) with AB strain wild type embryos. For IVF, wild type female fish were anaesthetized using tricaine solution and rinsed with PBS. The female fish was then dried with a paper towel (any excess water could activate the eggs). The female fish was then transferred to a 6 cm diameter glass dish. A gentle pressure was applied to the ventral side of the fish with moist hands to release the eggs slowly into the Petri dish. Good eggs were yellowish, translucent and granular looking while whitish, watery and cloudy eggs are bad. The sperms stored in cryovials were then removed from liquid nitrogen and transferred to a 34°C water bath. The tube was immediately filled up with 500 μl of BSMIS preheated to 37°C. After gentle stirring with the pipette the sperms were quickly activated by adding 500 μl fructose solution and mixed by pipetting up and down once. This activated sperm solution was then immediately transferred to eggs. The Petri dish was kept stationary for about 30 seconds. The motility of sperm was checked under the microscope for another 40 seconds. As soon as the motility of sperm diminished, the dish was filled with water and

incubated at 28°C for about 3 hours before checking the fertility rate. The fertilized eggs were then raised as described by Westerfield (2007).

Identification of heterozygous carriers

Heterozygous carriers of the mutant allele were identified by performing random brother-sister mating. The offspring of these couples were then screened for the expected phenotype (reduced motility, curved axis or reduced birefringence). Once a batch of mutant offspring was identified, the couples were marked as heterozygous mutants and were crossed with the AB wild type strain to get rid of any background mutations. The subsequent generation was then screened again for heterozygous fishes by performing random incrosses.

2.2.2 Histological methods

Immunohistochemistry

Fixation of embryos

For immunohistochemistry and also for *in situ* hybridization, the embryos were dechorionated and given time to straighten up since mutants are curved and show a motility defect. About 3 hours post dechorionation, embryos were transferred to a tube and anaesthetized before exchanging fish water with freshly thawed BT-fix. For *in situ* experiments overnight fixation at 4°C was done whereas for immunohistochemistry, embryos were fixed for 1 hour at RT. The immunostaining protocol is well described by a recent method paper (Santos et al., 2018).

Immunostaining protocol

After fixation, BT-Fix was removed and embryos were washed 4 times in the interval of 5 minutes with 1x PTW (0.1% Tween-20 in 1X PBS) to remove the fixative completely. Post washing, to enhance the penetration cold acetone was added to the embryos and incubated at –20°C for exactly 7 minutes. Acetone was removed and the embryos were then washed thrice in 10-minute interval with 1X PTW. The embryos were then blocked by incubating in BDP (1% BSA, 1% DMSO in 1X PBS) solution for about 4 hours at RT. Blocking was followed by transferring the embryos in primary antibody solution, pre-diluted with blocking buffer. Embryos were incubated overnight at 4°C. On day 2, the antibodies could be collected for reuse and the embryos were washed 6 times with 1X PTW followed by blocking for about 30 minutes at RT. Post-blocking, prediluted secondary antibodies were added and incubated at RT for about 2 hours in dark. Embryos were then washed 4 times with 1X PTW at 10-minute interval. At this stage DRAQ5 diluted in 1X PBS (nuclear staining) was added in a few cases for about 10 minutes. At the end, embryos were washed a few times with 1X PBS before imaging.

Whole mount *in situ* hybridization (WISH)

This procedure was performed as described by Oxtoby and Jowett, 1993. For this thesis, particularly used to visualize expression in developing trunk and tail muscles at around 24 hpf.

Synthesis and labelling of DIG RNA probes

Templates for DIG-labelled RNA-probe synthesis were linearized plasmid DNA. About 1 µg of linearized plasmid was added to a 20 µl reaction in water containing 4 µl 5X transcription buffer, 1.5 µl T7/T3/Sp6 RNA polymerase and incubated for 2-3 hours at 37°C. After incubation, the synthesized RNA probe was diluted with 10 µl RNAse free water and to this 3.75 µl 2 M NaOAc (pH4), 65 µl 100% ethanol was added for precipitating the RNA. It was then incubated at -80°C for 30 minutes. After incubation, the solution was centrifuged at 4°C for 30 minutes and the supernatant was discarded. The RNA pellet was seen at the bottom of the tube and was washed once with 70% ethanol by centrifuging for 5 minutes at 4°C. The supernatant was completely removed and the pellet was air dried at RT for about 10 minutes. Resuspension of the RNA was done in 11 µl of RNase free water. To check the quality of the RNA, 1 µl of RNA was loaded onto a 1% agarose gel. The concentration of RNA was assessed using a spectro-photometer, 10 µl of HYB buffer was added and it was stored at –20°C.

In situ protocol

Overnight fixed embryos were washed 3 times with 1XPTW and incubated overnight in 100% methanol (samples were stored in methanol until processed further). All the hybridisation steps were carried out in 0.5 ml Eppendorf tubes. Embryos were re-hydrated by sequential transfer from 100% to 75%, 50%, 25% methanol solutions. Subsequently the embryos were washed 4 times in the interval of 5 minutes with 1X PTW and digested with Proteinase K depending on the stage of the embryos. After digestion, proteinase K was removed and the embryos were washed thrice in the interval of 5 minutes with PTW. After washing, the embryos were incubated in HYB buffer for 2-3 hours followed by overnight incubation with the DIG labelled RNA probe diluted in preheated HYB buffer (1:300 or 1:400) at 65-70°C. Washing buffers were incubated along overnight with the embryos. After overnight incubation, embryos were washed twice with wash buffer 1 in a 30 minutes interval, once with wash buffer 2 for 15 minutes, twice with wash buffer 3 in a 30 minutes interval and at the end once with wash buffer 4 for 15 minutes to remove unhybridized probe completely. All the washing steps were done at 65-70°C. After washing, the rest of the steps were done at RT. Embryos were washed once with the blocking buffer for 15 minutes followed by an overnight incubation at 4°C in anti-DIG antibody diluted in blocking buffer (1:4000). On the third day, the antibody solution was removed and the embryos were washed 5 times in a 15 minutes interval with PTW, once with staining buffer for 5 minutes. The embryos were then transferred to a 24-well plate carefully and washed once with staining buffer again. For staining, the substrates BCIP (0.5 mg/ml final concentration) and NBT (0.188 mg/ml final concentration) were mixed in staining buffer and 500 µl of this solution was added per well. Staining was carried out in the dark to avoid background staining and was stopped through repeated washes with PTW. The background staining was removed by washing with 100% ethanol for about 10-15 minutes followed by washing with PTW several times for re-hydrating the embryos before imaging (This step makes the staining blue and the embryos get curved).

TEM sample preparation

Mutants and wild-type like siblings at 3 days post fertilization were collected, anaesthetized in tricaine solution followed by fixation in 500 µl Karnovski fixative solution at 4°C. Post fixation, the samples were washed twice at 10 minutes interval with 0.1 M PIPES, re-fixed with 500 µL $OsO_4/K_3[Fe(CN)_6]$ solution on ice for 1 hour, washed twice for 15 minutes with 0,1 M PIPES and finally twice for 15 minutes with ddH_2O. Tissue contrasting was achieved through overnight incubation in 2% uranyl acetate in 25% EtOH/75% ddH_2O at 4°C.

Epon embedding

Samples were dehydrated by successive washing steps with increasing concentration of ethanol (twice, 10 minutes with 50% ethanol → twice, 10 minutes with 70% ethanol → twice, 10 minutes with 95% ethanol → 4 times, 15 minutes with anhydrous ethanol). Following complete dehydration, the embryos were washed twice for 5 minutes in dried 1,2-propylene oxide (PO). The glycid ether 100 - epoxy resin (EPON) was stored at – 20°C to avoid polymerization and was kept at room temperature before use. EPON was also added to the embryos in increasing concentration (60 minutes in 33% EPON in PO → 60 minutes in 66% EPON in PO → 30 minutes in 100% EPON and final incubation for 10 minutes in 100% EPON). To embed the samples, rubber moulds were used which were first half-filled with EPON with labels and incubated at 65°C for 2 hours for polymerization. This is usually done so as to be able to orient the embryos in the middle of the mold. After polymerization, resin-soaked embryos were transferred into these labeled polymerized beds and positioned transversely. Post embedding of embryos, an overnight incubation at 65°C was done to completely polymerize the resin.

Trimming, sectioning and imaging

Polymerized EPON blocks were trimmed with a Leica REICHERT ULTRATRIM before subjecting them to ultra-sectioning using a Diamond DIATOME knife. For Toluidine blue staining, 350 nm thick sections were cut with a Leica Ultramicrotome EM UC6 which float over the water chamber of the knife and collected with a Diatome Perfect Loop section collector, placed on a glass side. The sections were then stained with a freshly prepared Toluidine Blue O solution (15 µl filtered Toluidine Blue O (1%), 35 µl 0,1M borate buffer (pH 9,5) and 950 µl ddH_2O) for about 5-7 minutes on a heating block at 80°, washed with ddH_2O to remove the dye from the section and dried again. Post staining, sections were covered with a thin layer of EPON resin and a glass cover slip, placed on a 80°C heating block overnight for polymerization before imaging. For TEM, 70 nm thin sections were cut and collected on a palladium-copper grid precoated with a thin formvar. These grids with the samples were stored on a rubber sample holder to prevent mechanical or electrostatic damages. Imaging was done with a Zeiss EM 910 Leo, 80kV Transmission electron microscope.

Evans blue dye injection

Evans blue dye is a membrane impermeable dye which was used to check the muscle fiber integrity in the mutant embryos. The dye powder was dissolved in Ringer's solution and

filtered through a sterile syringe filter. It was then injected into the peri-cardiac sinus of 48 hours old embryos which were previously anaesthetized and embedded in low melting agarose. After injection the embryos were carved out and incubated until the 72-hour stage the in dark. Imaging was carried out using a compound microscope. The detailed procedure is described by Smith et al., 2015.

2.2.3 Molecular biology methods

Genomic DNA extraction (HotSHOT)

For checking the mutational efficiency of the CRISPR guide RNAs prior to raising, genomic DNA from the injected embryos was extracted using the HotSHOT method previously described in Etard et al. (2017).

Genotyping the adult fishes

To check and select the genetically modified fishes created via CRISPR guide injection, adult zebrafish were genotyped by fin biopsy as described by Meeker et al., 2007. Adult fishes were anaesthetized using tricaine and were laid laterally on a plastic tray. A smasll piece of the tail fin was then cut using a sharp scalpel. The tail fin-cuts were transferred with forceps into a tube containing 75 µl KOH solution. The fish was then placed into a labelled box in fresh fish water which allows zebrafish to wake up. The solution containing tail fin cuts were incubated at 95°C for 20-30 minutes and cooled down to 4°C in a thermocycler. To this, 75 µl of neutralization buffer was added and mixed well using a pipette. About 5 µl of this solution was then used for setting up a 25 µl PCR reaction (Table 5).

Genomic DNA extraction for whole genome sequencing

Sample collection

Whole genome sequencing was done to identify the allele responsible for the observed phenotype in the previously uncharacterized mobility mutant lines we revived from ENU screens (Table 4). From a heterozygous couple, about 50 mutant embryos (showing a phenotype, 3 days post fertilization) and 50 phenotypically wild-type siblings were collected in a tube. The embryos were anaesthetized and the water was removed (as much as possible). The tube was then rapidly frozen by using liquid nitrogen. The samples were stored at -80°C until subjected to genomic DNA extraction.

Extraction protocol

To the collected samples, 500 µl of extraction buffer without proteinase K was added and subjected to strong pipetting events so as to completely smash the embryos into the solution. The supernatant was removed as much as possible (embryos coagulate at the bottom of the tube so can be simply sucked up and transferred into a new tube using a precut plastic pipette). To this, 500 µl of extraction buffer with proteinase K (final concentration 1 mg/ml) was added. This solution was then incubated overnight at 65°C without agitation. Genomic

DNA was then extracted by adding 500 µl of phenol: chloroform: isoamylalcohol (25:24:1) solution and gently shaking it at room temperature (RT) to avoid shearing of genomic DNA. This solution was then centrifuged for 10 minutes at 13,000 rpm at RT and the supernatant was transferred to a fresh tube using a precut 1 ml pipette tip. To this, 500 µl of 100% isopropyl alcohol was added and centrifuged at RT for about 10 minutes at 13,000 rpm. The supernatant was removed and the obtained pellet was washed with 75% ethanol by centrifuging it for 5 minutes at the same conditions. The supernatant was removed and the pellet was dried at RT for about 15 minutes. The pellet was resuspended in 100 µl of deionized water for about 10 minutes at 40°C. Genomic DNA was stored at 4°C and was extracted not more than a day before library preparation. The quality of the extracted DNA was assessed by Nanodrop (Thermofisher Scientific) and the quantification of the sample was assessed by a Qbit (Invitrogen) at the sequencing facility here at KIT.

Transformation of bacteria with plasmid DNA (Retransformation)

To get a larger quantity of the plasmid DNA (DNA fragment cloned into a plasmid), chemically competent bacteria were transformed by adding around 0.6 µl of plasmid solution to a previously thawed tube containing 100 µl of competent bacteria. After adding the plasmid solution, bacteria were incubated on ice for about 45 minutes followed by a heat shock by incubating this tube at 42°C for 42 seconds. After heat shock, the tube was incubated on ice for about 5 minutes. Out of this bacterial solution, around 30 µl was plated on LB agar plates containing a suitable antibiotic.

Isolation of plasmid DNA

For sequencing of uncharacterized clones or for restriction analysis, a small-scale plasmid DNA extraction (“miniprep”) was carried out using a Macherery-Nagel mini prep kit whereas for plasmid DNA preparation on a large scale a midi or maxi prep kit was used. Overnight cultures of bacteria colony in LB-medium in a specific volume were used as the starting material for the kit. All other instructions were followed as given by the manufacturer. The concentration of the plasmid DNA at the end was determined using a Nanodrop spectro-photometer.

Phenol-chloroform extraction

Purification of nucleic acids was carried out by this method. DNA solutions were subjected to equal volumes of phenol: chloroform (1:1) and vortexed for about 10 seconds. This mixture was then centrifuged for about 20 minutes and 13,000 rpm at 4°C to allow phase separation (the aqueous phase, the interphase and the organic phase). Nucleic acids were retrieved from the supernatant (aqueous phase) carefully without the interphase and transferred to a new tube. To this, about 100 µl of chloroform was added, mixed vigorously and centrifuged at 13,000 rpm, 4°C for about 20 minutes. The supernatant was retrieved again and about 100 µl of isopropanol was added to it. The mixture was briefly vortexed and incubated at -80°C for about 30 minutes. This incubated solution was then centrifuged for about 25 minutes at 4°C, 13,000 rpm. The supernatant was discarded and the precipitated DNA was washed once with

70% ethanol by brief centrifugation for about 5 minutes. The supernatant was discarded and the pellet was air dried for about 10 minutes at room temperature. Finally, the pellet was resuspended in about 30 µl water.

Restriction digest and ligation of DNA

Digestion of DNA was done with restriction endonucleases according to the manufacturer's instructions. The enzymes were used with proper buffer conditions and approximately one unit of enzyme was used to digest around 1 µg of DNA when incubated for 1 hour or even overnight at 37°C. Ligation of DNA fragment (insert) to a specific vector was carried out at a molar ratio (vector: insert) of 1:3 or 1:5. The amount of insert was calculated with the following equation:

$$\boldsymbol{vector(ng)\ X\ \frac{vector\ size\ (kb)}{insert\ size\ (kb)}\ X\ \frac{ratio\ insert}{vector} = insert\ (ng)}$$

Polymerase Chain Reaction (PCR)

The amplification of DNA fragments from genomic DNA or cloned fragment in the form of plasmid was performed by PCR. Taq polymerase (GoTaq polymerase, Promega) was the polymerase of choice for the PCRs where proofreading was not required as it is faster than proof reading polymerases (Q5 Hifi DNA polymerase, New England Biolabs or Phusion DNA polymerase, Thermo Scientific) which were used for cloning purposes. The PCR reaction was set up according to the following protocol, adjusting the annealing temperature and elongation time according to the primers and size of the amplified fragments respectively.

Table 5. Standard PCR reaction and normal PCR cycle

Reaction components	Volume
5X Go Taq Reaction buffer	5 µl
25 mM dNTPs	0.25 µl
10 µM Primer mix (forward+ reverse)	0.25 µl
25 µM $MgSO_4$	1.5 µl
DMSO	1.25 µl
Template*	5 µl (fin clip /gDNA) or 50 ng/µl plasmid
Go Taq Polymerase	0.25 µl
Water*	11.5 µl
Total	25 µl

Cycle		Step
94°C ---- 7 min		Initial denaturation
94°C ---- 30 sec	30-40 cycles	Denaturation
X°C* ---- 30 sec		Annealing
72°C ---- Y sec*		Amplification
72°C ---- 7 min		Final extension
10°C ----- ∞		Hold

Agarose gel electrophoresis

For separation of DNA fragments, to check the size of the PCR product and also to check RNA quality, gel electrophoresis was performed. The exact protocol has been practically described by Lee et al., 2012. For experiments in this thesis, the digested plasmid, PCR product or RNA was added on a 1-3% agarose gel with loading dye. For visualization, ethidium bromide (3

µl/100 ml) was added to the agarose solution. An electrophoresis chamber was loaded with TAE buffer and the solidified gel was immersed into it. After loading the samples onto the gel, electric current was applied to allow DNA fragments to move towards the positive electrode. For estimating the fragment length of the samples, a DNA/RNA ladder was also loaded onto the gel along with the samples. The results were checked on a UV-transilluminator.

Isolation of DNA from agarose

To clone the fragment, to check the sequence of the PCR product or to select positive clones; the bands of DNA stained with ethidium bromide appears glowing when visualized using UV transilluminator. Bands corresponding to the expected size were cut out from the agarose gel using a scalpel. The fragment was then retrieved from the gel using a Macherey-Nagel gel extraction kit following manufacturer's instructions. To sequence the fragments, around 200 ng of the product was sent along with appropriate primer to Metabion AG.

pGEMT-vector sub cloning

PCR derived; gel extracted fragments were cloned into pGEMT-Easy Vector (Promega). Since this vector contains 3´dT overhangs at its multiple cloning site, the product should have 3´A overhangs. To create these GoTaq was used alone or in combination to Q5 polymerase during PCR. The cloning was done as described in the manufacturer's protocol. Overnight incubation at 16°C was done and subsequently the ligated product was used for transformation of the competent bacteria.

Extraction of total RNA for sequencing

RNA extraction for RT PCR or RT qPCR was done by following Step 1 of the Macherey-Nagel gel extraction kit. Step 2 was followed only when RNA extraction was done from the mutants and wild type siblings to check the differences at the transcriptional levels (RNA sequencing).

Sample collection for RNA sequencing

From three heterozygous couples, 50 embryos each mutant and wild type were collected in 2 ml Eppendorf tubes. The stage for sample collection was dependent on the phenotype recognition which was clear around 3 days post fertilization. The collected embryos were frozen using liquid nitrogen and stored at -80°C until RNA extraction was started. For RNA extraction only autoclaved tubes, filter tips, and DEPC water were used.

RNA extraction

Step 1: To the frozen embryos, 1ml of the Trizol reagent (Invitrogen) was added and homogenized using a syringe or pipetting and vortexing until no tissue was visible. The homogenized solution was incubated at RT for about 5 minutes followed by addition of 200 µl chloroform. The chloroform was mixed by vortexing the mixture for about 15 seconds followed by incubation at RT for about 2 minutes before centrifuging at 13,000 rpm at 4°C for 20 minutes. After centrifugation, the upper aqueous phase was transferred to a clean 1.5 ml

tube. [About 1 µl glycogen (Ambion) was added to the collected aqueous phase when there was not enough starting tissue.]. To the aqueous phase 500 µl of isopropyl alcohol was added, mixed by vortexing and incubated for 45 minutes at -80°C. After incubation, it was centrifuged at 13,000 rpm for 1 hour at 4°C. The supernatant was completely removed and the pellet was seen at the bottom of the tube. The pellet was washed with 500 µl 75% ethanol and centrifuged at the same conditions for about 5 minutes. Ethanol was removed and the pellet was air dried for about 10 minutes at RT. The dried pellet was then resuspended in 100 µl DEPC water.

Step 2: The second precipitation step was followed to purify the RNA for sequencing purposes. To 100 µl of the RNA solution (from step 1), 100 µl of phenol: chloroform: IAA (25:24:1) mixture was added, vortexed and centrifuged at 4°C for 30 minutes at 13,000 rpm. The upper aqueous phase was the transferred to a clean 1.5 ml tube. To this, 10 µl of sodium acetate DEPC (pH 4.5) and 250 µl 97% ethanol were added and incubated either overnight at -20°C or for 1 hour at -80°C. Following incubation, the tubes were centrifuged at the same conditions for about 1 hour. The supernatant was removed after centrifugation and washed with 250 µl of 75% Ethanol. Ethanol was removed and the pellet was completely air dried for 10 minutes at RT. The dried pellet was resuspended in 25 µl DEPC water.

The RNA concentration was measured with a nanodrop and integrity was checked by gel electrophoresis where 28 S rRNA and 18 S rRNA of all samples appeared as two bands with almost a 2:1 ratio; and further by checking the RIN number.

cDNA synthesis for RT PCR

DNase treatment of the RNA

To prevent genomic contamination in the resulting cDNA, DNase treatment was done prior to cDNA synthesis. 1µg of RNA was digested with 1U DNase I (Promega) by incubating it at 37°C for 30 minutes in DNase buffer in a 10 µl reaction. The reaction was stopped by adding RQ1 DNase stop solution (Promega) and incubating at 65°C for 10 minutes.

cDNA synthesis reaction

cDNA synthesis was done using the Maxima First Strand cDNA Synthesis Kit following the manufacturer's protocol. The reaction mixture contained DNase treated RNA with Maxima first strand reaction buffer and enzyme. This mixture was incubated at 25°C (RT) for 10 minutes followed by 1 h incubation at 50°C. A final inactivation step (65°C for 10 minutes) stopped the reaction. The resulting cDNA was stored at -20°C and diluted before use.

CRISPR/Cas9 deletion strategy and guide RNA synthesis

To disrupt the function of the gene, Crispr/Cas9 mediated gene editing was performed for understanding function of *apobec2a (apo2a)* and *apobec2b (apo2b)* genes. To create knockouts, a deletion strategy was chosen where two guide RNAs were injected together to create a big deletion with a hope of disrupting gene function completely. The best guide RNAs (20 nucleotides long) for each gene were chosen from the Chopchop website online <https://chopchop.cbu.uib.no > and were synthesized by cloning-free guide RNA synthesis

(Gagnon et al., 2014). Following this protocol, 60 nucleotides long oligos containing a T7 promoter sequence, the 20 base target site without PAM and a complementary region were annealed to a constant oligonucleotide. Annealing of both the oligonucleotides was done by adding T4 DNA Ligase to the oligos, followed by incubation at 12°C for 20 minutes to make double stranded DNA. The double stranded DNA was subjected to column purification (Gel and PCR clean up kit, Macherey-Nagel) and used for RNA synthesis using Megashortscript T7 kit, Ambion. The quantity of guide RNAs was checked using Nanodrop, aliquoted and stored at -80°C.

Knockout of *apobec2a* and *apobec2b* genes

Mutants for the *apobec2a* and *apobec2b* genes were generated using the CRISPR/Cas9 genome editing technique (Varshney et al., 2015a) by a two guide-deletion strategy where two guides (one in exon1 and the other in intron 1 or both guides in different exons; 250 ng/µl each) were injected with Cas9 protein to create big deletions (Figure 11A´´, B´´). The wild-type eggs were injected at the one celled stage and raised to an F0 generation. The F0 generations were screened for mutations by genotyping individual fishes. From three different combinations of injections, I retrieved only positive founders for one of the deletions between exon1 and intron 1 in *apobec2a* (official nomenclature of this allele: ***apobec2a***^{ka98}). Similar to *apobec2a*, a deletion of part of exon1 and intron 1 of apobec2b with an additional 7 bp insertion (Figure 11B´´) was passed to next generation (official nomenclature ***apobec2b***^{ka99}). The F0 founders harboring big deletions were outcrossed with wild-type fishes and the F1 mutant generations were raised separately for *apobec2a* and *2b.* F1 generations were further screened for mutants where the mutants were identified from the heterozygous or wild-type fishes by PCR. Primers were made in the deleted part and to amplify the leftover product after deletion. The positive fishes for *apobec2a, 2b* were then in-crossed to check for any defects pertaining to loss of *apobec2a* or *2b* separately. The heterozygous fish from *apobec2b* were outcrossed with *apobec2b* heterozygous fishes to obtain double heterozygous mutants (Table 6). Further crossing schemes were set up to reach homozygosity; ***apobec2a***$^{ka98/ka98}$***; apobec2b***$^{ka99/ka99}$ (Table 7, Table 8).

2.2.4 Crossing schemes

Crossing scheme to obtain double heterozygous *(apobec2a; apobec2b+/-)* mutants

Table 6. Incrossing *apobec2a+/-* to *apobec2b+/-* gives rise to 25% *apobec2a; apobec2b+/-* (double heterozygous) mutants (green).

AaBB (*apobec2a+/-*) X AABb (*apobec2b+/-*)

	AB	AB	aB	aB
AB	AABB	AABB	aABB	aABB
Ab	AABb	AABb	aABb	aABb
AB	AABB	AABB	aABB	aABB
Ab	AABb	AABb	aABb	aABb

Wild-type

Double heterozygous

Crossing scheme to obtain double homozygous *(apobec2a; apobec2b-/-)* mutants

Table 7. Crossing of double heterozygous (*apobec2a+/-; apobec2b+/-*) gives 6.25% of *apobec2a*; *apobec2b-/-* (double homozygous) mutants (green)

AaBb (*apobec2a+/-, apobec2b+/-*) X AaBb (*apobec2a+/-; apobec2b+/-*)

	AB	Ab	aB	ab
AB	AABB	AAbB	aABB	aAbB
Ab	AABb	AAbb	aABb	aAbb
aB	AaBB	AaBb	aaBB	aabB
ab	AaBb	Aabb	aaBb	aabb

Wild-type

Double homozygous

Crossing scheme 2 to obtain double homozygous mutants

Table 8. Incrossing of *apobec2a-/-; apobec2b+/-* (homozygous for *apobec2a* and heterozygous for *apobec2b)* gives 25% of apobec2a; apobec2b-/- (double homozygous) mutants (green)

aaBb (*apobec2a-/-, apobec2b+/-*) X aaBb (*apobec2a-/-; apobec2b+/-*)

	aB	ab	aB	ab
aB	aaBB	aabB	aaBB	aabB
ab	aaBb	aabb	aaBb	aabb
aB	aaBB	aabB	aaBB	aabB
ab	aaBb	aabb	aaBb	aabb

Wild-type

Double homozygous

3 Results

3.1 Assessing guide RNA cutting efficiencies with a simple PCR based method

gRNA/Cas9 complex when injected in the zebrafish embryo causes the induction of different indels and frequently not all target sequences are mutated, resulting in a mix of wild-type and different mutant alleles. Also cutting efficiencies of gRNAs are quite variable. Therefore, to assess the cutting efficiency, we applied TIDE (Tracking Indels by sequence trace DEcomposition) to zebrafish and developed an improved method and software for it which we called PCR-F-Seq (Polymerase Chain Reaction-Fragment- Sequencing). We chose highly efficient guides available in our lab where phenotypes could be seen already in F0 generations. Guides for *rp2 gene* shows highest efficiency followed by *bbs1*, *pik3r4* and from our experience with *bbs4* being a highly inefficient guide and was used as a negative control. PCR-F-Seq takes advantage of the heterogeneity in mutant allele generation, to assess the cutting efficiency of gRNAs specifically applied to zebrafish model system. Genomic DNA flanking the target site of the gRNA is amplified from genomic DNA which was prepared from a pool of zebrafish embryos injected with specific gRNAs and Cas9 protein (Figure 7A). The resulting mixes of mutant and wild-type PCR fragments were directly Sanger sequenced without cloning into a plasmid. The derived sequencing profiles which deviate around the PAM sequences show reduced height and heterogeneity of sequencing peaks at positions downstream of it (Figure 7B, Figure S 1A-H) because sequences representing different indels are averaged. In parallel, to assess the efficacy of mutagenesis directly, we determined the number of mutant sequences among randomly picked individual subclones of the PCR fragment pools by sequencing of individual subclones (Figure 7C, Figure S 1, Figure S 2). High cutting efficacy results in a high number of mutant clones among the subcloned individual fragments and therefore the guide against *rp2* shows highest efficiency followed by *bbs1*, *pik3r4* and *bbs4* as highly inefficient guides. The sequence profiles of fragment pools derived from gRNAs with such high cutting efficiency revealed a clearly reduced sequencing signal that showed strong heterogeneity of base specific peaks at the positions downstream of the mutated region in the direction of sequencing (Figure 7B, Figure S 1).

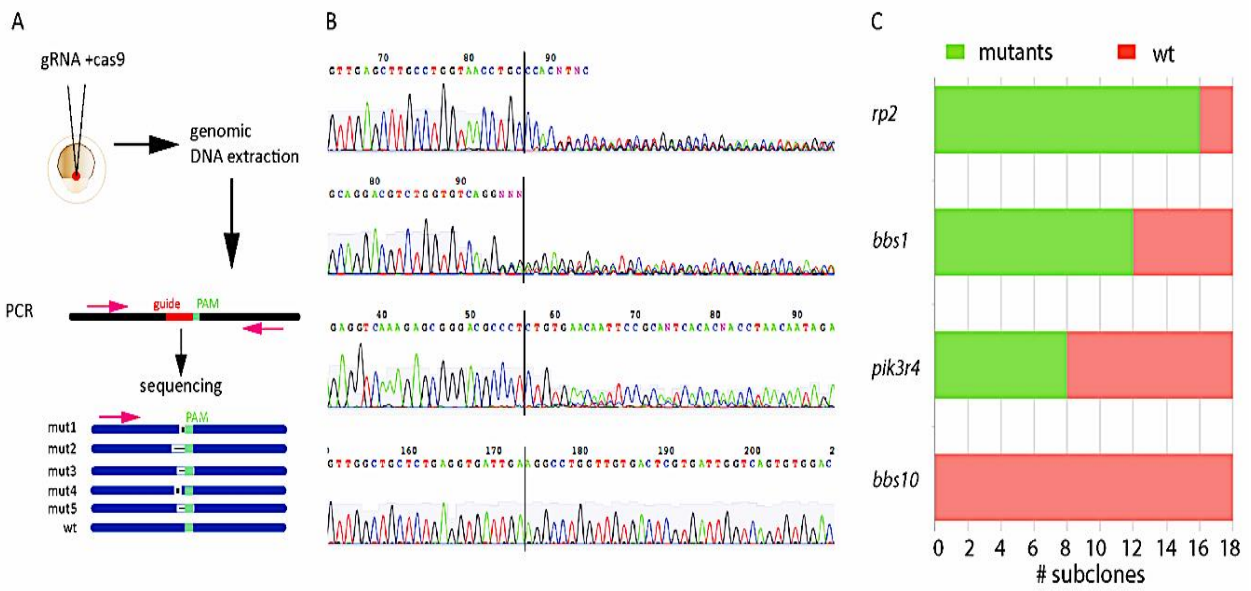

Figure 7. Sequence profiles derived from four amplified fragment pools containing CRISPR/Cas9 target sites quantify efficacy of gRNA mediated mutagenesis.

(A) Scheme illustrating steps of PCR-F-Seq: Zebrafish eggs were injected with gRNA and Cas9 protein. Genomic DNA was extracted from pools of 15 one-day old embryos, and the DNA flanking the PAM site was PCR-amplified. One of the amplification primers was used for Sanger sequencing of the PCR fragments (Figure S 2B). (B) Examples of sequencing profiles obtained from sequencing of the PCR fragment pools of four different gRNA/Cas9 injections. gRNAs directed against *rp2*, *bbs1* and *pik3r4* resulted in sequence profiles of fragment pools with strongly reduced electropherogram peaks downstream of the PAM sequence (vertical line). In contrast, the gRNA directed against *bbs10* yielded a sequence profile of the PCR fragment pools that appeared unchanged downstream of the PAM sequence. (C) Chart showing the number of mutant (green) and wild-type (red) subclones for each of the gRNAs tested in (B). PCR fragments were subcloned and a total of 18 subclones for each gRNA were sequenced. The 18 sequenced fragments comprised more than 50% mutant fragments when gRNAs directed against *rp2*, *bbs1* and *pik3r4* were injected. In contrast, and as revealed also by the sequencing profile shown in (B), injection of a gRNA against *bbs10* did not result in any mutant fragment among the 18 tested subclones.

3.1.1 Quantification of cutting efficiency

These observations suggest that the efficiency of gRNA performance may be deduced quantitatively from the degree of deviation from the wild-type sequencing profile present in the mutant profile: Downstream of the indels in direction of sequencing, we expect a certain level of randomization at individual sequence positions that should quantitatively correlate with the abundance of mutant sequence in the PCR pool. We extracted the relative maximum peak intensities within 50 nucleotides before and 50 nucleotides after the PAM sequence and calculated the median of these intensities in the two areas (Figure S 3). In this way, peaks that are perfectly randomized attain only 25% (1/4 for every nucleotide) of the maximum relative height observed when there is no deviation from the wild-type pattern. To convert these relative median heights to a cutting efficiency, we scaled the two obtained values to the

interval [0,1], such that the lowest possible relative height of 25% was set to 1 (maximum cutting efficiency) and the larger median value corresponded to 0 (no cut, wild-type sequence). We analyzed the sequencing profiles summarized in Figure S 1A-H with this method (Figure 8A). The PCR-F-Seq based quantification of the cutting efficiency of the tested gRNAs correlates well with the cutting efficiencies obtained from sequencing single subclones (Figure 8B).

We next wished to assess the sensitivity of PCR-F-Seq and tested at which ratio we could detect a single mutant sequence mixed with a wild-type sequence. With the PCR-F-Seq method, we detected as little as 6% mutant fragment in a wild-type fragment background (Figure 8C).

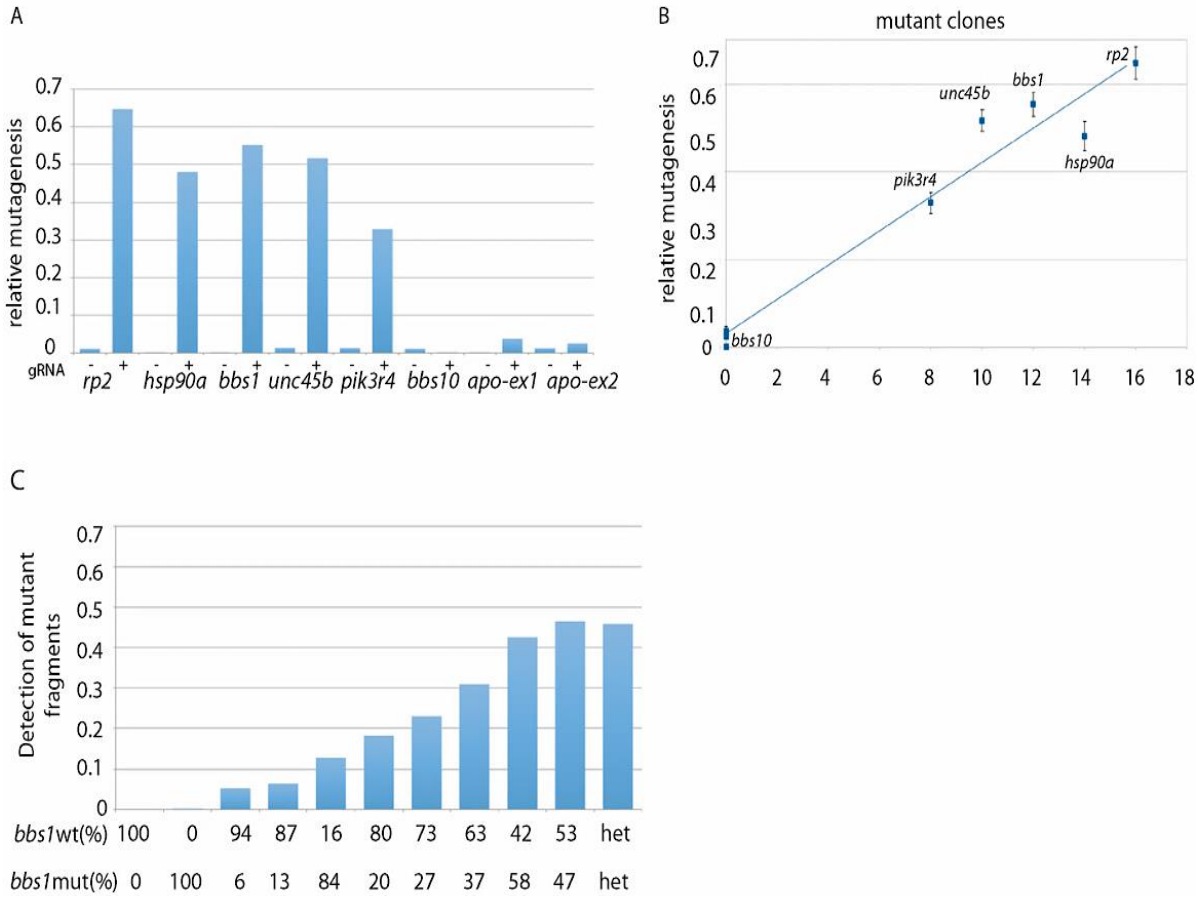

Figure 8. Quantification of mutagenesis efficiency by different gRNAs assessed with the PCR-F-Seq method.

(A) Chart showing relative cutting efficiency calculated from the sequencing profile of the PCR fragment pool derived from 15 embryos 24 hours after injection with gRNAs directed against *rp2*, *hsp90aa1.1* (indicated as *hsp90a*), *bbs1*, *unc45b, pik3r4, bbs10*, *apobec2a-exon1* (indicated as *apo-ex1*) and *apobec2a-exon2* (indicated as *apo-ex2*). +, embryos injected with the indicated gRNA/Cas9; -, uninjected sibling controls. (B) Mutagenesis efficiency calculated from sequencing profiles with the PCR-F-Seq method was plotted against the proportion of mutant PCR fragments among 18 subcloned fragments (Figure 1C, Figure S 1A-H). The regression coefficient R^2 is 0.954. (C) Wild-type fragment was mixed with a mutant fragment at variable ratios ranging from 100% wild-type to 100% *bbs1* mutant fragment and each fragment mix was Sanger sequenced. The presence of mutant sequence was calculated from the sequencing profiles using the PCR-F-Seq method. Good correlation with the increasing amount of mutant sequence in the mixes was noted. For comparison, the same fragment was amplified from a heterozygous *bbs1* zebrafish, subjected to Sanger sequencing as pool, and the resulting sequencing profile analyzed by the PCR-F-Seq algorithm. As expected for the 50% abundance of the mutant fragment in this pool, the relative detection of the fragment was 0.5. Thus, the method also allows identification of heterozygous animals. Please note that the method detects differences between the sequencing quality before and after the PAM sequence. Therefore, 100% wild-type or 100% mutant fragment both show relative mutagenesis values of 0. For more details see Figure S 4.

3.1.2 PCR-F-SEQ as a web interface

Since much higher efficiencies are required for gRNAs to be good tools for genome editing (Shin et al., 2014) (Hoshijima et al., 2016), the sensitivity of PCR-F-Seq is more than sufficient. When applying the method to genotyping of the progeny of mutant carriers, tracing of individual heterozygous carriers (Figure 8C) and distinguishing them from homozygous mutant or wild-type animals is easily achieved. To facilitate use of the PCR-F-Seq method, we designed a user-friendly, open source web interface which allows to derive cutting efficiencies of gRNAs by simply importing the sequence trace files in the SCF format (*.scf) (Figure 9, http://iai-gec-server.iai.kit.edu). The web interface automatically generates a preview image for each of the sequences to refine the location of interest (i.e. the PAM location) and subsequently allows evaluating the cutting efficiency.

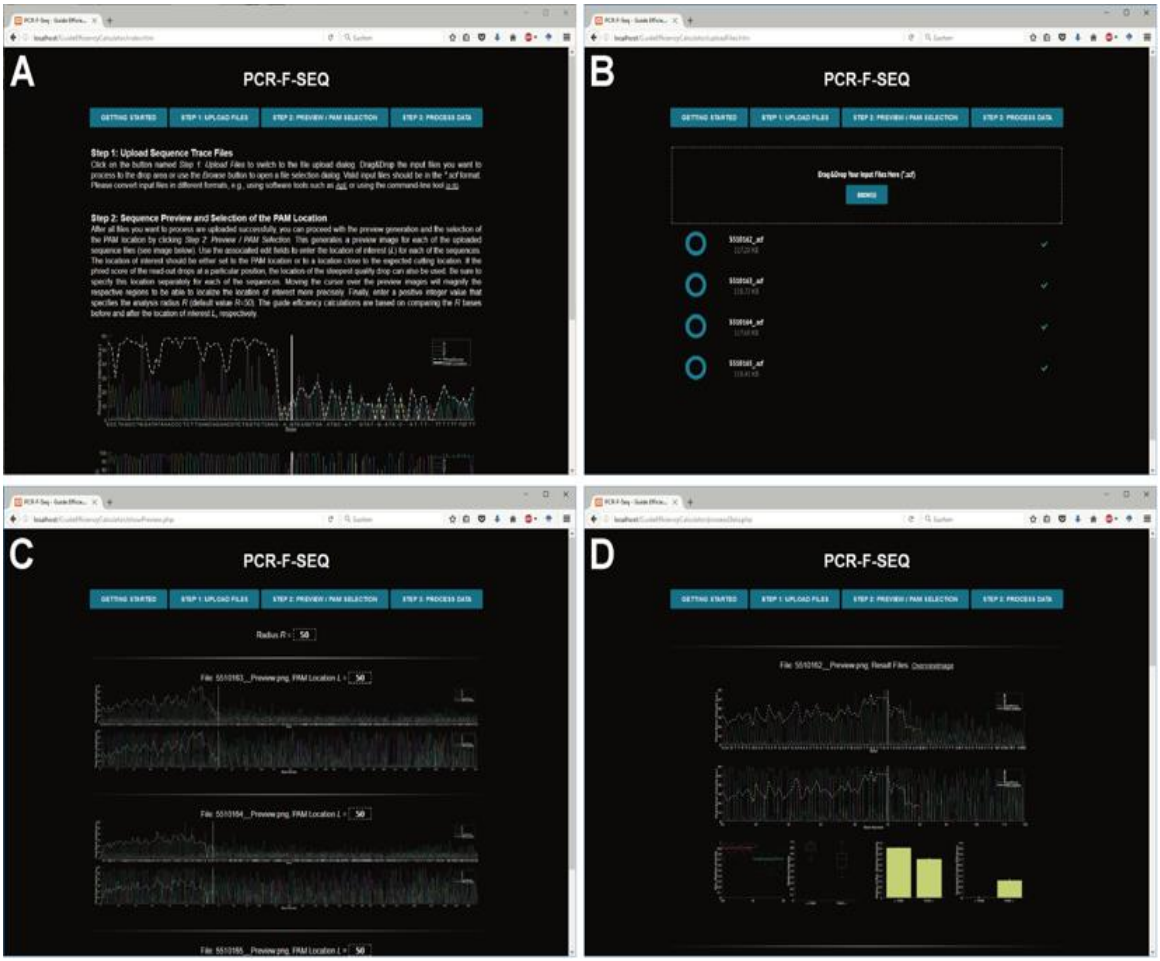

Figure 9. Web interface for applying the PCR-F-Seq method to sequence trace files provided in the SCF format (*.scf).

The interface provides a brief introduction to the usage of the tool (A) where all the steps are explained in detail. For the first step, a file upload section (B) appears where the file* containing peaks was uploaded. A preview dialog that allows to adjust the PAM location as well as the radius to use for cutting efficiency calculations (C) appears immediately after the upload is completed and finally a dialog for automated cutting efficiency estimation on a per-sequence basis (D) is produced. Results can be viewed online or downloaded for subsequent analyses.

*The original Sanger sequencing peaks in AB1 format were converted to SCF format by simply exporting the original files as SCF files using the plasmid editor, ApE. Figure courtesy: IAI, KIT.

3.2 Understanding the role of *apobec2a* and *2b* genes in muscle development

apobec2a and apobec2b genes are predominantly expressed in skeletal muscles and are important for muscle fiber integrity

The *apobec2a* and *apobec2b* genes are paralogues and share 68% amino acid identity at protein level. Therefore, both of them are predominantly expressed in skeletal muscles during embryonic development (Etard et al., 2010). The expression starts around 18 somite stage and reaches its peak at around 24 hpf (hours post fertilization). The expression of *apobec2a* and *2b* genes at 24 hpf can be clearly seen in chevron shaped somites (Figure 10A, B). Additionally, the expression of both the orthologues was also seen in the head.

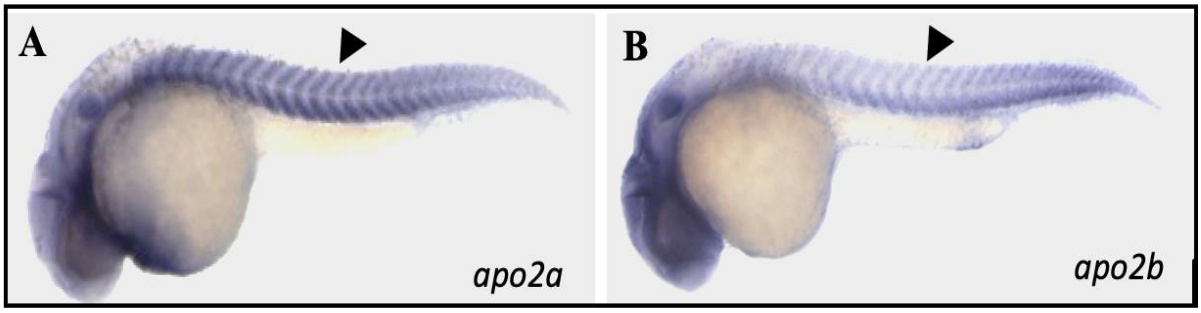

Figure 10. In situ hybridization with *apobec2a* (A) and *apobec2b* (B) anti-sense probe at 24 hpf.
The lateral view of the embryos shows mRNA expression of both genes predominantly in the skeletal muscles marked with arrowheads.

Previous studies with APOBEC2 deficient mice, show no effect on health, fertility or survival and the histological examination of muscles did not reveal any abnormalities (Mikl et al., 2005a). *apobec2* being duplicated in teleosts, the paralogs; *apobec2a* and *2b* were found in zebrafish and reported to play a structural role in maintenance of muscle integrity during contractions and morpholino mediated knockdown leads to a loss of embryonic motility due to loss of myosepta integrity, causing myofibrils to get detached (Etard et al., 2010). The structure of Apobec2 is very close to Apobec1 which shows a C to U deaminase activity. Therefore, we hypothesized that it might play an enzymatic role as well. With a view of understanding its molecular function, I created a genetic knockout model for the *apobec2a/2b* genes. To make the knockouts, I employed CRISPR/Cas9 based genome editing for which choosing the best guide RNA holds utmost importance as it impacts target DNA cleavage efficiency and off target binding. For choosing the right guide RNA we employed the TIDE (Tracking Indels by sequence trace DEcomposition) method in zebrafish.

3.2.1 *apobec2a* and *2b* knockout using CRISPR/Cas9

For creating a pure mutant model for the *apobec2a* and *2b* genes, I used a deletion strategy because deletion of a large genomic fragment was expected to totally disrupt the gene

function. Deletions were successfully performed by choosing different guide combinations: close to the start codon and the first intron, in the first intron and second exon or in the first and last exon to delete the whole gene. Other attempted deletions were not transmissible in the germline and therefore were not detected in the F1 generation. The only combination which was germline transmissible in both genes is schematically shown in Figure 11A, B. in order to check the mutational efficiency of the guide, 24 h after injection each batch was tested by the PCR-F-SEQ method. The Sanger sequencing electropherograms (A´, B´) showcase multiple peaks near the PAM sequence due to sequence polymorphisms, indicated by the dotted box, where sequencing practically stops. In *apobec2a*, a DNA fragment of 4.6 kb was snipped off consisting of partly exon1 and intron1 sequence; disrupting the splice junction. Similar to that, in *apobec2b* a deletion of 2.2 kb excising the splice junction was made. An additional insertion of 7 bp was observed, creating a frameshift. The exact mutation in both cases was further confirmed in the F1 generation by genotyping using fin clips, and exact indels were shown by multiple sequence alignment (Figure 11A´´, B´´).

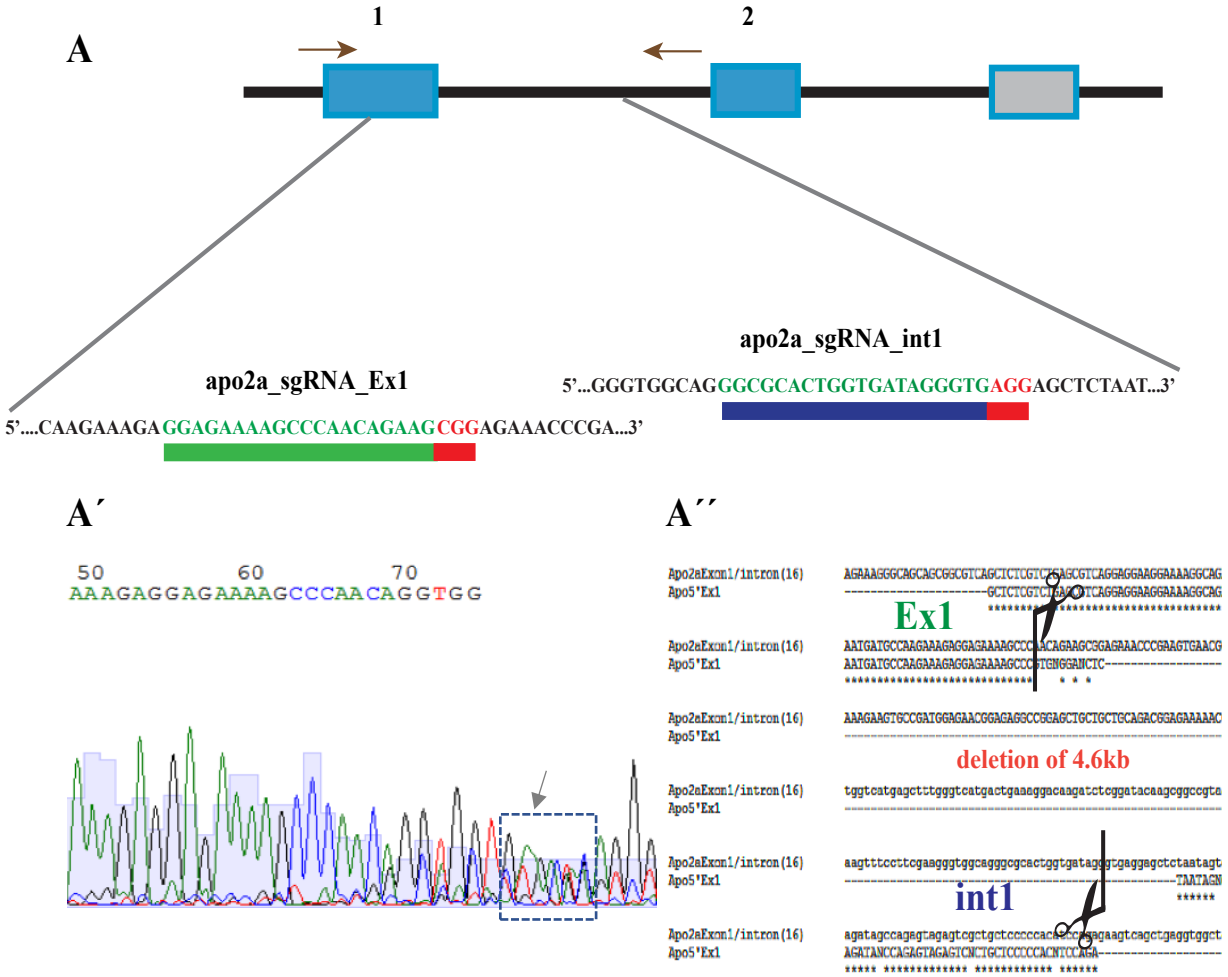

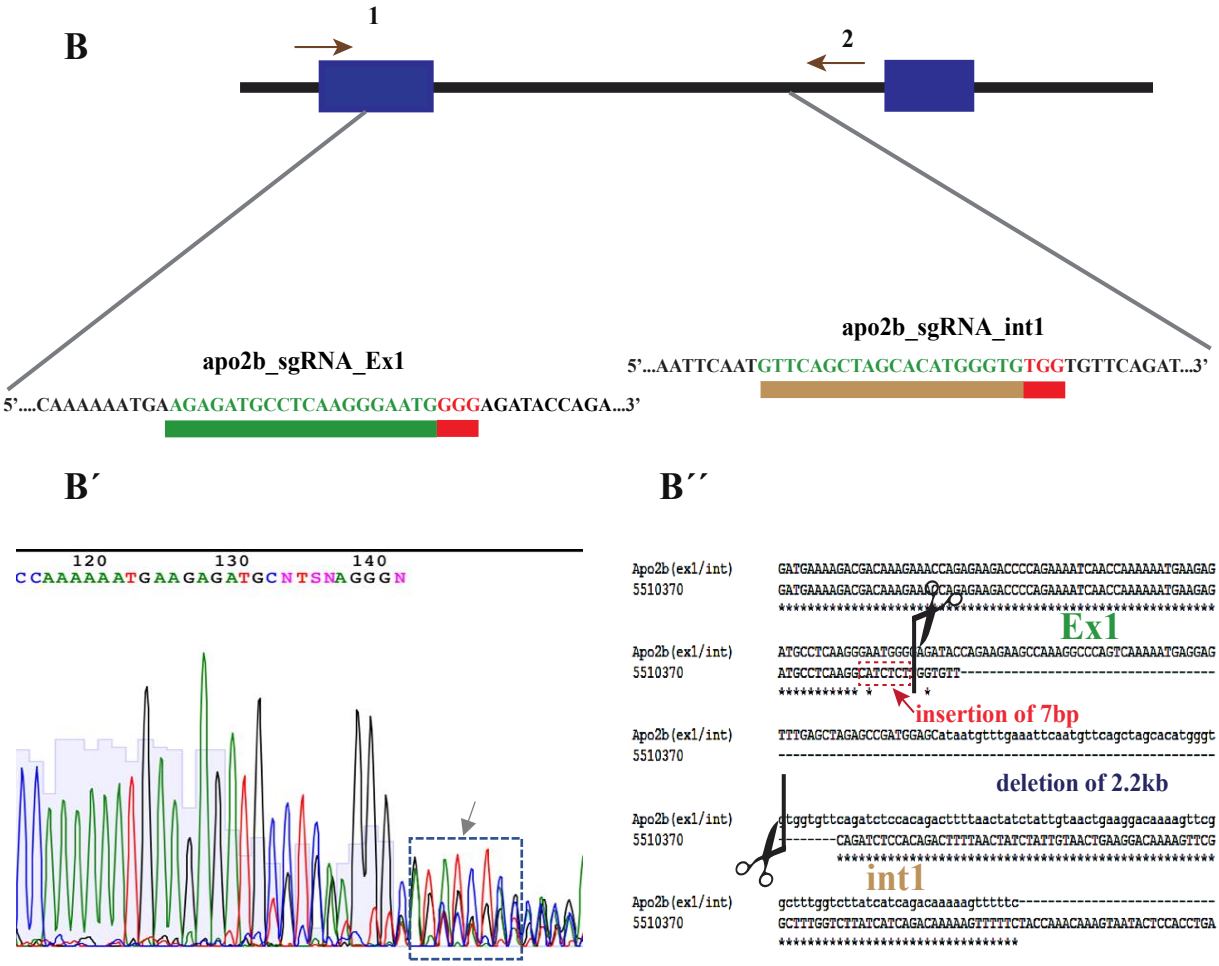

Figure 11. *apobec2a* and *apobec2b* guideRNA design and description of the mutations.
(A, B) Schematic overview of the strategy to make big deletions in the *apobec2a* and *2b* genes. The intron is marked in black and the coding exons of *apobec2a* and *2b* are labelled in light blue and dark blue respectively, the target sites are indicated by grey lines in exon1 and intron followed by the target sequences where PAM sequences are highlighted in red. The location of PCR primers (Forward and reverse) is indicated by arrows in both the cases. (A´, B´) Sanger sequencing chromatogram of PCR amplified fragment left from the injected batch (F0) showcasing indels in the form of multiple peaks near the PAM, indicated by the rectangular dotted box marked with an arrow. (A´´, B´´). Sequence alignment of the fragment amplified from F1 positive fish to that of wild-type sequence, showing a deletion of a 4.6kb fragment and a deletion of a 2.2kb fragment along with an insertion of 7 bases marked by a red dotted box, in *apobec2a* and *apobec2b* respectively.

In zebrafish, the paralogues, *apobec 2a* and *2b* both contain two exons and a cytidine deaminase domain which might have a function of mRNA editing, converting C (cytidine) to U (uridine). The *apobec2a* gene is located on chromosome 22 and encodes for a 267 amino acid long protein whereas, the *apobec2b* gene encodes for a 273 amino acid protein on chromosome 23. The cutting efficiency of guides used was about 60% and only one mutation was germline transmissible in each of them. Therefore, I used these alleles to generate stable single knockout lines (*apobec2a*^{ka98} *and apobec2b*^{ka99}*)*. The deletion causes removal of the splice junction and hence might affect mRNA splicing events. For *apobec2a*, the allele with a deletion of 4.6 kb (*apobec2a*^{ka98}) remains in-frame and is predicted to translate into a shorter

protein having 222 amino acids. Since the splice junction is deleted, another protein is also predicted which might result from retainment of the part of intron1, leading to a premature stop codon forming a very short protein of 50 amino acids.

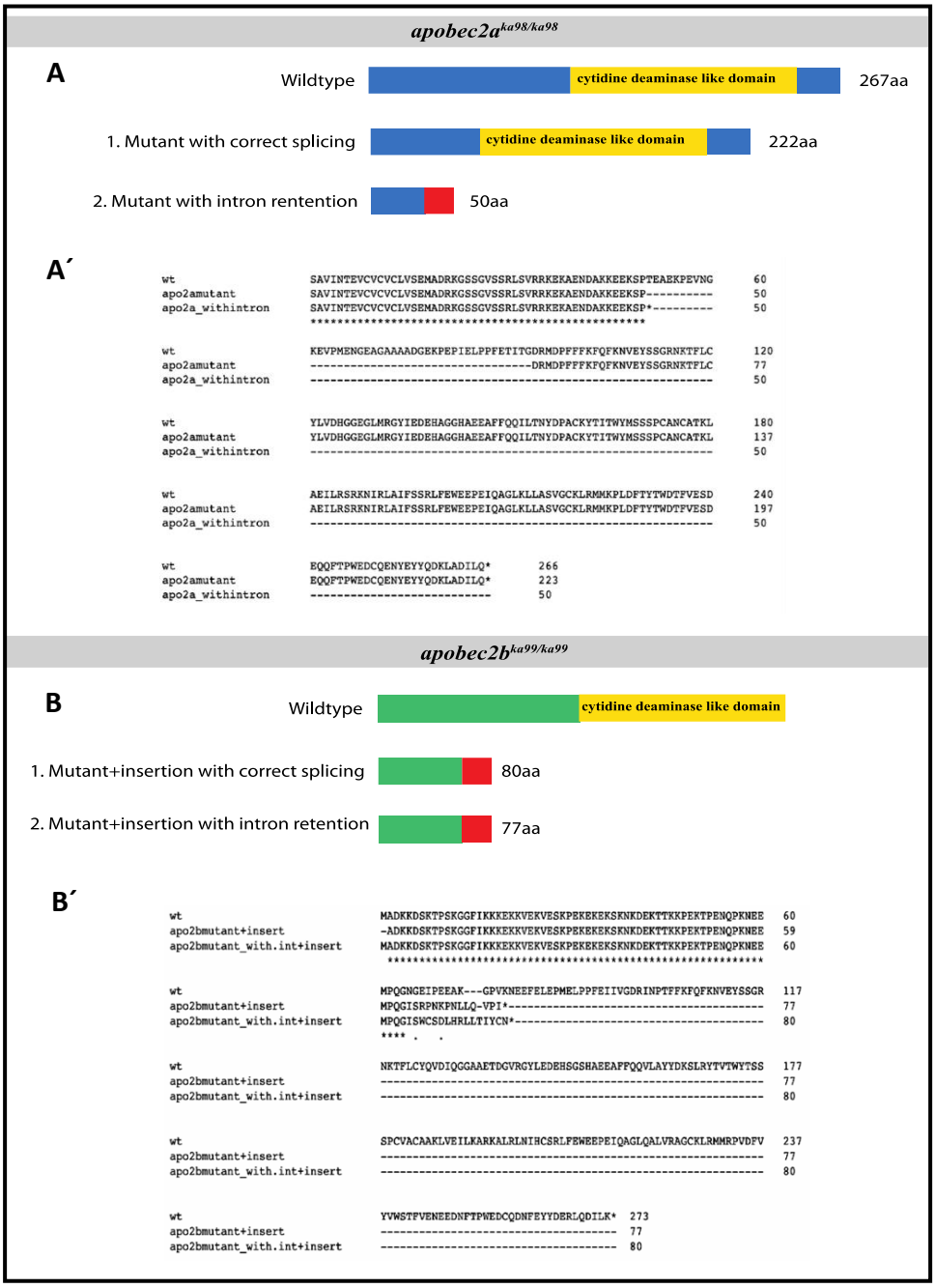

Figure 12. Prediction of Apobec2 proteins after deletion.
(A, B) Schematic drawings of the predicted sequence of Apobec2a and 2b mutant proteins. (A´) Putative sequence of the Apobec2a mutant protein with properly spliced product gives a truncated 222 amino acid protein where part of exon1 is missing whereas in the case of aberrant splicing, the intron is retained which leads to a premature stop codon giving a 50 amino acid protein lacking the cytidine deaminase like domain. (B´) Apobec2b mutant allele with a 2.2kb deletion along with a 7bp insertion which lead to a frameshift with a premature stop codon with or without correct splicing. The putative truncated proteins would lack the cytidine deaminase like domain. aa= amino acids.

3.2.2 Double homozygous mutants do not show any muscular defect

Mutants were crossed to homozygosity, *apobec2a*$^{ka98/ka98}$ and *apobec2b*$^{ka99/ka99}$. Both the individual homozygous lines were viable and fertile. There were no visible defects observed. The double homozygous mutants were then generated by incrossing, as per the scheme (Table 7, Table 8) to establish a pure double homozygous mutant generation. The maternal-zygotic double mutants were also established and henceforth called *apobec2a*$^{ka98/ka98}$*; apobec2b*$^{ka99/ka99}$ or double mutants. Unlike morphants, double mutants do not show any early phenotype as well. Neither any obvious motility defect nor any lethality was seen. The muscle integrity of *apobec2a*$^{ka98/ka98}$*; apobec2b*$^{ka99/ka99}$ mutants was maintained as shown by birefringence (Figure 13A´, B´) which is similar to the unrelated wild-type embryos of same age.

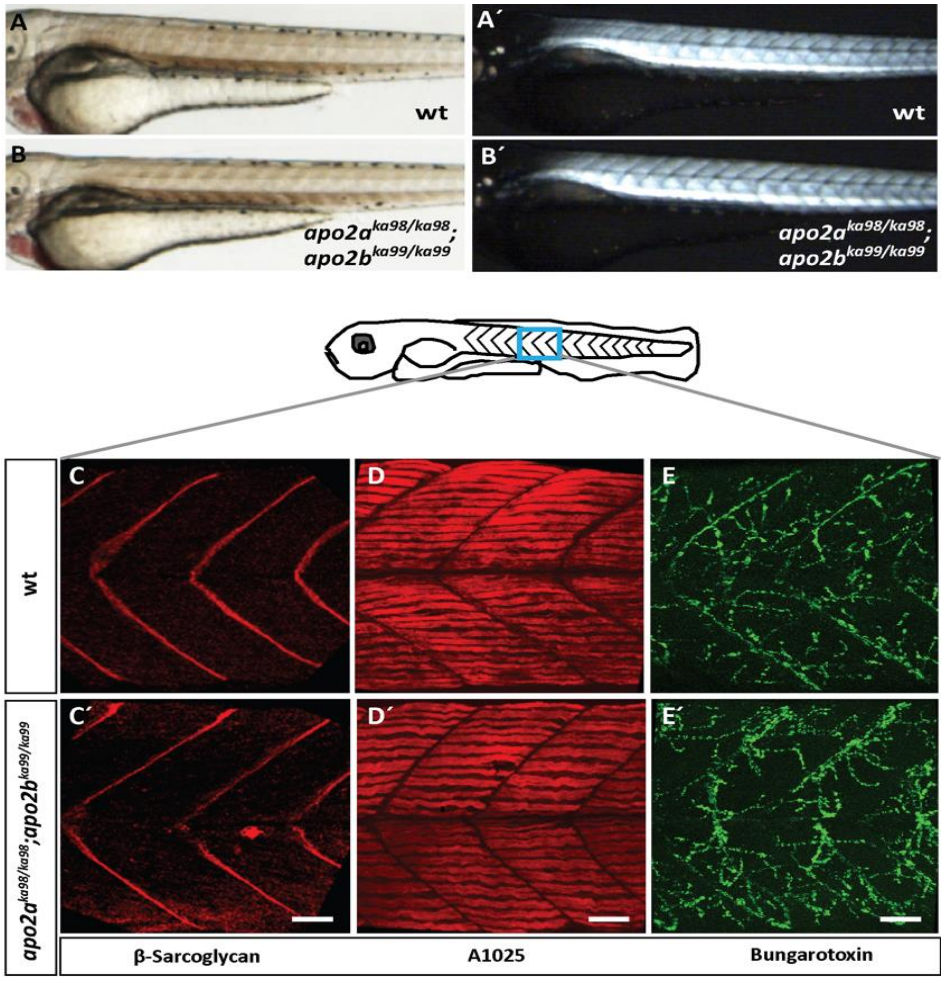

Figure 13. Double homozygous (*apobec2a*$^{ka98/ka98}$*; apobec2b*$^{ka99/ka99}$) mutants do not exhibit a muscle defect.

At 48 hpf, birefringence of mutants is similar to their wild-type siblings. Immunohistochemistry with **(C, C´)** β-sarcoglycan antibody staining sarcomere boundaries, **(D, D´)** A1025 antibody staining all muscle myosin and **(E, E´)** nAchRs at NMJ stained by α-bungarotoxin do not reveal any difference in mutants **(C´, D´, E´)** compared to wild-type **(C, D, E)** at 72 hpf. nAchRs- nicotinic acetylcholine receptors, NMJ- neuromuscular junction. Scale bars = 20 μm.

To investigate the muscle components in depth, immunohistochemistry was performed. The myofibrillar components F-actin (Figure 14A,D), all types of muscle myosin (Figure 13D, D'), and β-sarcoglycan (Figure 13C, C´) were all properly localized just like in the wild-type embryos and show no defects. Further, the characterization of neuro-muscular components like nicotinic acetylcholine receptors (nAChR) by fluorescently labeled bungarotoxin binding irreversibly to γ subunits of the receptor showed a punctate pattern similar to that of wild-type siblings (Figure 13E, E´).

3.2.3 Pax7 positive cells were not affected in the mutant

Previous in vitro experiments with single myofiber cultures of APOBEC2 knockout mice showed a significant reduction of satellite cells (Ohtsubo et al., 2017). To examine any such changes in the number or localization of Pax7 positive nuclei in our double mutants, immunohistochemistry was performed at 72 hpf. Pax7 positive nuclei were located along the transverse and horizontal myosepta (TM, HM), dorsal and ventral edge (DE and VE), and normal migration to the central portion was seen in later stages as shown in Figure 14. Immunostainings of the mutants (Figure 14B, B´) did not show any defect in number and localization of satellite cells compared to wild type.

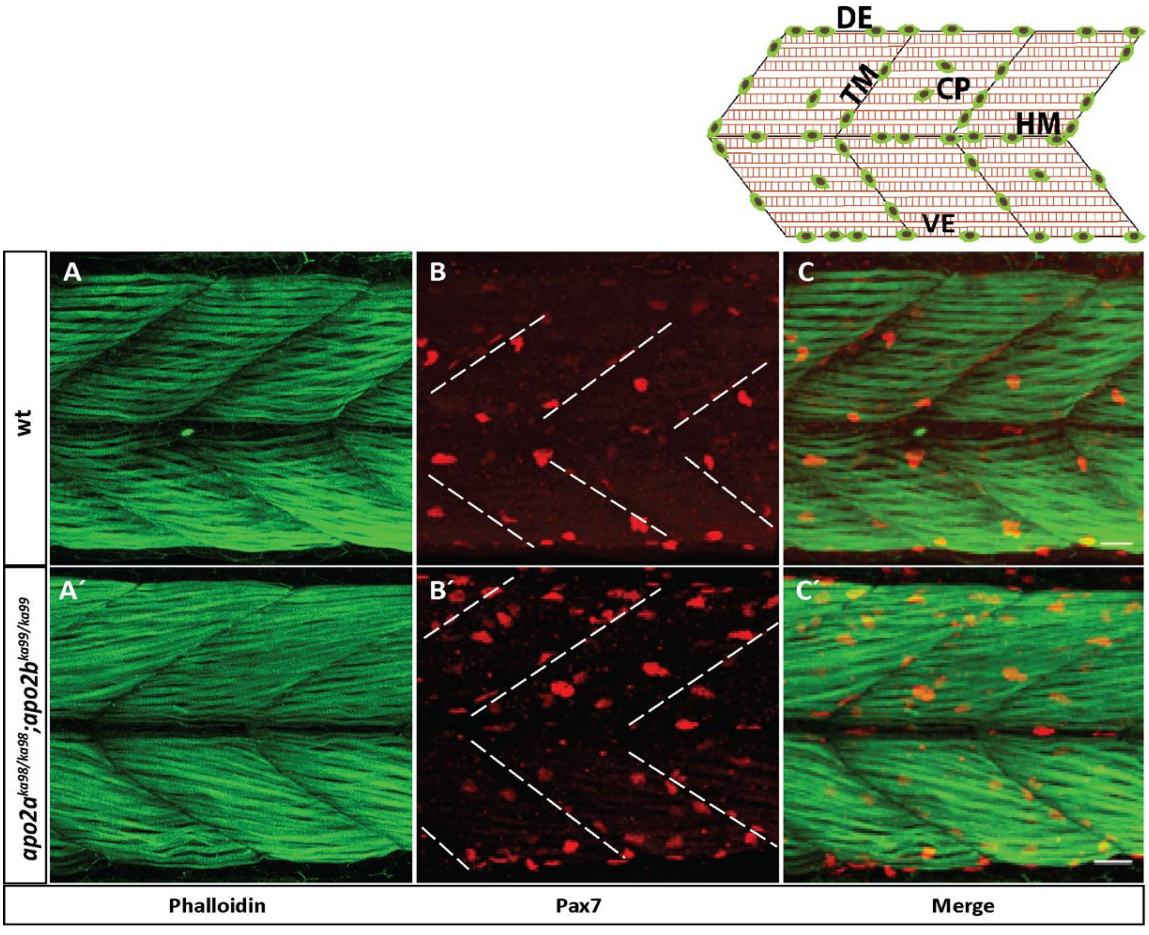

Figure 14. Satellite cells are not affected in *apobec2a*$^{ka98/ka98}$; *apobec2b*$^{ka99/ka99}$ double mutants.
Schematic representation of the location of satellite cells in zebrafish muscles is shown on top right for reference. **(A, A´)** Immunohistochemistry with phalloidin (green) marking F-actin, **(B, B´)** Pax7 staining for satellite cells located at the dermomyotome, **(C, C´)** merged images do not show any differences between unrelated wild-type **(A, B, C)** and **(A´, B´, C´)** mutants at 72 hpf. DE, VE = dorsal and ventral edge respectively; HM, TM = horizontal and transverse myosepta respectively; CP= central portion. Dermomyotome consists of DE, VE, HM, TM.

3.2.4 *apobec2a/2*b mRNA transcript is absent in *apobec2a*$^{ka98/ka98}$; *apobec2b*$^{ka99/ka99}$ mutants

The consequences of genomic sequence deletion on the mRNA transcript were analyzed using RT-PCR. mRNA was extracted from double homozygous mutants and unrelated wild-type at 24 hpf. The RT-PCR product corresponding to Exon2 of both *apobec2a* and *2b* genes was completely absent in mutants (Figure 15), suggesting early mRNA degradation of both *apobec2a* and *2b*. Several other combinations of primers were not able to amplify any product in mutant sample.

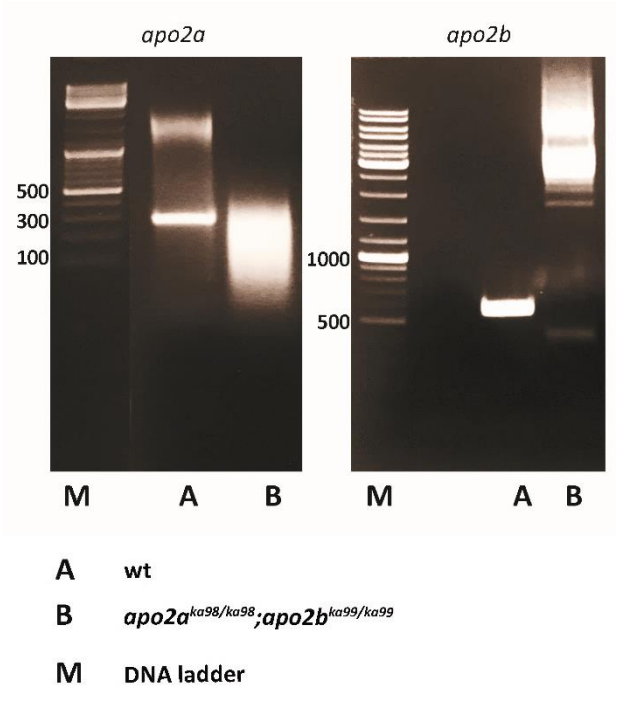

Figure 15. RT-PCR confirms mRNA degradation in mutants.
WT and mutant allele RT-PCR products resolved on 2% agarose gel. On the left panel, the *apobec2a* profile in wild-type embryos (A) shows a clear band of about 300 bp which is missing in the double homozygous mutant (B). Similarly, on the right panel, the *apobec2b* profile in wild-type embryos (A) shows a band of about 600 bp which is missing in the double homozygous mutant (B). M= marker.

3.2.5 Knockdown of *apobec2a* in *apobec2a*$^{ka98/ka98}$; *apobec2b*$^{ka99/ka99}$ mutants

Injection of the start-site morpholino against *apobec2a* (Mo[ATG]-*apobec2a*) was previously shown to impair embryonic motility (Etard et al., 2010). Since neither *apobec2a*$^{ka98/ka98}$ nor *apobec2b* $^{ka99/ka99}$ show any muscle phenotype, I injected the same morpholino as previously described into *apobec2b*$^{ka99/ka99}$ as well as double *apobec2* mutants. These injections induce a motility defect, pericardial edema as well as smaller eyes in both the lines (Figure 16).

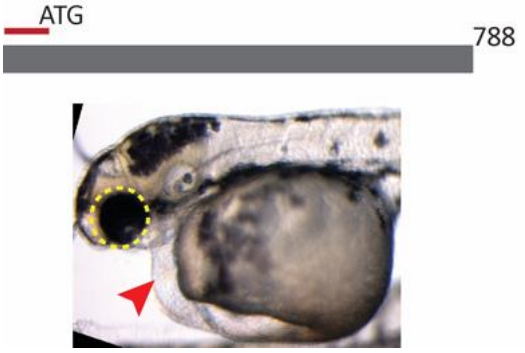

Figure 16. *apobec2a* morpholino position and injection.
The morphant exhibiting pericardial edema shown by an arrowhead and smaller eyes is shown by a dotted circle. Additionally, the morphants had a curved body axis.

3.2.6 Loss of *apobec2a* might be compensated by *apobec2b* mRNA upregulation

To check the mRNA profiles in the *apobec2a*$^{ka98/ka98}$; *apobec2b*$^{ka99/ka99}$ mutants, I performed chromogenic ISH for *apobec2a* and *2b* at 24 and 48 hpf. The expression patterns of both the genes are quite similar, primarily in the somites and the expression peaks at 24 hpf (Figure 17A-D). Surprisingly, the expression of *apobec2a* was completely lost in the mutants at 24 hpf (Figure 17A´) whereas the expression of *apobec2b* was upregulated at this stage as shown by the arrow (Figure 17B´). By 48 hpf, the expression of both *apobec2a* and *apobec2b* was completely lost in the mutants (Figure 17C´, D´). This suggests that the upregulation of *apobec2b* in the double mutants might be accounted for by genetic compensation.

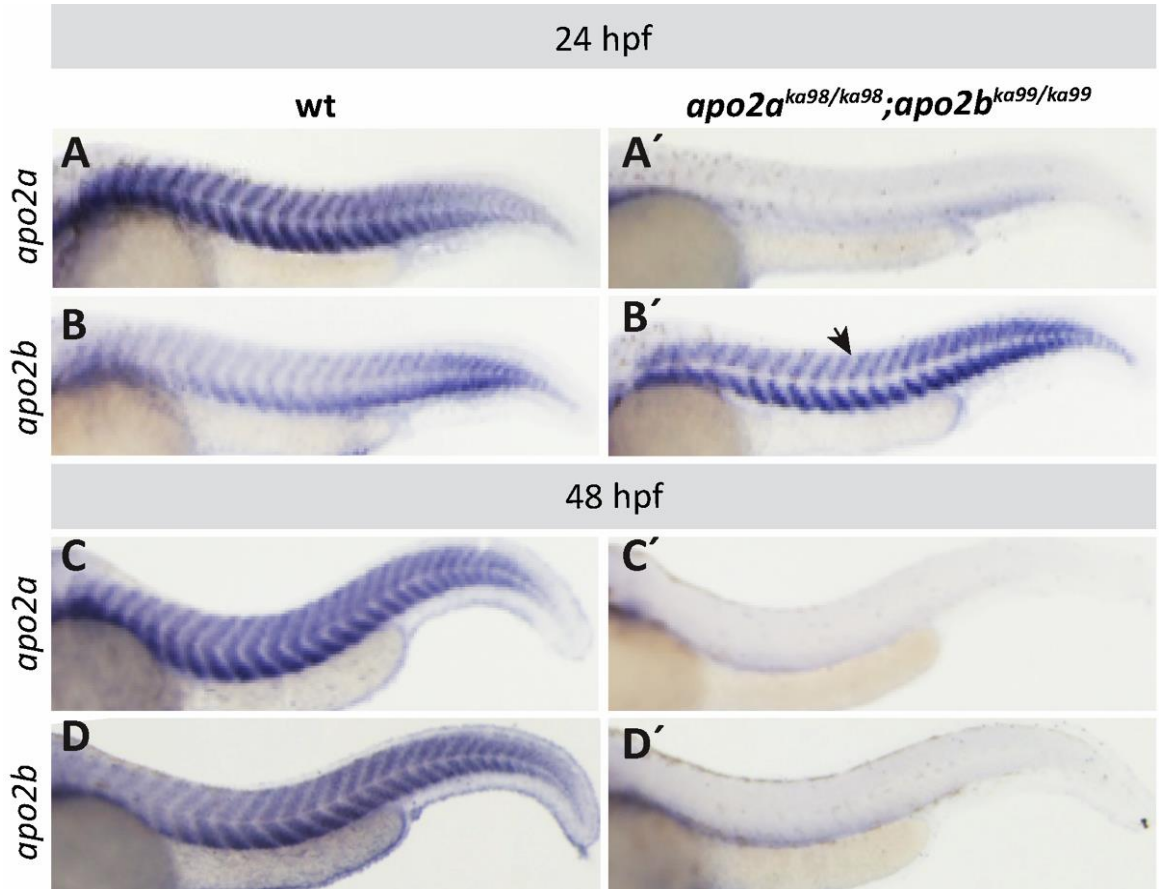

Figure 17. *apobec2b* is upregulated in double mutants at 24 hpf.
(A, A´) At 24 hpf, in situ hybridization (ISH) with *apobec2a* anti-sense probe shows a clear expression in skeletal muscles in wild-type and complete absence in mutants. (B, B´) ISH at 24 hpf with *apobec2b* anti-sense probe in wild-type also shows expression in somatic muscles but it is upregulated in mutants, shown by the arrow. At 48 hpf, (C, C´) *apobec2a* expression can still be seen in wild-type embryos but not in mutants whereas the expression of *apobec2b* (D, D´) is completely lost by this stage in mutants but not in wild-type. The orientation of embryos in the images is anterior to the left, lateral views are shown.

3.3 Forward genetic approach to study the existing mobility mutant lines

Several hundreds of the mutants were isolated in large-scale mutagenesis screens which were done at the Max Planck Institute of Developmental Biology, Tübingen in 1993 and 2004 (1st and 3rd screens respectively). These phenotypic screens were done in order to retrieve putative developmentally relevant genes. Many of the mutant lines from these screens were stored at the EZRC in the form of frozen sperm stocks and remain uncharacterized. We thus took the advantage of studying some of these uncharacterized lines and for that, we revived a few of them as mentioned in Table 4. We chose the lines which exhibit drastic muscle or mobility phenotypes with a hope to discover new developmentally critical muscle genes. The lines were revived by IVF and each of them was randomly incrossed at around 3 months, to find heterozygous couples as depicted in Figure 19. To characterize the mutant lines, I followed a series of common steps with each line. The strategy is shown in Figure 18 .

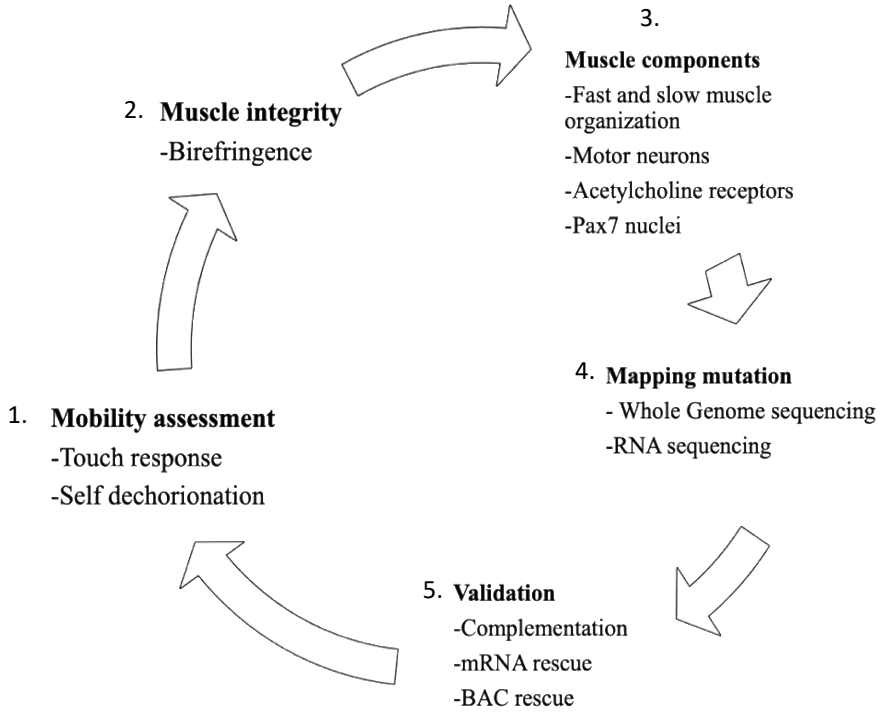

Figure 18. Strategy for systematic study of revived ENU mutant lines.
A series of steps were followed in order to discover the cause of the phenotype in each uncharacterized line. After crossing the heterozygous couples for each line, step 1. mobility assessment of the mutants was performed where ability to self dechorionate and response to touch were noted. After the identification of mutants, in step 2 birefringence was recorded to confirm if there is a muscle disruption. In step 3 a detailed study of the various muscle components was performed by immunostaining. The mutation was then mapped by whole genome or RNA sequencing (step 4). After curating the candidate gene list, the best candidate was validated in step 5 by complementation or rescue experiments.

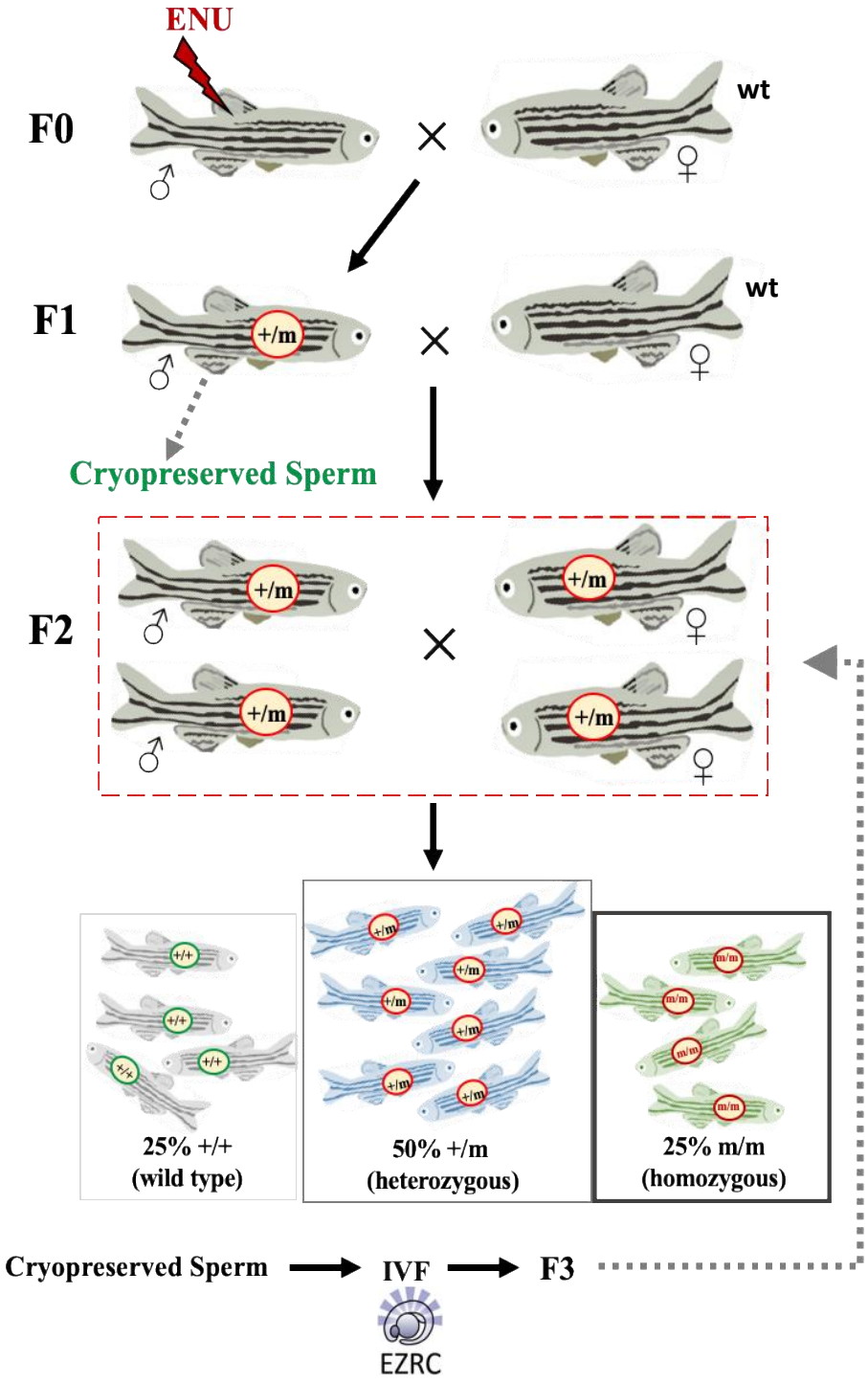

Figure 19. Overview of an ENU based-forward genetic screen.
ENU treated males were outcrossed with wild-type females and the progeny (F1) were raised and crossed to identify heterozygous couples based on the phenotype observed in the progeny. Identified heterozygous F1 males were sacrificed and the samples of cryopreserved sperm were archived. Sperm from each identified carrier was used then to generate an F2 generation through *in-vitro fertilization* (IVF), done in house at the EZRC and heterozygous carriers were then retrieved by progeny screening (25% motility defect). ENU = Ethyl nitrosourea, +/m = mutation carrier, +/+ =wild-type, m/m = mutant fish, wt =wild-type, IVF= *in vitro* fertilization.

Phenotypic groups of the revived mutant lines

After retrieval of 6 lines by IVF from the 1st Tübingen screen, I was successful in recovering mutant couples from 4 lines. The other 2 mutant lines when revived had a low fertility rate and only females survived. Whereas, from the 3rd Tübingen screen, out of 5 revived lines, I could recover positive couples from only 2. After many random crossings for other 3 lines, I couldn't see any phenotype in the progeny as described earlier. For all of the identified lines, a simple and fast motility test was carried out on the progeny. As mentioned by (Granato et al., 1996), most of the locomotion mutants are embryonically lethal. Accordingly, we found that the homozygous alleles were not viable. Motility mutants from 1996 Tübingen screens belong to three major groups: Group A no or reduced motility combined with reduced muscle striation; Group B no obvious muscle defects but reduced/ abolished embryonic locomotion, Group C no obvious muscle defects and motility abnormal (Granato et al., 1996). The mutant lines from the 3rd Tübingen screen were identified based on their satellite cells using antibody staining against Pax7, with the aim to identify new genes involved in satellite cell specification and regeneration (R. Geisler, personal communication).

3.3.1 Mutants with reduced motility combined with reduced trunk muscle striation (Group A)

duesentrieb (dus^{tq250}) and frozen (fro^{to27c}) were classified under this group. Mutants in this group were further subdivided into four distinct phenotypic groups where *fro^{to27c}* belongs to the A1 subtype (immotile mutants with no or reduced striation) and *dus^{tq250}* belongs to A2 subgroup (mutants with reduced motility, reduced striation). *fro^{to27c}* mutants are not able to hatch due to compromised motility and upon manual dechorionation, they remain curved for a few hours since straightening up is passive. The mutants are easily distinguished from the unaffected siblings due to their enlarged pericardium with blood accumulation over the yolk (Figure 20C). At 24 hpf, the mutants cannot escape on touch, they only twitch in response to external stimuli and by 72 hpf they become completely immotile. They are viable only until 4 dpf (days post fertilization) although there is no significant difference in the heart rate to that of the wild-type embryos. The *fro^{to27c}* mutants exhibit a drastic muscle phenotype as seen by birefringence images (explained in Methods) where the mutants show significantly reduced brightness compared to their unaffected siblings (Figure 20A, A´). Apart from the dystrophic muscles, the mutants also exhibit an unusual otolith number. Otoliths are crystalline deposits of calcium carbonate and proteins which are clearly visible as pairs under a dissecting microscope in each otic vesicle of zebrafish larvae (Whitfield et al., 2002). The two sensory patches that develop in the larval ear are called the maculae. Utricular and saccular macula tethers the stones with the help of arrays of sensory hair and supporting cells present on the epithelium. The ear stones help in hearing and maintaining body balance in adult fish. The unaffected siblings of *fro^{to27c}* have two otoliths in each ear (2+2) (Figure 20D) whereas the mutants exhibit three otoliths in one ear and two in the other (2+3) (Figure 20D´) or sometimes even three otoliths in both ears (3+3). Quantification of the otolith number confirmed our

findings where most of the mutants lie in the 2+3 category whereas, the siblings remain unaffected (Figure 20E).

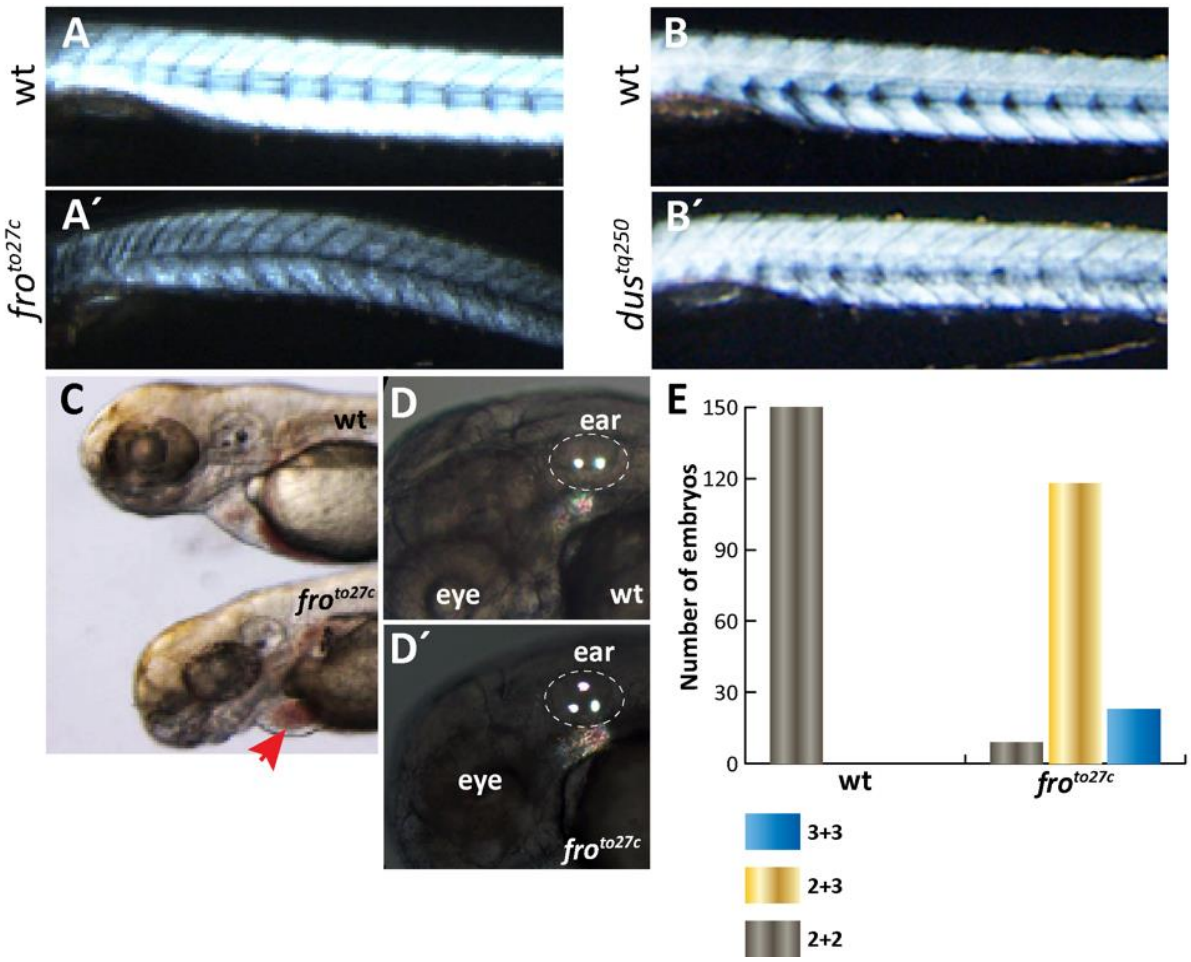

Figure 20. Muscle integrity of *fro*^{to27c} and *dus*^{tq250}.
At 48 hpf, (A, A´) birefringence of the *fro*^{to27c} mutants is considerably reduced compared to their wild type-like siblings and (B, B´) the birefringence of *dus*^{tq250} mutants is similar to their wild-type-like siblings, showcasing no obvious defect in muscle architecture, (C) *fro*^{to27c} mutants additionally exhibit an enlarged heart cavity and (D, D´) abnormal otolith number. (E) Quantification of the number of otoliths in mutants (*fro*^{to27c}) and unaffected siblings (wt). 86% of the mutants show abnormal number of otoliths from which 16% show 3 otoliths in each ear and 70% lie in 2+3 category. Only 14% outliers were seen and n=150.

To investigate the phenotype in detail, immunostaining against various muscle components was performed. *fro*^{to27c} mutants at 24 hpf show a clear loss of the Z-line indicated by patchy α-actinin staining (Figure 21B, H). At higher magnifications the difference between wild-type and mutants can be clearly noted (Figure 21B´, H´). Only few residual striated fibers were seen in the mutant embryos depicted by arrows (Figure 21J´). The fast and slow twitch fibers also remain unorganized (Figure 21D, J and E, K respectively) and only residual striations were seen in the mutant embryos as shown by the arrows in higher magnification images (Figure 21D´,

J´ and E´, K´ respectively). By 72 hpf, the muscle fibers show almost no striations and slow muscle myosin does not retain any organization (Figure 22A, A´). Titin, a giant protein connecting Z line to the M line is also completely disorganized (Figure 22B, B´).

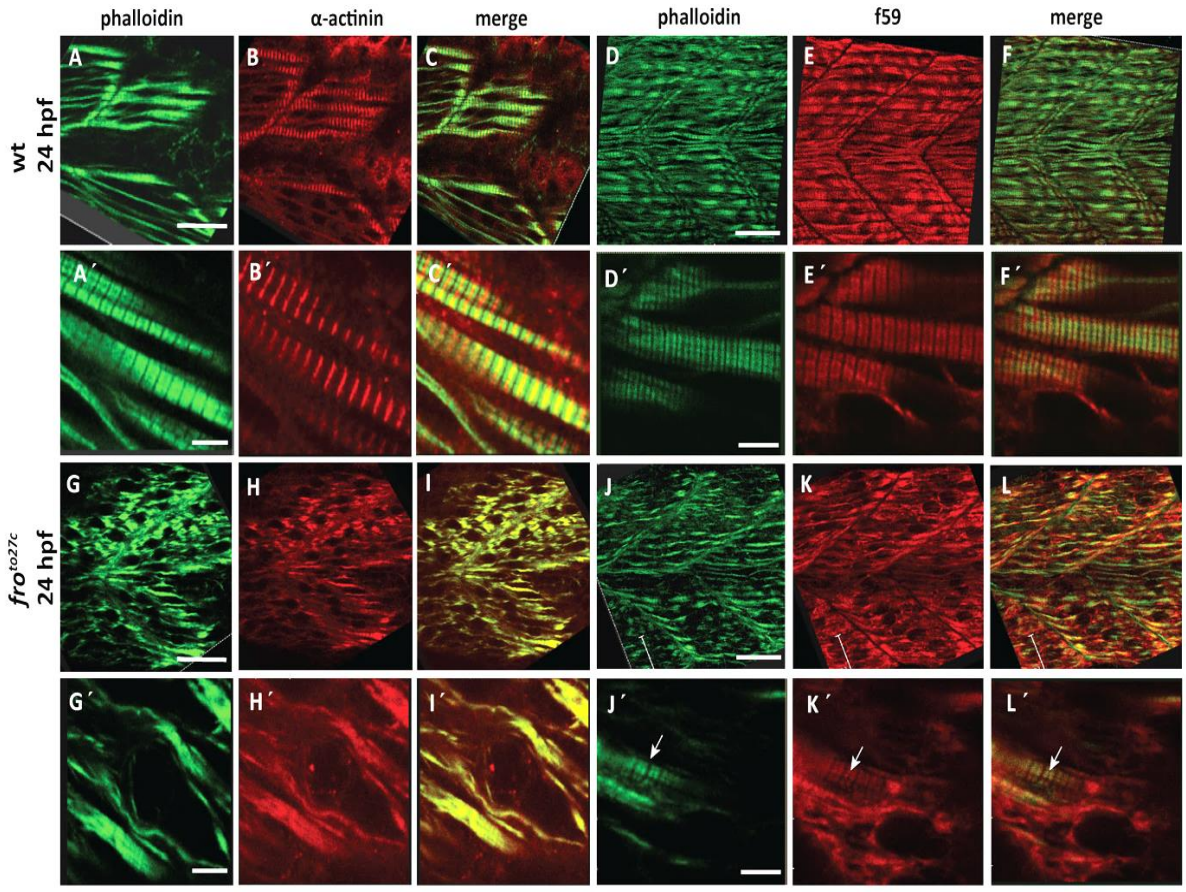

Figure 21. *fro*^{to27c} shows disorganized muscle fibers.
Immunohistochemistry of wild type and mutants with phalloidin (green) marking F-actin (fast muscle fibers), α-actinin marking z-discs (red), and merge (A-C, G-I respectively). Higher magnification images (A´- C´) of wild type siblings show a proper organization of α-actinin on Z-discs and complete disorganization in mutants (G´-I´). Actin and slow muscle myosin are properly organized in wild-type (D-F) and at higher magnifications (D´-F´). froto^{27c} shows complete disorganization of the fiber architecture (J-L) and only residual organized fibers were seen at higher magnifications (J´-L´). Scale bars A-F, G-L = 25 μm, A´-F´, G´-L = 6 μm.

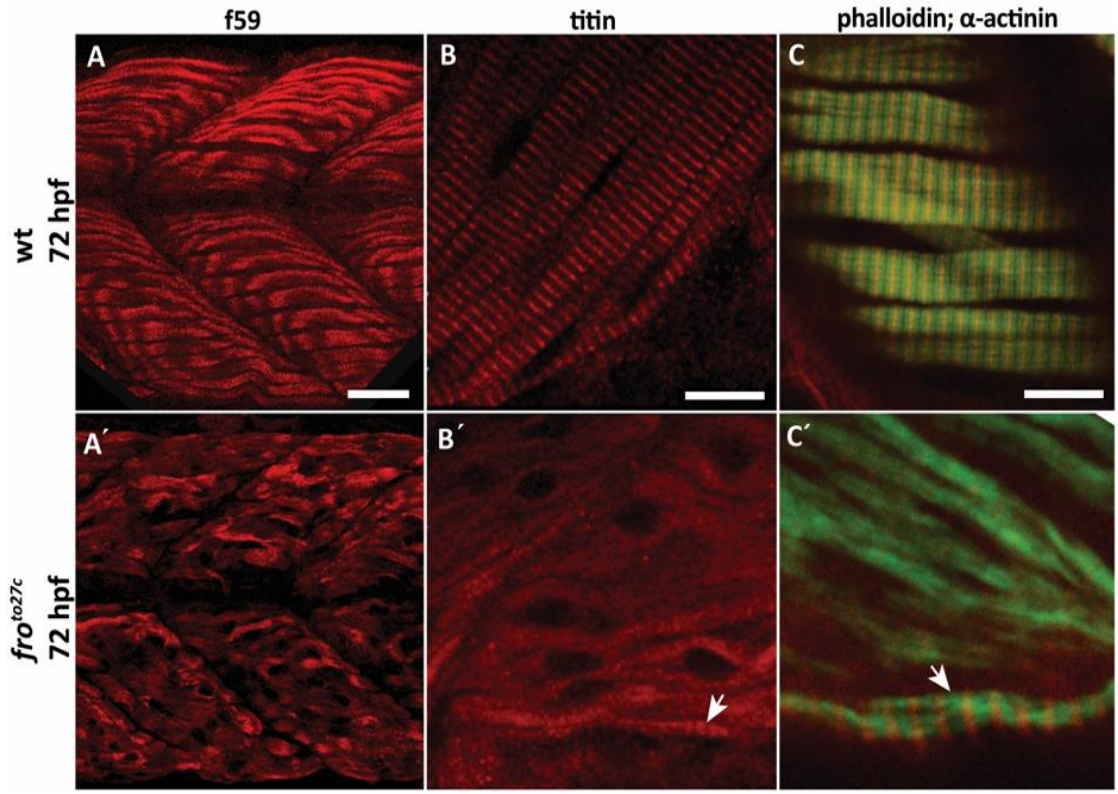

Figure 22. Complete degradation of muscle fiber structure was seen in mutants by 72 hpf. *fro*^{to27c} mutants show completely disorganized slow twitch fibers (A, A´). Titin staining also shows complete disruption of overall sarcomeric organization in mutants (B, B´), F-actin (green) and α-actinin (red) co-immunostaining show well organized actinin at Z-discs, in rare cases some structural organization in the fibres was seen as shown by the arrow (B´, C´). Scale bars A, A´ = 25 μm, B, B´, C, C´= 12 μm.

Embryos mutant for *dus*^{tq250} (duesentrieb, internal allele name *AQ50A)* can hatch from their chorion but only react with a low-speed escape response to external stimuli. The escape response worsens over time and mutants can be fully distinguished from wild-type siblings at 72 hpf. The muscle architecture seems intact as indicated by birefringence showing no obvious difference compared to the unaffected siblings (Figure 20B´, B respectively). The mutants die within a week due to the drop-in heart beat rate over time. To investigate in detail, I performed immunostaining of muscle components of the mutants at different stages of development and there were no visible differences observed organization of fast and slow muscle myosin. Since, muscles were not affected but the mobility was impaired, I investigated the motor neuron profile and the acetylcholine receptors at the NMJ. Both of the stainings shows no visible difference to those of the siblings.

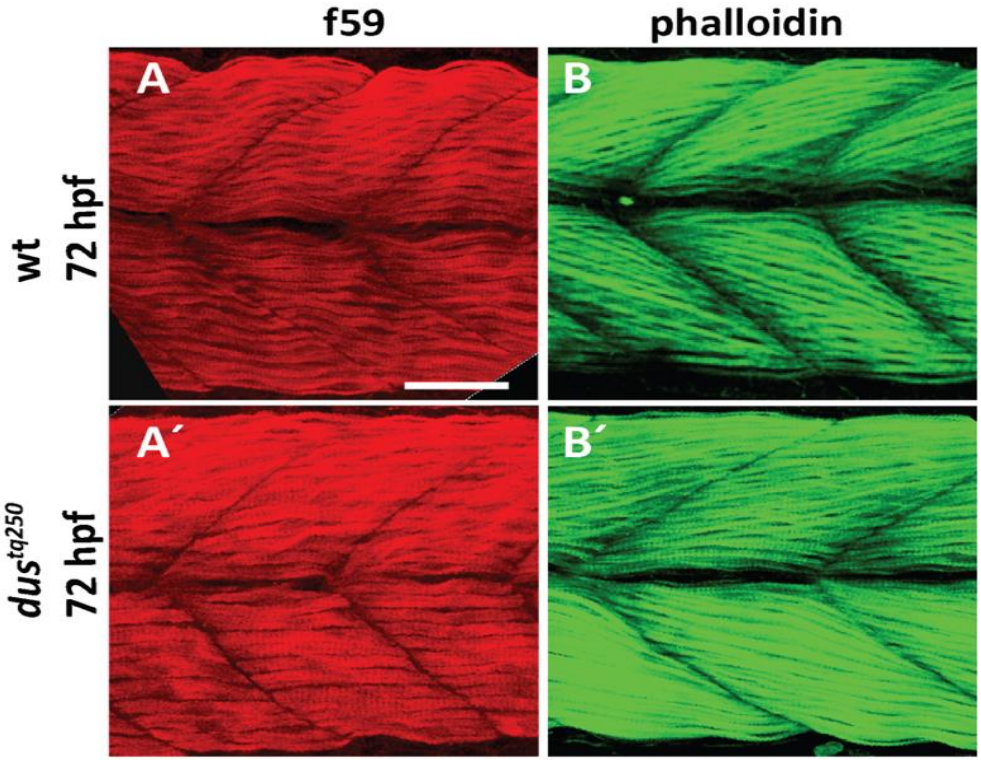

Figure 23. Immunostaining of fast and slow muscle fibers of *dus*^{tq50} mutants and wild-type siblings.
Slow twitch muscles (red) and actin filaments (green) are properly organized in the mutants.

3.3.2 Mutants with reduced embryonic locomotion (Group B)

Two of the revived mutant lines from the Tübingen I screen, *slm*^{tt208} and *tk64* were classified under this phenotypic group. *slm*^{tt208} (*slumber*, internal allele name *AT08B*) was further placed in subgroup B6 (mutants with reduced motility). The mutant *slm*^{tt208} do not dechorionate due to reduced motility and after manual dechorionation they remain curved. At 48 hpf, the mutants only twitch in response to an external stimulus whereas the wild-type escapes rapidly. The muscle architecture remains intact as shown by birefringence (Figure 24A, A´). The homozygous mutants are not viable, they die within 5 days. Investigating the muscle architecture of *slm*^{tt208} mutants in detail was done by immunostaining for different muscle components like actin and myosin filaments, as well as titin which holds myosin filaments. Additionally, bungarotoxin staining was performed to check the profile of acetylcholine receptors at neuromuscular junctions (NMJ). F-actin stained by phalloidin (Figure 24B, B´) and myosin stained by A1025 antibody (Figure 24C, C´) at 48 hpf do not show any disorganization. At 72 hpf, bungarotoxin shows punctate staining in the mutants similar to that of their unaffected siblings (Figure 24D, D´). Titin staining also shows no defects in mutants as shown by the zoomed images compared to their wild-type siblings (Figure 24E´-G´ and Figure 24E-G respectively).

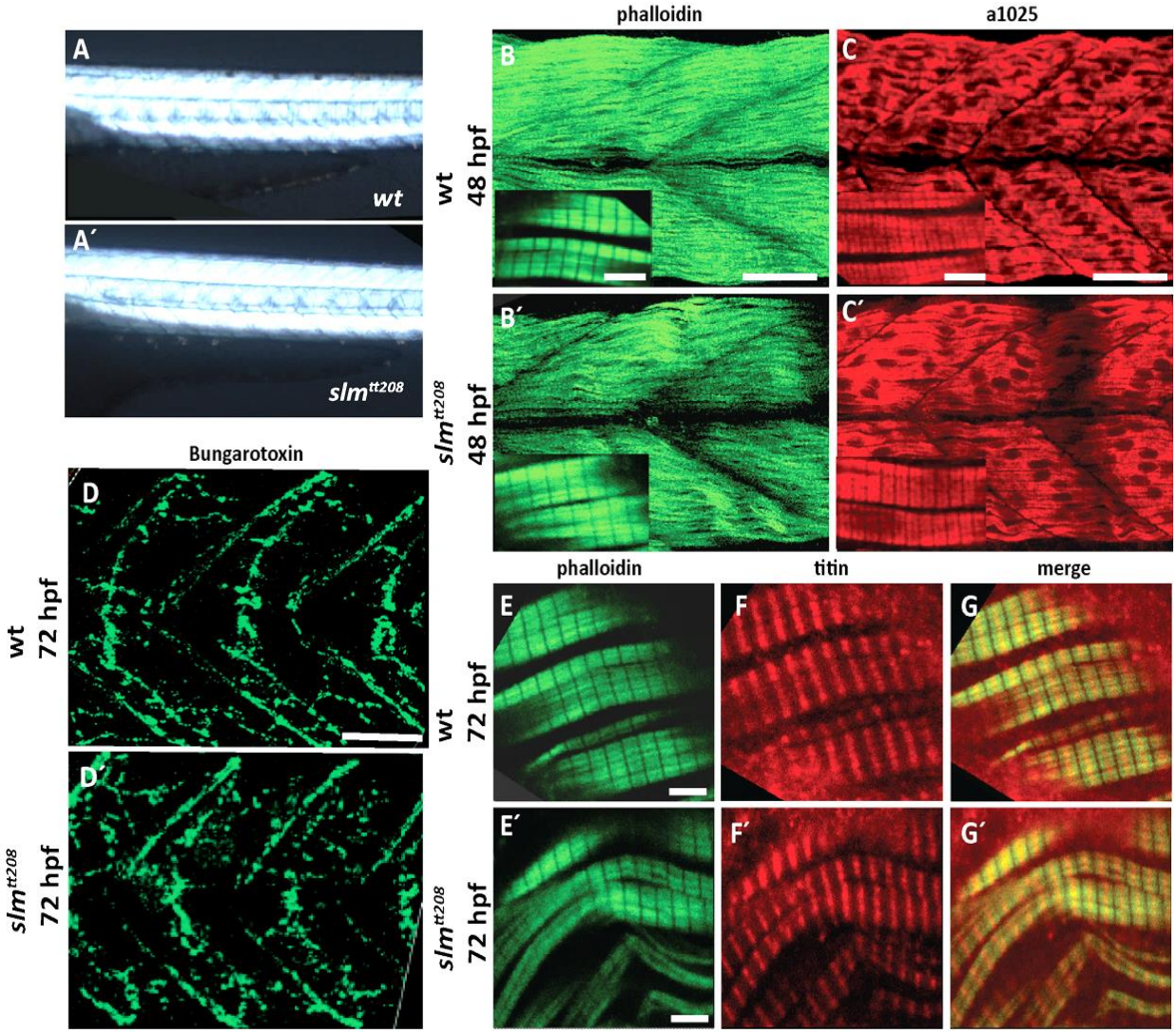

Figure 24. Phenotype of *slm*^{tt208}.
Birefringence of *slm*^{tt208} mutants (A´) is similar to wild-type siblings (A). Immunohistochemistry with phalloidin labeling F-actin (B, B´), A1025 labeling all muscle myosin (C, C´) at 48 hpf and α-bungarotoxin (D, D´) and titin (F, F´) at 72 hpf do not reveal differences between wild-type (B, D, E, F, G) and *slm*^{tt208} mutants (B´, D´, E´, F´, G´). Scale bars B, B´, C, C´, D, D´= 20 μm and E, E´, F, F´, G, G´= 6 μm.

tk64 exhibits practically very similar phenotype like that of *slm*^{tt208} mutants. The homozygous mutants remain unhatched and curved upon manual dechorionation (Figure 25C). Around 3 hours post-dechorionation, the mutants straighten up and cannot be distinguished from their wild-type siblings (Figure 25B) until assessed by touch response. The response of mutants to touch worsens over time. However, the integrity of the muscles was also conserved in these mutants as shown by birefringence (Figure 25D, E) and in-depth analysis of the skeletal muscle components showcases no obvious defects (Figure 25F-I). The myofibrillar components like F-actin, myosin, α-actinin, β-sarcoglycan were all properly localized and show no defects. Post synaptic ACh receptors were labelled using florescent-conjugated alpha-bungarotoxin. Both *Chata*^{tk64} and wild-type larvae show well developed postsynaptic receptor clusters (Figure 25J, K).

The presynaptic vesicular acetylcholine transporter responsible for transporting acetylcholine into secretory vesicles is also not affected in the mutants (Figure 25L, M).

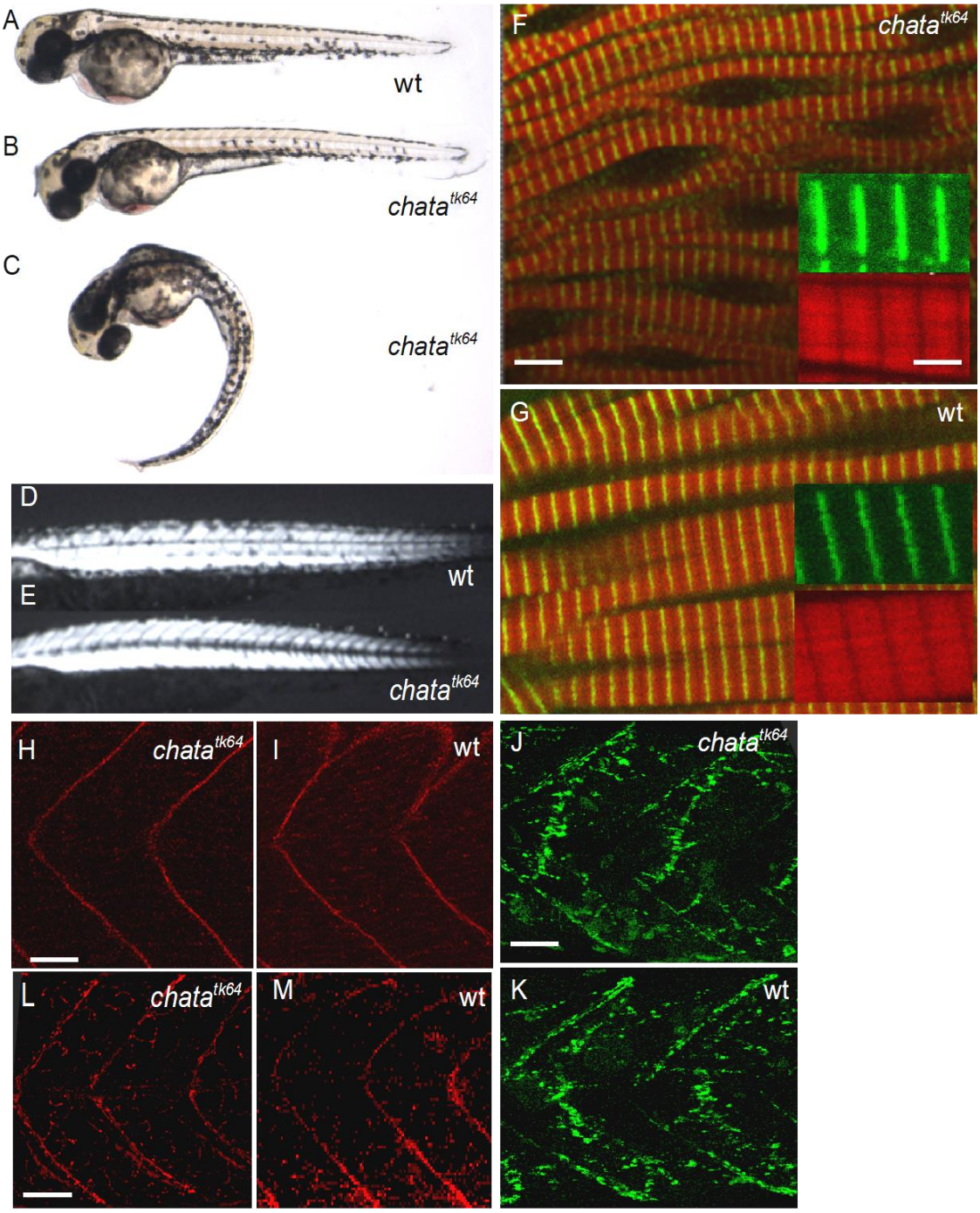

Figure 25. Phenotype of *chata*^{tk64}.
Wild-type embryo (A), *chata*^{tk64} mutant 3 hours after de-chorionation (B) and immediately after de-chorionation (C). Note that (B) is indistinguishable from (A). Birefringence is similar in wild-type (D) and *chata*^{tk64} mutant (E). Immunohistochemistry with phalloidin (red) marking F-actin, and α-actinin (green) (F, G), β-sarcoglycan (H, I), α-bungarotoxin (J, K) and VAChT (L, M) do not reveal differences between wild-type (G, I, K, M) and *chata*^{tk64} mutant (F, H, J, L) at 48 hpf. Scale bars F, G = 6 μm, insert F, G = 2 μm; H-K = 20 μm.

3.3.3 Motility mutants isolated in the Tübingen EU screen

t30064 (internal allele name *LH005QAV*) and *t31198* (internal allele name *NS078SA*) were isolated as satellite cell mutants in the Tübingen EU screen. Mutants of *t30064* line exhibit a phenotype very similar to *fro*^{to27c}, where mutants show no escape response when stimulated on touch, they only twitch. The muscle architecture is affected as clearly indicated by a decreased birefringence (Figure 26A). Along with the skeletal muscle dysfunction, the mutants also exhibit a heart phenotype as indicated by the red arrow (Figure 26B) with an enlarged pericardium and accumulation of blood over the yolk was seen around 24 hpf. The mutants also show an abnormal otolith number like *fro*^{to27c} (Figure 26C, D) and the condition worsens over time and the mutants do not survive over 72 hpf.

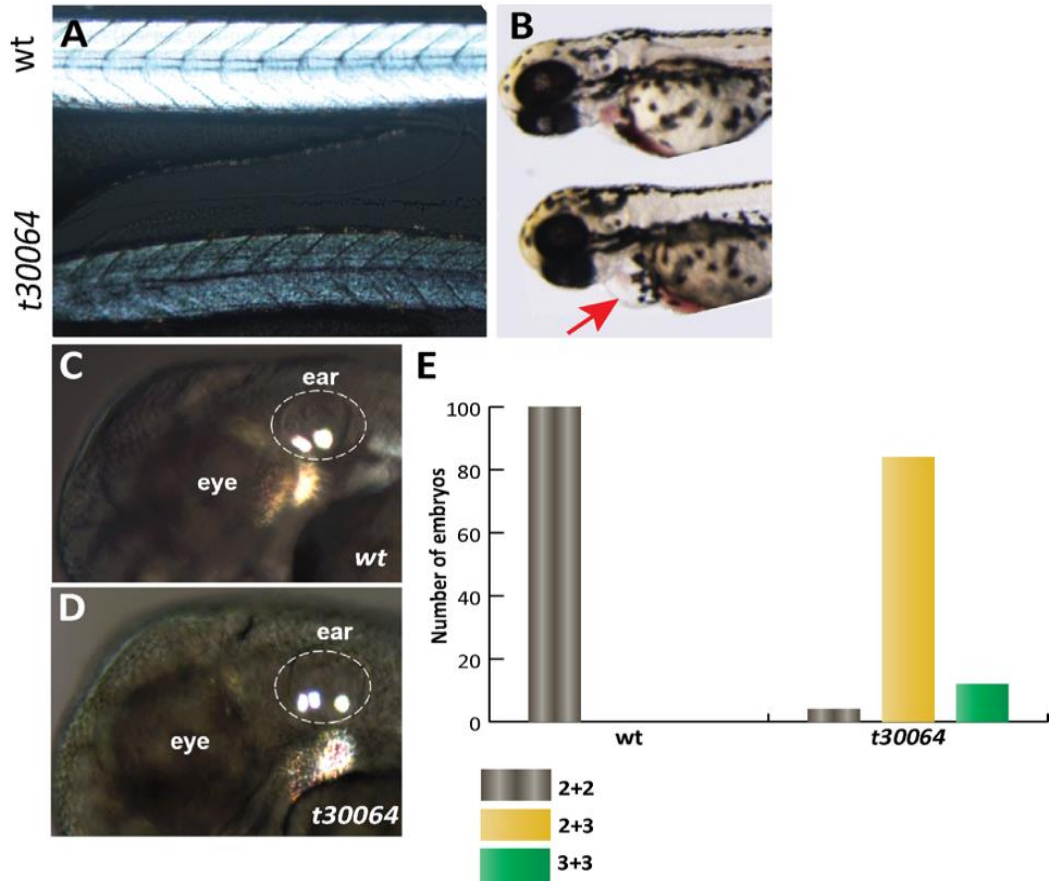

Figure 26. *t30064* mutants show multiple defects.
(A) Birefringence of mutants at 48 hpf is drastically reduced to that of their unaffected wild-type siblings. (B) Mutants show enlarged pericardium marked by red arrow and accumulation of blood over the yolk. (C, D) the number of otoliths in mutants is also affected. (E) Quantification of the possession of varied number of otoliths in mutant embryos: most of the mutants, around 85% fall in 2+3 case and a few, around 12% in 3+3 and 100% of the wild-type embryos in 2+2 case. Only 3% outliers were seen in the mutants. n=100.

Since this line shows a phenotype quite similar to *fro*^{to27c}, I had to verify that both lines carry mutation on different genes. Thus, I performed complementation test by setting up 3 independent crosses between heterozygous *fro*^{to27c} and *t30064* fishes. All three independent crosses gave wild-type like embryos, clearly indicating that the mutations of both genes complete each other and thus are two independent mutations responsible for the observed phenotype. Further detailed study of the muscle structure shows a clear absence of muscle fiber architecture in mutants (Figure 27A, A´). Immunostainings revealed disruption of both slow and fast muscle fibers, only some residual striations were present (Figure 27B, C and B´, C´ inserts). α-actinin localized on Z-discs is completely disorganized in mutants at 48 hpf (Figure 27D, D´ and E, E´ respectively), although integrity of myoseptal proteins is not affected in the mutants as shown by immunostaining with β-sarcoglycan antibody (Figure 27F, F´) at 48 hpf. Additionally, the nAchRs subunits and motor neurons do not show any obvious defects in mutants at 72 hpf (Figure 27G, H, I and G´, H´, I´).

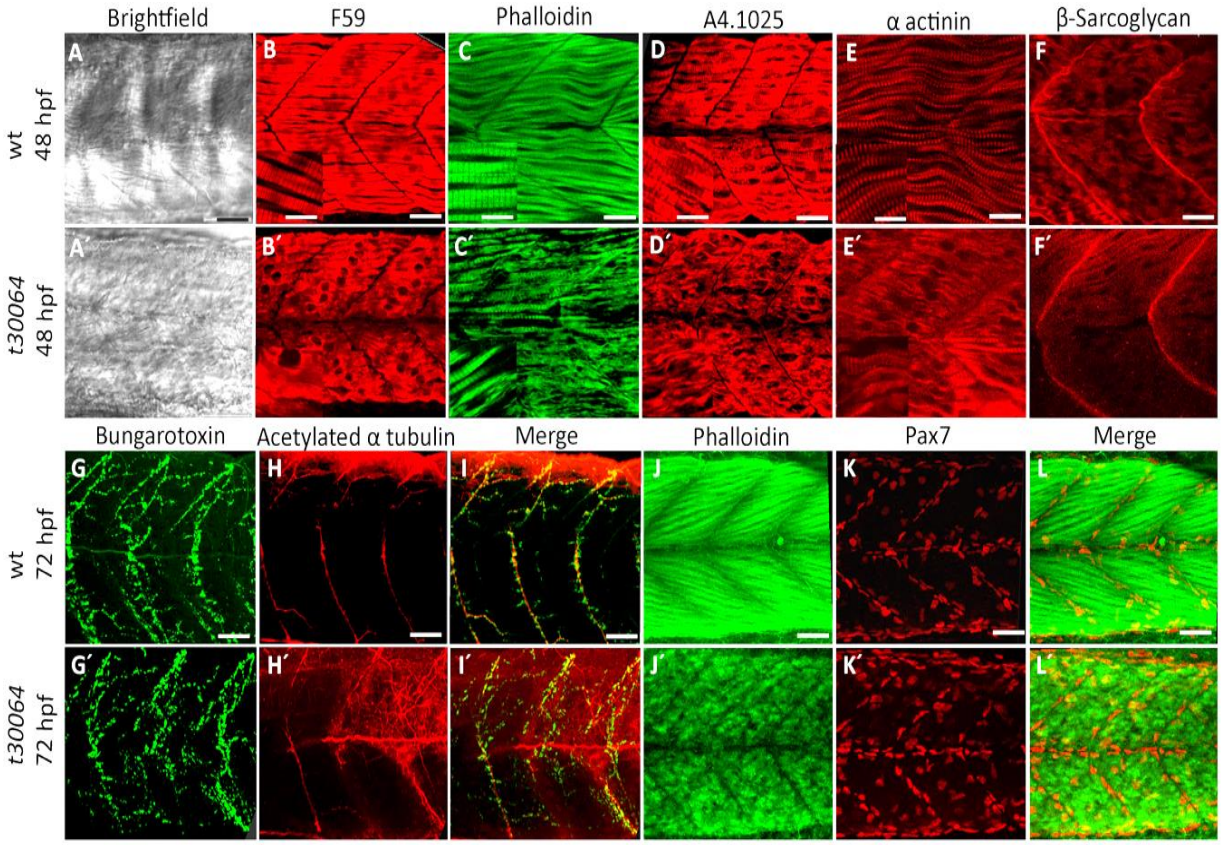

Figure 27. *t30064* exhibits massive muscle wasting.
(A, A´) Brightfield images of the mutant show absence of striated muscle fibers. At 48 hpf (B, B´) the slow muscle fibers are unorganized which can be seen in the zoomed inserts in the images, (C, C´) the fast fibers in mutants are also completely unorganized and only residual striations can be seen in the mutants, (D, D´) all muscle myosin and (E, E´) α-actinin are also completely disrupted, (F, F´) β-sarcoglycan is properly organized at the myosepta similar to their wild-type siblings. At 72 hpf, double staining for nAChR subunits and acetylated tubulin show no difference in mutants where (G, H, I) corresponds to wild-type siblings and (G´, H´, I´) to *t30064*. Double staining of F-actin (J, J´) and satellite cells (K, K´) shows a complete degradation of actin filament structure in mutants but no effect on the profile of satellite cells as seen in merged images (L, L´). Scale bars A-L, A´-L´ = 20 μm; B-E, B´-E´ insert = 6 μm.

As this line was identified as a satellite cell mutant, I investigated the number and profile of satellite cells by performing double immunostaining for F-actin and Pax7 antibody (Figure 27L, L´). At 72 hpf, mutants show almost no residual striations (Figure 27J, J´) and to our surprise the number and location of satellite cells were also not affected in mutants (Figure 27K, K´).

Mutants from *t31198* on the other hand also show an abnormal escape response which worsens over time. The overall muscle architecture was not affected in the mutants as indicated by birefringence (Figure 28A) which is similar to their wild-type siblings. At 5 dpf, *t31198* mutant embryos exhibit an uninflated swim bladder (Figure 28B) because of which the mutants stay at the bottom of the cage and die around 14 dpf.

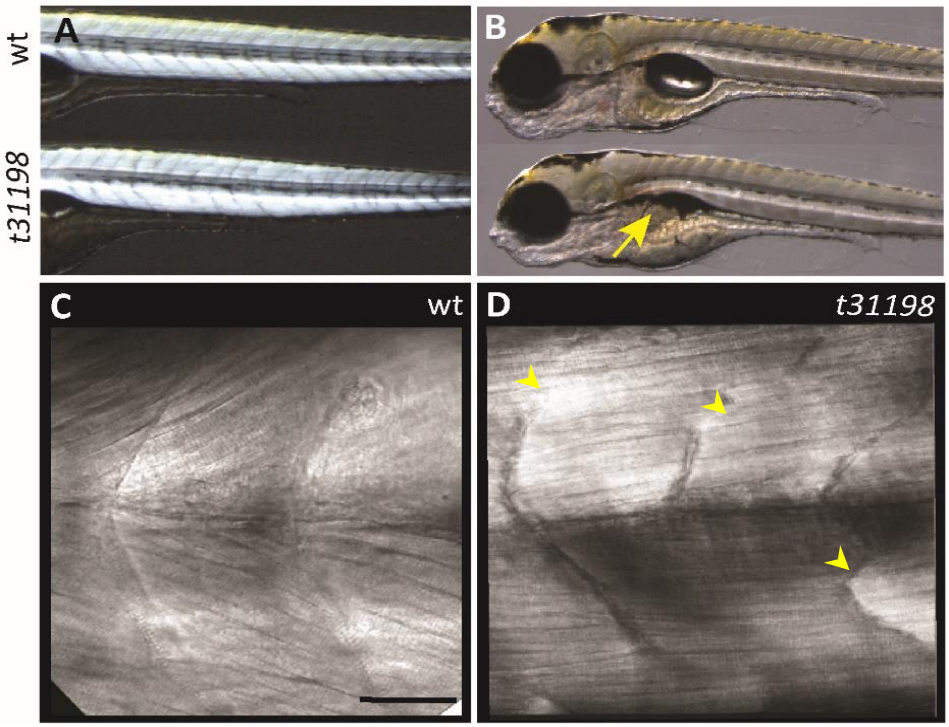

Figure 28. Phenotype of t31198 mutants.
(A) mutants do not reveal difference in birefringence to their wild-type siblings at 48 hpf. (B) At 120 hpf, mutants lack swim bladder (arrows). (C, D) Confocal brightfield image of mutants shows discontinuous horizontal myosepta (arrowhead). Scale bar C, D = 30 μm.

A detailed analysis of the muscle components revealed disrupted horizontal myosepta in mutants as shown by the arrowheads (Figure 28C, D and Figure 29A´, B´). The slow muscle (Figure 29A, A´) and fast muscle (Figure 29B, B´) fiber architecture was maintained in the mutants although the myofibrils span across the defective somite boundaries and continue until the next boundary to adhere to, as shown by arrows (Figure 29B´). Since nAchR subunits are also present at the myosepta, immunostaining showed that the receptor localization follows the pattern of broken myosepta in the mutants as shown in Figure 29C, C´. Additionally, the satellite cell localization was also affected by the broken myosepta as the satellite cells were also aligned to the broken myosepta as shown by dotted lines (Figure 29D,

D′) pointing at the horizontal myosepta being a cue for the organization of other myoseptal proteins. At 72 hpf, the choline receptor subunits are completely unorganized (Figure 29E, E′) and myoseptal proteins like β- sarcoglycan belonging to the DGC complex also mislocalized (Figure 29F, F′).To check the integrity of muscle fibers, evans blue dye was injected in the pericardinal vein at 48 hpf. The dye doesn't leak out suggesting intact fiber structure however, we found that the mutants also exhibit defects in intersegmental vessel (SE) patterning (Figure 30). The regularly spaced arrangement of SE was affected both in trunk and tail regions of the mutants.

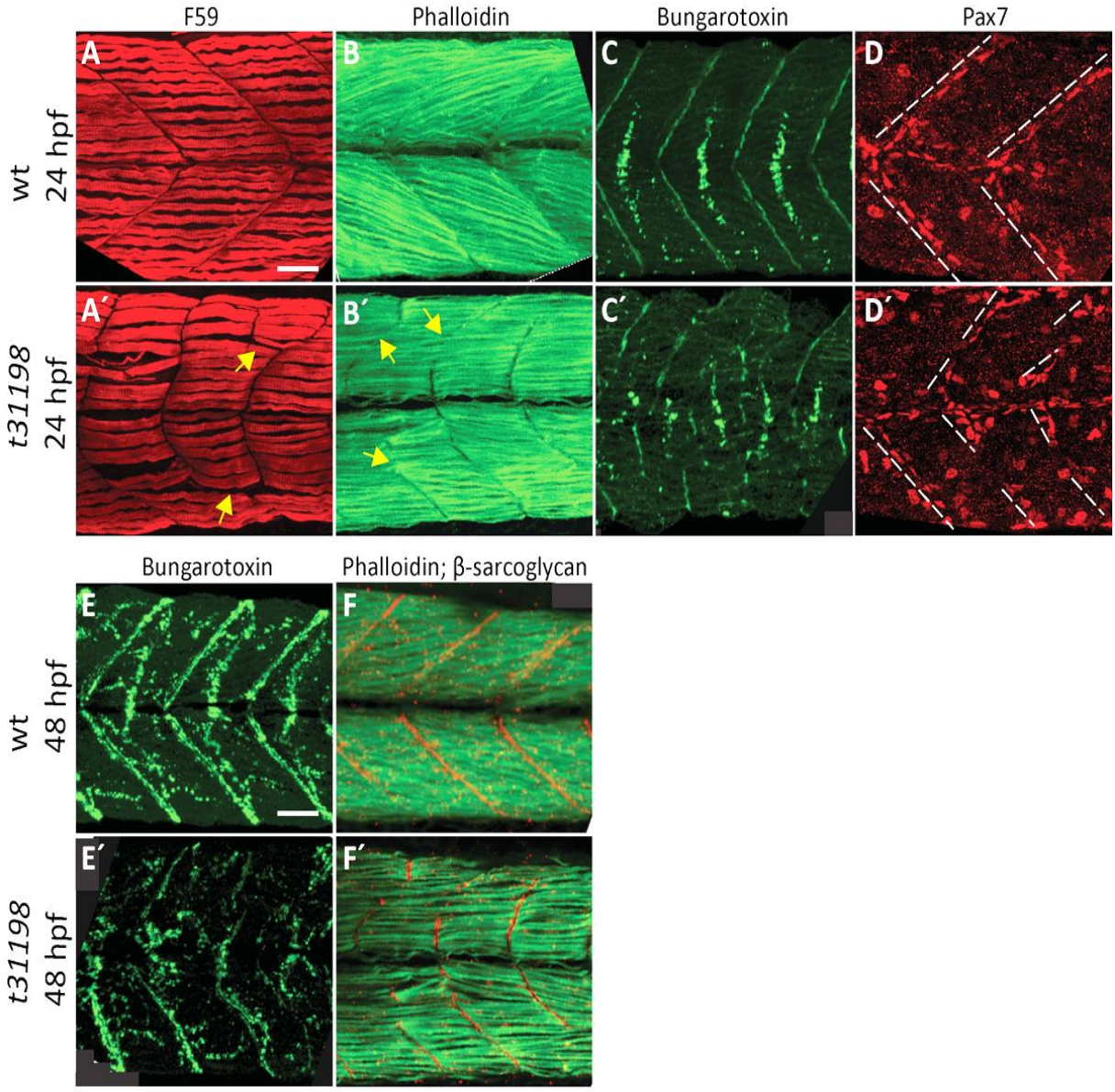

Figure 29. Immunostaining of t31198 mutants show fibers spanning across disrupted myosepta. At24 hpf, (A, A′) slow twitch fiber integrity is maintained and both slow and fast-twitch fibers span over the broken myosepta in mutants (arrows) (B, B′) fast muscle fibers also maintain their structural organization (D, D′) anti-Pax7 staining for satellite cells reveals clear differences between wild-type and mutants at 24 hpf. The satellite cells also follow the broken myospeta. At 48 hpf, (E, E′) α-bungarotoxin clearly also aligns to the broken myosepta in the mutants Additionally, (F, F′) double staining for F-actin (green) and β-sarcoglycan (red) also obey the same trend. Scale bar = 20 μm.

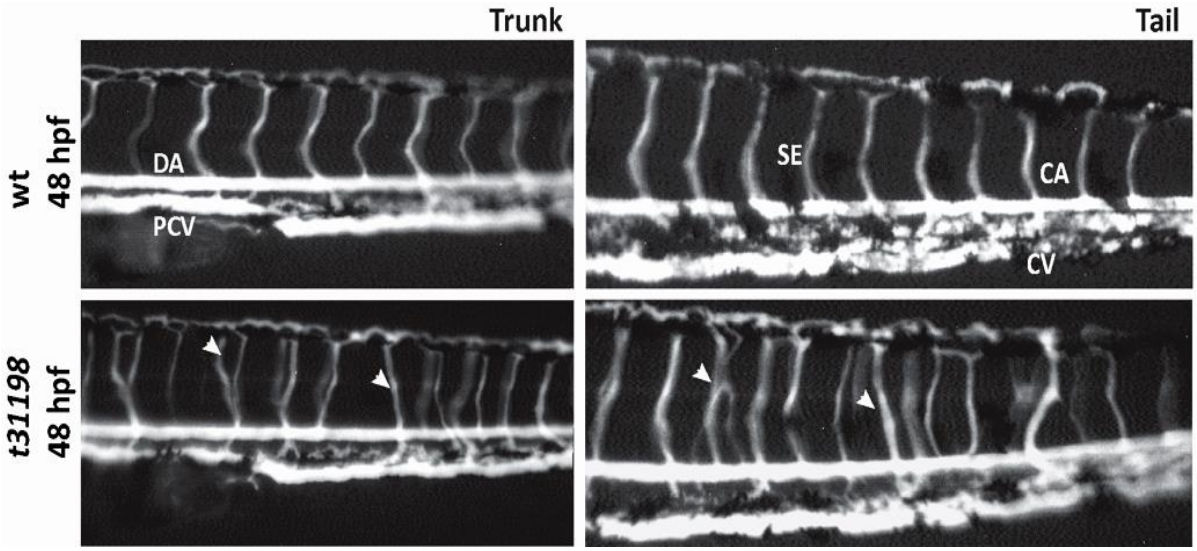

Figure 30. Vessel patterning was affected in t31198 mutants at 48 hpf.
Injection of 0.1% Evans blue dye in the pericardinal vein was injected in mutants and wild-type siblings. An overall patterning defect was seen in mutants as shown by arrows in the intersegmental vessels of trunk and tail regions. (DA) Dorsal artery and (PCV) pericardinal vein; (CA) caudal artery, (CV) caudal vein, (SE) intersegmental vessels.

3.4 Next generation sequencing for mutation mapping

To map the mutation in all the revived lines, whole genome DNA sequencing (WGS) was performed at our in-house sequencing platform with a HiSeq 1500 machine (Illumina) in a paired end and multiplexed fashion. For WGS, the genomic DNA was extracted from mutants and wild-type siblings of each line except *t31198*, where a new strategy of mapping mutation with mutants only was demonstrated by my colleague Sanamjeet Virdi who also performed the bioinformatic analysis for all mutations (for more detailed information on this please see Virdi, 2019). After sequencing, a quality check was performed, followed by aligning the reads to the zebrafish reference genome across all 25 chromosomes. Post alignment, homozygosity mapping was performed by *Zyg-score* (in-house script). The chromosome showcasing maximum homozygosity was identified (homozygosity curves for each mutant line can be seen in (Figure S 5, Figure S 6, Figure S 7; marked by the dotted box). Homozygous variants not found in the wild-type (SNPs, single nucleotide polymorphisms) were scanned in this area and were analyzed for their effect by Variant Effect Predictor software which ranks variants as high, modifier and low impact variant depending on its effect on protein. All the mutant lines were mapped successfully and annotated with the curated gene that is the best candidate for each mutation (Table 9).

Table 9. Mapped locus for each mutant line, the exact mutation and the best candidate gene linked to the phenotype (from Virdi, 2019).

Mutant	Chromosomal location	Mutation	Gene
frozen	**10**:44,410,930	A to G	*myosin-XVIIIb*
duesentrieb	**9**:43,246,289	T to G	*titin, tandem duplicate 1*
slumber	**18**:35,663,390	C to A	*ryanodine receptor 1b (skeletal)*
tk64	**13**:29,288,858	A to T	*choline acetyl transferase a*
t30064	**1**	Δ260 kb	*dual specificity phosphatase 27*
t31198	**21**:4,631,175	G to T	*notch1a*

3.5 Validation of the candidate genes

3.5.1 Mutants classified under group A

In *fro*^{to27c}, a splice site variant on LOC100333206 encoding for an unconventional myosin-18b like mRNA was identified as the best candidate as other members of this family, *myo18aa* and *myo18ab* having already been studied for their role in muscle fiber integrity. This gene was found in the critical region in previous zebrafish genome assemblies, even though it was unannotated in the current one. Parallel to our investigation, Gurung et al. identified the mutation by synteny analysis (Gurung et al., 2017). They reported an A to G mutation at a splice acceptor site causing a 26 bp truncation of exon32 of this gene. We also found a splice acceptor mutation, T to C which is most likely the same mutation. Validation of this candidate gene was not possible by mRNA rescue due to cloning bottlenecks as this gene is very huge (6303 bp). A third mutant line, *schläfrig (sig)* from an independent ENU screen (Berger et al., 2017) was also linked to *myo18b* which shows this gene´s importance in maintenance of muscle structure thus suggesting that it is the correct candidate gene for *fro*^{to27c}.

The second mutant categorized under the group A mutants, *dus*^{tq250} when sequenced was found to have 20 missense mutations in the gene *titin, tandem duplicate 2* (*ttn.2* or *ttna*) and one frameshift insertion in its paralog *titin, tandem duplicate 1* (*ttn.1* or *ttnb*). These genes have been extensively studied over many years in other zebrafish mutants like *(pik) pickwick* (Xu et al., 2002a)*, runzel* (Zhou et al., 2007) and *(hel) herzschlag* (Myhre et al., 2014). Mutation in *pickwick* was found to be a premature stop codon in a heart-specific exon of the *ttn.1* gene, therefore only pericardial edema, reduced heartbeat, smaller eyes and head were noticed but

skeletal muscles were not affected. The locus containing the mutation in *hel* was found to contain the titin gene cassette, where the two paralogous copies of the gene, *ttn.1* and *ttn.2* were present. Since this mutant showed trunk muscle dystrophy along with pericardial edema, the *ttn.1* gene was the best candidate. *hel* and *pik* did not genetically complement each other, confirming that they are mutant alleles of the same gene (Myhre et al., 2014). We compared our mutant *dus*^{tq250} with *hel* by performing genetic complementation. Three independent crosses of heterozygous mutant *hel+/-* and *dus*^{tq250} *+/-* adult fish were set up and the offspring were assessed. We found that 98% of larvae were normal suggesting that both alleles could complement each other. This led to the conclusion that the mutation *dus*^{tq250} carries does not affect the same locus as *hel*, as it could compensate the loss. Therefore *ttn.2* is the more likely candidate. However, since, titin is the largest protein known and shows heterogeneity of phenotypes depending on the mutation (exon-dependent phenotypes) which could lead to partial intragenic complementation, we could not confirm the exact mutation in the *titin* locus responsible for the phenotype of *dus*^{tq250}.

3.5.2 Mutants classified under group B

The *slm*^{tt208} line was sequenced by a mutant only strategy reducing the overall expense of sequencing. 2 mutations were found to be of highest impact; a premature stop codon in *ryr1b* and a splice site mutation in AL844192.1. The *ryr1b* gene encodes for one of the ryanodine receptors which are a family of intracellular Ca^{2+} release channels that regulate the flux of Ca^{2+} from internal stores (endoplasmic and sarcoplasmic reticulum) to the cytosol (Ingham, 2009; Wu et al., 2011). One of the five zebrafish *ryr* genes, *ryr1b* is expressed in both fast and slow muscles functions in excitation-contraction coupling in striated muscles resulting in muscle contraction. Embryonic development requires maintenance of Ca^{2+} gradients and mutations in human homologs of RyRs affect Ca^{2+} influx and efflux causing cardiac diseases and myopathies. On the other hand, AL844192 is a long intergenic non-coding RNA (lincRNA). LincRNAs have been found to play an essential role in numerous biological processes and transcriptomic studies in other model organisms point out their role in skeletal muscle contraction, as well as targeting genes in muscle growth and development (Zou et al., 2017). Since the muscle architecture of *slm*^{tt208} mutants was intact, *ryr1b* remained the best candidate gene which could cause the defective motility in the larvae through abnormal levels of calcium which would worsen with time eventually rendering the mutants completely immotile. To check whether *ryr1b* is the right candidate gene responsible for the motility defect in our mutant line, we revived an already existing Sanger mutant line, *ryr1b*^{sa14191} containing a stop codon in exon22 of this gene. A genetic complementation test was performed between *ryr1b*^{sa14191}+/- and *slm*^{tt208}*+/-* heterozygous adult fishes. The phenotype of the progeny from three such independent crosses was then assessed and we saw that 25% of the embryos possessed a similar phenotype to *slm*^{tt208} homozygous mutants (i.e. they couldn't complement) suggesting that both are mutant alleles of *ryr1b* gene. This mutant was thus a successful example of mapping without sequencing wild-type siblings.

The second mutant from this category, *tk64* was sequenced in parallel with wild-type siblings. Around 101 variants were identified, out of which after curating for effect of variants only two missense mutants were left for our investigation. An A to C transversion in *cxcl18a.1* gene (*chemokine (C-X-C motif) ligand 18a, duplicate 1*) and a T to A transversion in *chata (choline O-acetyl transferase a)* gene was seen. Mutation in *chata* was predicted to be deleterious in nature while that in *cxcl18a.1* was tolerated. *cxcl18a.1* belongs to a protein family having chemokine activity whereas *chata* is a well-known gene involved in neuromuscular transmission. This gene codes for an enzyme, *choline O-acetyl transferase a* which catalysis the synthesis of a major neurotransmitter, acetylcholine (ACh). Mutations in this gene are reported to have an effect on muscles in humans. An already existing *chata* mutant in zebrafish called *bajan* was reported (Wang et al., 2008) containing a point mutation (A to C) at the splice acceptor site of the second intron of *chata.* This line was revived by us for performing genetic complementation testing. Three independent crosses of heterozygous mutant *bajan+/-* and *tk64 +/-* adult fish were set up and the phenotype of offspring were assessed. We found 25% of larvae were affected suggesting that both are mutant alleles of *chata* gene. To further confirm, a rescue experiment was done by injecting wild-type mRNA into the mutants and 99% rescue of the phenotype was seen (Figure 34 B) (Joshi et al., 2018).

3.5.2.1 tk64 was identified as a novel mutant allele of zebrafish *chata*

To find the exact cause of the observed phenotype we performed whole genome sequencing at the NGS facility of KIT. The sequencing was done in a paired end, multiplexed manner. The reads obtained were first checked for the quality (per base) and mapped for homozygosity. The maximum homozygosity was found on chromosome 13 shown by the elevated orange peak (Figure 31). The bioinformatic analysis was done by my colleague Sanamjeet Virdi, ITG, KIT. The variants in this area were identified by comparing to the wild-type, and categorized as low, modifier, or high impact variants with respect to their effect on the protein. After careful curation, a T to A transversion giving rise to a serine to arginine substitution at position 102 in *chata* (*choline-o-acetyl transferase a*) was predicted to have a deleterious/high impact effect on the protein. Also, the function of this gene perfectly fits to the observed phenotype. In humans, mutations occurring in this gene correspond to a disease called congenital myasthenic syndrome with episodic apnea (CMS-EA) causing muscle weakness and sudden, recurrent episodes of respiratory arrest but a large number of these patients remain still genetically undiagnosed due to clinical variabilities within patients.

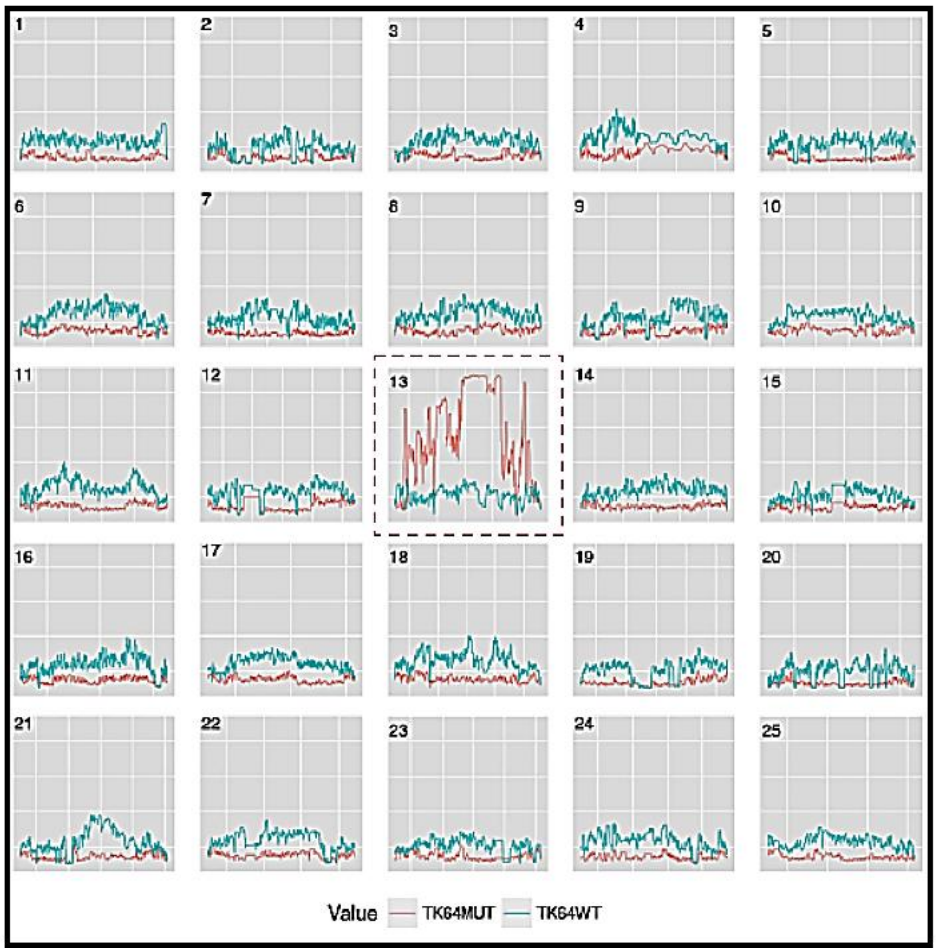

Figure 31. Homozygosity score plot for tk64 covering all chromosomes.
The homozygosity score in mutant (orange) and wild-type (blue) samples shows maximum homozygosity in chromosome 13. Figure courtesy: Sanamjeet Virdi.

3.5.2.2 Serine 102 is a part of evolutionarily conserved domain of zebrafish ChATa

The mutated amino acid that we found was never reported to be critical for the proper functioning of this gene. However, it is highly conserved amongst its vertebrate orthologs, suggesting its functional importance (Figure 32). The active site containing a histidine residue and the mutated amino acid serine are marked by the dotted box and the black arrow, respectively.

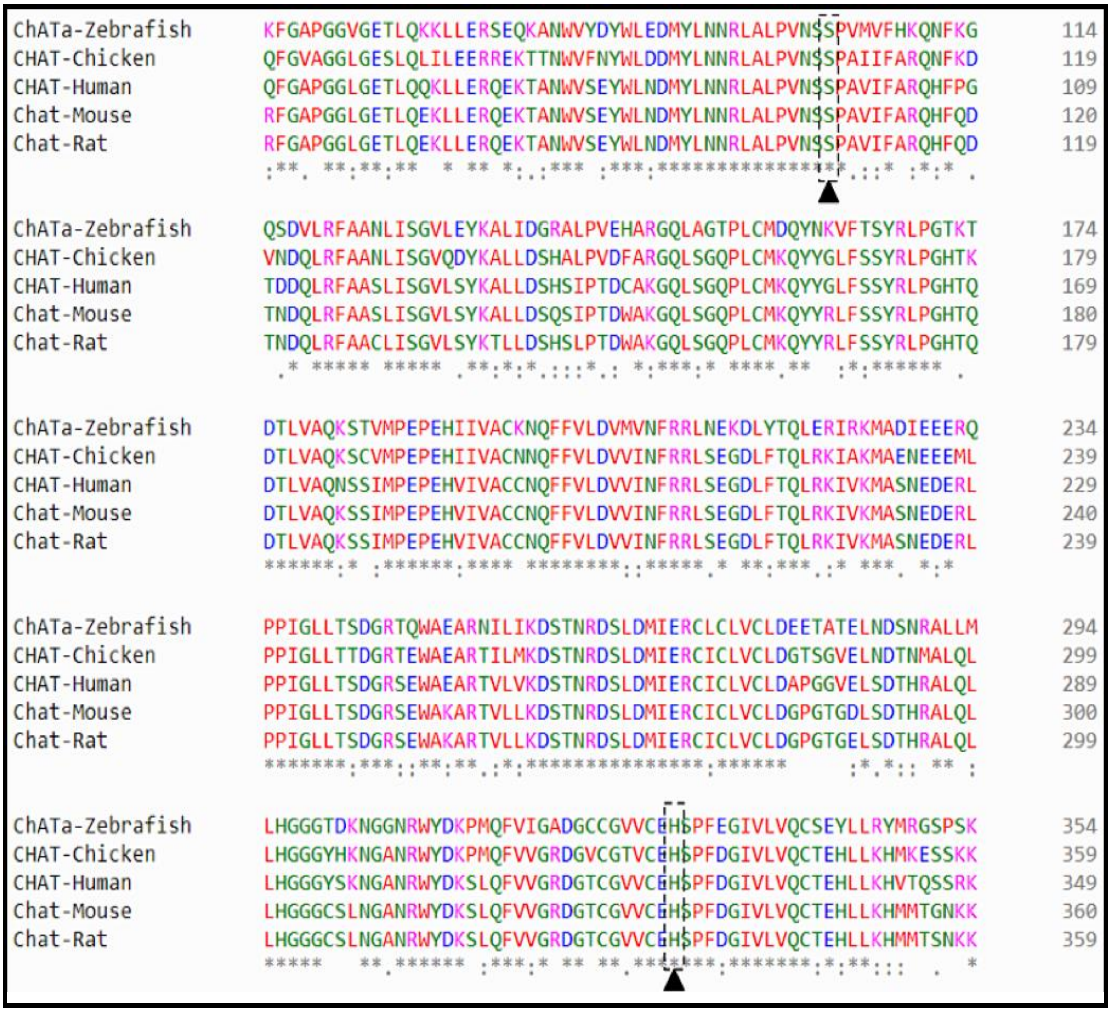

Figure 32. Multiple sequence alignment show conservation
Vertebrate transcripts (residue range 50-349 in human 70kDa CHAT Isoform R, UniProtKB ID: P28329-3) showing that serine and histidine (active site) residues are highly conserved among zebrafish, human, mouse, rat and chicken. Figure courtesy: Sanamjeet Virdi.

3.5.2.3 Amino acid change from serine to arginine might affect protein stability

In silico analysis for protein conformation was done by my colleague Sanamjeet Virdi, using several prediction programs, in order to determine the functional effect of the mutation on the protein structure. Introducing a serine to arginine change was predicted to give an unstable protein (Cutoff Scanning Matrix program (mCSM) (Pires et al., 2014). mCSM measures the difference of the Gibbs free energy of unfolding between wild-type and mutant proteins. The program predicted a stability change (ΔΔG) of -0.98 Kcal/mol, where the negative value categorizes the change as destabilizing. The functional impact of the S102R substitution was also checked with PANTHER-PSEP (Position-Specific Evolutionary Preservation) v9.0 (Tang and Thomas, 2016) which predicted the change as "probably damaging" because the position in the protein has been evolutionarily conserved for more than 450 million years. The structure prediction of zebrafish ChATa was done using another

software, Phyre[2] (Protein Homology/analogY Recognition Engine v2.0)(Kelley et al., 2015). When the structure of human ChAT was compared to zebrafish ChATa, as expected around 68% identity was observed. Serine 97 resides in the catalytic domain of the protein, in the vicinity of active site containing histidine 324 within a distance of 5 Å (PDB ID 2fy2) (Figure 33A-C). To check the effect of serine mutation, the human ChaT structure was used. We found that while introducing amino acid change S97R, the protein structure accommodates the arginine without any clashes but the arginine forms new salt bridges and introduces a charge into the buried center of the protein (close to the active site) by removing polar uncharged serine (Figure 33D, E). This introduction of charge could affect protein structure and likely hamper the catalytic efficiency.

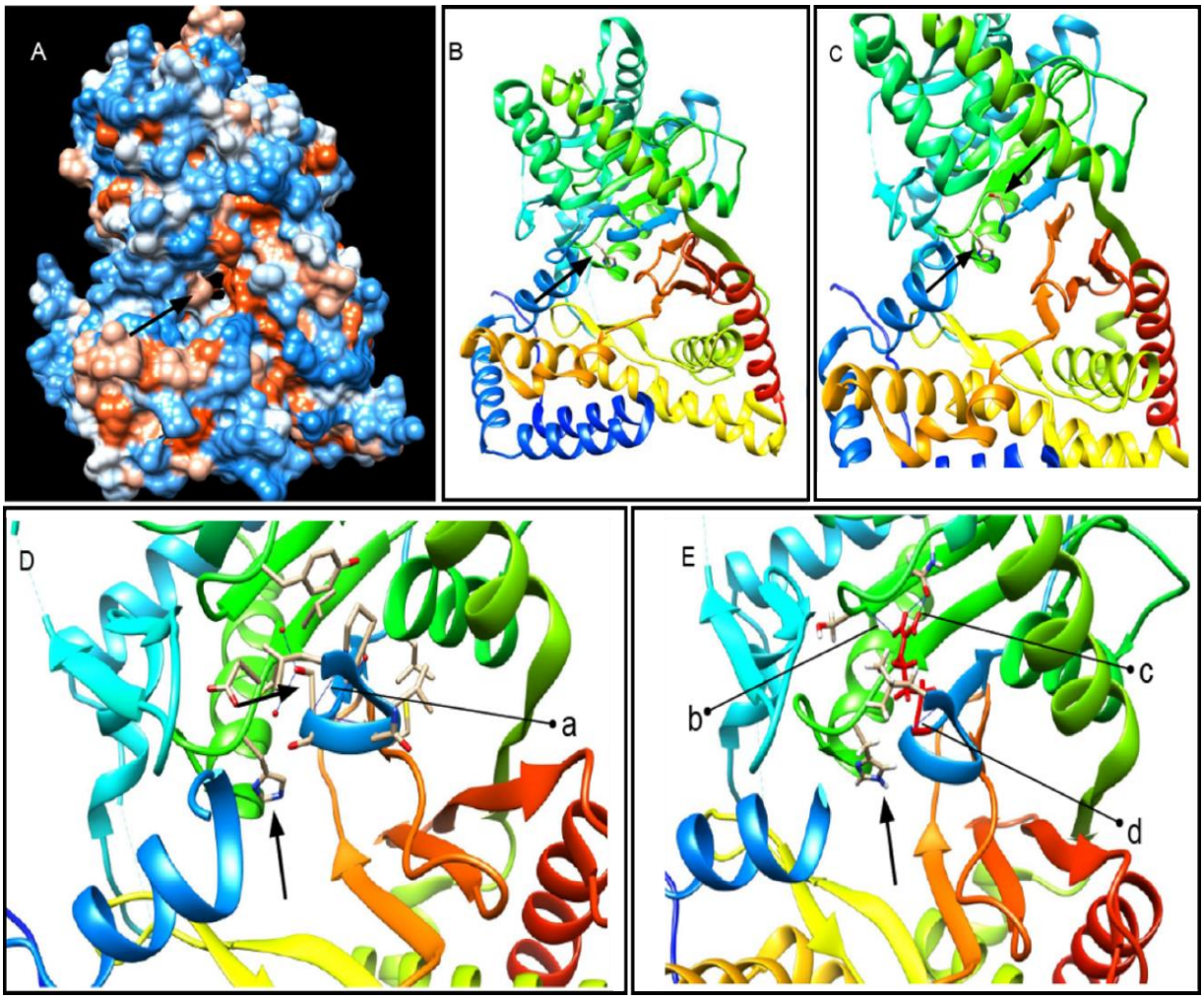

Figure 33. Human ChAT protein crystal structure and predicted effect of the *chata*^{tk64}mutation.
(A) Front view of protein crystal structure of human ChAT showing catalytic tunnel and **(B)** active site histidine H324. Residues 90 to 391 comprise the catalytic domain according to the human ChAT protein structure PDB ID 2fy2 (90–394 in 70 kDa ChAT Isoform R, UniProtKB ID: P28329-3 (Kim et al., 2006). The length of the N-terminal domain of the protein differs by 118 residues from the canonical protein isoform M (UniProtKB ID: P28329-1) and the structure starts at residue 8 (Arredondo et al., 2015). **(C)** Serine residue in the vicinity of active site in the protein (residues 90–95 are removed from the structure for better visualization). **(D)** Wild-type serine residue S97 forming a salt bridge a = 1.80 Å with residue L92 (residues 88–91 and 235–243 are deleted from the structure for better visualization). **(E)** Serine to arginine mutation S97R after structure minimization in UCSF chimera. R97 (in red) forms a new H-bond with serine S307 b = 2.50 Å; salt bridge with L92 d = 1.80 Å; and two new H-bonds with glutamine 309 c = [2.43 Å and 1.64 Å] (residues 86–90 and 236–246 are deleted from the structure for better visualization).

3.5.2.4 Complete rescue was achieved by injecting wild-type *chata* mRNA

To prove that the missense mutation found in chata^{tk64} is indeed responsible for the observed phenotype, we performed rescue experiments. Wild-type chata and chata^{tk64} allele were cloned from cDNA derived from wild-type and mutant embryos, respectively (Figure 34A). Synthetic mRNAs of wild-type and mutant *chata*^{tk64} carrying the missense mutation were injected into zygotes obtained from heterozygous *chata*^{tk64} incross. Embryos were examined at 48 hpf for their motility by the touch response assay. Since *chata*^{tk64} is recessive, 25% homozygous mutant embryos from crosses of heterozygous parents show the mutant phenotype in uninjected controls (Figure 34B). However, only 1% of the embryos resulting from such crosses injected with wild-type *chata* mRNA showed a motility defect upon touch, suggesting behavioral rescue (Figure 34B). As expected, the S102R mutant *chata*^{tk64} mRNA did not rescue the phenotype (Figure 34B) resulting in approximately 25% motility mutants, thus confirming that the missense mutation causing S102R is responsible for the observed motility phenotype. Surprisingly, in the course of our cDNA amplifications; we noted a shorter fragment that is weakly present in PCR fragments amplified from wild-type and more strongly in PCR fragments from mutant cDNA (Figure 34A). Sequencing of the PCR fragments revealed that these shorter fragments represent the same mRNA variant that lacks exon3. This suggests that this variant, henceforth called as ΔEx3, is naturally expressed in both wild-type and mutants but its abundance is increased in the *chata*^{tk64} mutants. Because exon3 encodes part of the catalytic site of ChAT, the deletion is predicted to abolish its enzymatic activity. To exclude any possibility that this variant contributes to the observed motility phenotype, a synthetic mRNA encoding ΔEx3 was injected into embryos derived from *chata*^{tk64} heterozygous incross. This variant was unable to rescue the phenotype: approximately 30% embryos showed the motility defect (Figure 34B). Moreover, the remaining 70% of embryos did not show any additional defects, suggesting that at least under these assay conditions ΔEx3 is non-functional and does not contribute to the observed motility defect phenotype. Our results on *tk64* have been published (Joshi et al., 2018).

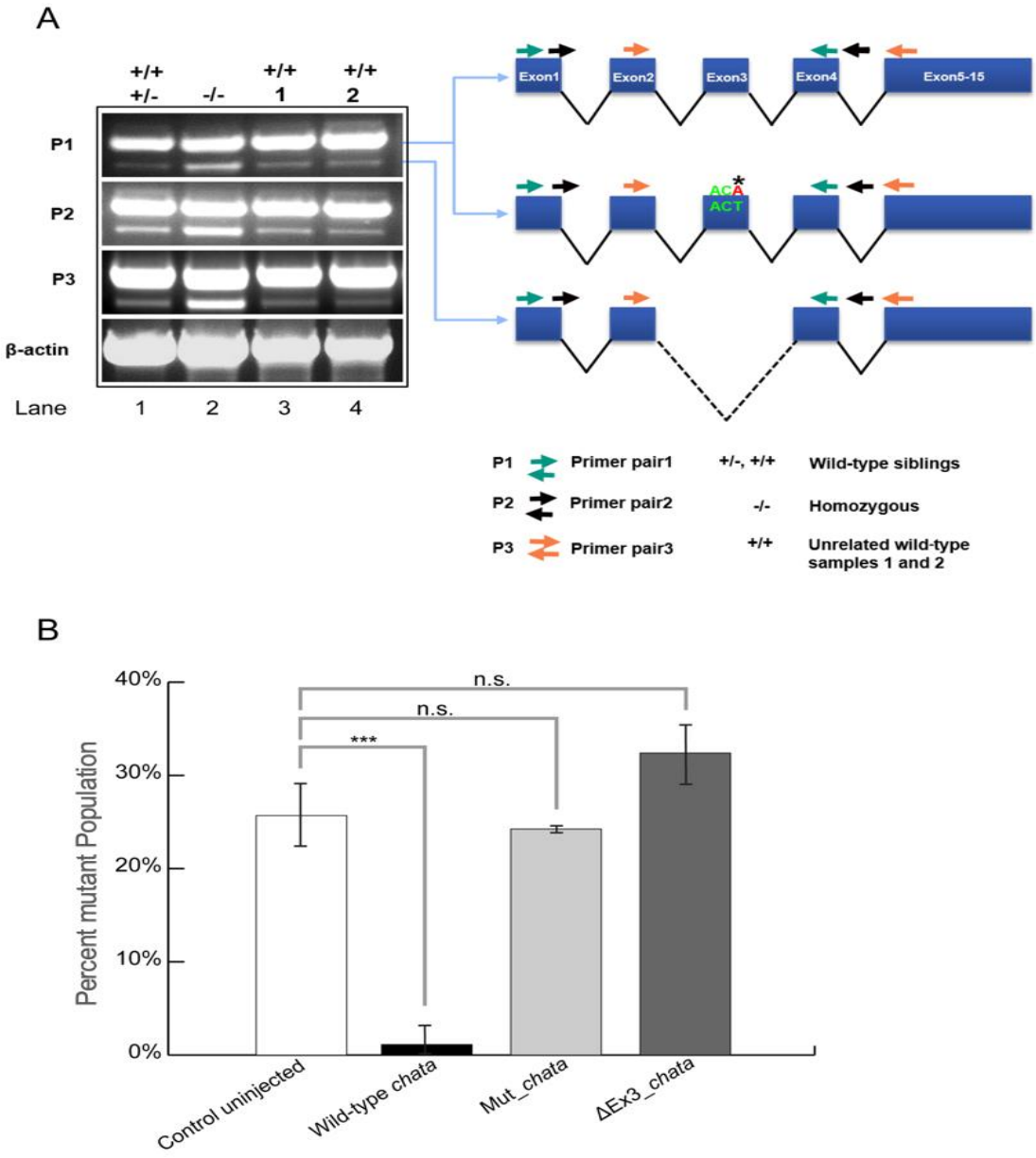

Figure 34. Variants of *chata* mRNA and rescue of the mutant phenotype.

A. cDNA fragments amplified by RT-PCR, left: Overlapping RT-PCR amplicons obtained with three different primer pairs (P1, P2 and P3). With each of the primer pairs two different PCR products, with and without exon3 were amplified from wild-type siblings, *chata*^{tk64} and unrelated wild-type cDNAs and confirmed by Sanger sequencing. From left, lane 1 wild-type siblings; lane 2: homozygous *chata*^{tk64}; lane 3 and 4: unrelated wild-type embryos. Right: Schematic diagram of the sequenced PCR products of zebrafish *chata*, top: wild-type; middle: *chata*^{tk64}; bottom: ΔEx3. For each of the primer pairs, the ΔEx3 product is more pronounced in the mutants than in the siblings or unrelated wild-types. **B.** Wild-type *chata* mRNA rescues the *chata*^{tk64} phenotype. Embryos were assessed with respect to their motility phenotype at 72 hpf after injection. In the wild-type mRNA injected embryos only 1% were mutants showing 99% rescue whereas the mRNA with missense mutation as in *chata*^{tk64} (Mut_*chata*) and lacking exon3 (ΔEx3_*chata*) gave a Mendelian ratio of mutants in the injected population. Significance was checked with Student's *t*-test at $P<0.05$. Asterisks and "n.s." above the bars represent significant and non-significant *p* values respectively. Data shown is mean ± standard deviation (n ≥ 17).

3.5.3 Mutants from the Tübingen EU screen

t30064 was mapped to the telomere region of chromosome 1. Since telomeres are repetitive areas and are not well annotated, there were many problems to pinpoint the exact candidate as none of the genes could explain such a drastic muscle phenotype. Therefore, we performed total RNA sequencing to check the transcriptomic profile of genes in mutants in comparison to their wild-type siblings. Differential gene analysis revealed more than half of the top differentially regulated genes to have a negative fold change value. These genes were found to be clustered altogether on the telomere. To confirm the results of RNA sequencing, I performed qPCR for 5 genes in this cluster and found that the mRNA of all these genes was completely absent which indicated a big telomeric deletion of about 260 kilobases. While comparing our results with previous genome assemblies (Zv9) in order to find the candidate responsible for muscle defect, *dusp27* (*dual specificity phosphatase 27*) was found. This gene was missing in the latest assembly (GRCz11) and was located on KZ116034.1, an unplaced scaffold. This gene was shown to be predominantly expressed in muscles and mutations in this gene (*dusp*^{y241}) results in complete disorganization of sarcomere assembly and pericardial edema in zebrafish (Fero et al., 2014) just like *t30064* mutants. Since *dusp27* is also a very huge gene, cloning to rescue remained a bottleneck. The mutant line *y241* was brought from ZIRC to perform genetic complementation.

The other mutant line revived from this screen, *t31198* exhibiting discontinuous myosepta was mapped to chromosome 21 and three candidate genes were found where the mutation with the highest impact was found to be a premature stop codon in the *notch1a* gene. Among other candidate genes, *kcnt1 (potassium channel, subfamily T, member 1)* encodes a voltage gated potassium channel having diverse functions from regulating neurotransmitter release to smooth muscle contraction. Mutations found in these genes cause seizures in humans (Lim et al., 2016). Segmentation of somites is under the control of Delta-Notch signaling and zebrafish mutants showing segmentation defect predominantly fall in this pathway (van Eeden et al., 1996). *aei* (*after eight*) mapped to *deltaD*, *bea* (*beamter*) mapped to *deltaC*, *des* (*deadly seven*) mapped to *notch1a* and *fss* (*fused somites*) mapped to *tbx24* (Gray et al., 2001; Holley et al., 2000; Holley et al., 2002; Jülich et al., 2005; Nikaido et al., 2002) all show somite boundary defects. *Fss* mutants survive to adulthood while *des* mutants are late embryonically lethal like *t31198* mutants. Since the segmentation clock is controlled by oscillating delta and notch concentrations, *notch1a* having a stop codon was selected to be the best candidate.

4 Discussion

4.1 Importance of guideRNA efficiency for gene editing

The guide RNA molecule (gRNA) is the major component of editing a DNA target using CRISPR/Cas9 methodology. gRNAs bind to the target site via base complementarity, enabling precise cleavage by Cas9. The principal requirement for the success of a CRISPR experiment is the target accuracy and efficiency of the guide RNA chosen. Therefore, constant efforts are made in the community for optimizing the design of gRNAs. Many studies have led to rules of sequence composition of gRNA relating to its efficiency and validated them across many locations. One such rule is that sgRNAs with more than 50% GC content and a guanine adjacent to PAM show better activity whereas, one or two mismatches at the 5´ of the target hamper its activity. Although many such rules are followed, studies have found that none of them are statistically significant (Varshney et al., 2015a).

Many web based tools assist in designing sgRNA, such as CHOPCHOP, CRISPRscan and CasBLASTR (Kleinstiver et al., 2015; Montague et al., 2014; Moreno-Mateos et al., 2015). Some of these tools also take care of off-target matches and work only for a certain species. Others are designed for multiple species. Avoiding polymorphisms to prevent problems with binding of nucleases or primers, uniqueness of sequence to prevent off-targets recognition and avoiding multiple CpG residues in the target sequence to keep the target accessible to nucleases are three basic considerations for choosing a target in a gene to be manipulated (Varshney et al., 2015c). Even though these tools effectively provide information on the best locus-specific gRNA sequences with their probable efficiencies, the editing of the target loci is still neither perfect nor very efficient in many cases.

In zebrafish, CRISPR/Cas9 has been successfully used for gene knockouts and recently for knock-ins. Efficient gRNAs can generate bi-allelic mutations where the phenotypes of recessive mutations were seen in the F0 generation immediately. This implies that the efficiency of gRNAs could modulate phenotype visibility and hence is a crucial step for an

experiment. Due to the genome duplication in teleosts, to create zebrafish mutants; one needs to target multiple genes at once to obtain complete knockouts, making the process much more cumbersome. The standard procedure of screening for indels is often performed in the F0 generations by analyzing the genomic DNA of adults. This procedure is time-consuming as it requires a waiting time of about 2 months during which a possible inefficiency of gRNA used in the experiment cannot be ruled out. This calls for the development of sensitive, fast and reliable methods to evaluate the effectiveness of gRNAs. Moreover, genotyping on a large scale to maintain mutant lines needs a cost-effective solution.

Several assays have been developed to identify mutations of target loci and the most common method used was the DNA mismatch nuclease assay where T7 endonuclease (Jao et al., 2013) and surveyor nuclease (Qiu et al., 2004) are used to identify mutants. However, while this method is simple and cost effective it has poor specificity in zebrafish due to the very high polymorphism. Restriction fragment length polymorphism (RFLP) can be used to screen target mutagenicity (Hruscha et al., 2013) but this method is not design friendly as presence of a restriction enzyme site at the target loci reduces the possible targets. Both of these techniques do not provide precise information about the mutations. Recently an improvised technique, HRMA (high resolution melting analysis), was successfully used to take the readout of guide RNA efficacy as early as 4 h post injection (Parant et al., 2009; Samarut et al., 2016) in zebrafish. This technique combined DNA extraction using the HotSHOT method with fluorescent PCR reactions which monitors DNA denaturation at a very high resolution. Regardless of all its advantages, a need for an expensive light cycler and requirement of specific software for data analysis makes it unhandy for many laboratories.

To overcome all these limitations, we developed and applied TIDE (Tracking of Indels by DEcomposition) to zebrafish, which was applied independently to cells earlier by Brinkman et al., 2014. This method employs HotShOT to extract DNA from injected embryos followed by PCR amplification of the target locus which is then subjected to capillary sequencing and hence we call it PCR-F-SEQ in accordance to the sequential steps. Hence, we injected previously known guides of variable efficiencies to assess the competence of the method. The Sanger sequencing profiles were found to deviate around PAM for guides against *rp2*, *bbs1 and pik3r4* whereas, guide against *bbs4* do not. These deviations are due to profound heterogeneity of bases at this location which is caused by the indels. The subcloned PCR product for each guide was used to infer mutagenesis efficacy by randomly sequencing subclones. As expected, high cutting efficacy indeed leads to a high number of mutant clones.

To quantify the cutting efficiency of individual guides, we exploited the degree of deviation of peaks found close to the PAM site in Sanger sequencing derived electropherograms. The peak intensities before and after PAM varies significantly and therefore correlates well with the cutting efficiency. We also created an artificial mix of variable percentages of wild-type and mutant fragments to understand the potential detection window of this method. We found out that the method is quite robust and can detect as little as 6% mutant fragment in the wild-type background.

Moreover, this technique could even detect a single indel and is very much capable of deducing heterozygous fish by analyzing the chromatogram. In parallel, we developed an open access webtool (accessible to the community) which provides clear information on mutagenicity post injection. We thus demonstrated PCR-F-SEQ, a high-throughput method to screen the gRNAs in zebrafish by quantitatively estimating their cutting efficiencies. This method employs simple lab machinery and is rather cost effective.

4.2 Crispr/Cas9 and genetic robustness

To decipher the role of a gene, targeted interference with gene function has been widely used in the zebrafish community. Two of the many strategies known namely, targeted knock down and knock out of the gene have been employed. Transient knock down of gene function using morpholinos, an antisense reagent has been rigorously used in countless studies. They bind to target mRNAs and prevent their translation or splicing. Many morpholinos could efficiently phenocopy well- characterized mutants and hence became the tool of choice for interfering with the gene function. However, the occurrence of phenotypes caused by non-specific binding to unintended targets could not be differentiated therefore, raising questions on relying solely on them (Stainier and Schulte-Merker, 2014; Tao et al., 2011).

Meanwhile, our ability to evaluate gene function has been further heightened by the recent advancements in the field of reverse genetics. Efficient tools like TALE nucleases (TALENs) and the Crispr/Cas9 system have been implemented to generate targeted mutations. Even though they can bind and cleave off-target loci, mutations can be segregated away from the mutation of interest by subsequent outcrosses. The ease of generating mutants has provided an opportunity to compare morphant with mutant phenotypes. Despite of the same goal of functional inactivation, surprisingly many cases have supported the observation that these strategies can result in different phenotypes. Also, an overwhelming number of engineered mutants (knockouts) do not exhibit an obvious phenotype. Many mechanisms of such a genetic robustness of engineered mutants have been proposed; functional redundancy, genetic compensation and transcriptional adaptation being some of the major ones (El-Brolosy and Stainier, 2017; Rossi et al., 2015; Tautz, 1992).

APOBEC2 belongs to a family of proteins some of which having RNA editing capability. However, its target has remained elusive. It is abundantly expressed in skeletal muscles (Liao et al., 1999; Wedekind et al., 2003) but initial studies in knockout mice exhibit no muscle phenotype (Mikl et al., 2005b). To understand its role, another study on the same knockout line was performed by Sato et al. (2010b). They found a shift of fiber type from fast to slow in the soleus muscle of APOBEC2 deficient mice. Although the reduction of muscle mass and the fiber type switch were evident at younger ages, the histological evidence was seen only at an

older age. A follow up study has shown that even though apobec2 is localized at Z-lines, the sarcomeric structure in Apobec-deficient mice was not affected (Sato et al., 2018). Instead, the deficiency of apobec2 causes mitochondrial defects leading to increased mitophagy in 10-month-old mice.

Previous study in our group identified an interaction between muscle myosin, Unc45b and Apobec2b (Etard et al., 2010). It was also shown by our group that Apobec2 proteins show colocalization with Unc45b at the myoseptal boundaries which might act as an anchor for muscle fibers. Knockdown of *apobec2* genes in zebrafish leads to detachment of myofiber from the boundaries. Other studies in zebrafish have shown *apobec2* to be involved in regulating retina and optic nerve regeneration independent of any cytosine deaminase function that they could possibly have (Powell et al., 2012; Powell et al., 2014). Most of the members of this protein family are involved in either DNA or RNA editing (Conticello, 2008) but such a catalytic function of APOBEC2 has been questioned (Siriwardena et al., 2016).

In order to resolve such phenotypic discrepancies and to characterize the function of the gene, we decided to establish a genetic knockout zebrafish model. Therefore, we performed genetic manipulation of the *apobec2a* and *apobec2b* genes using the CRISPR/Cas9 technique. Various guide RNA combinations were used to delete large parts of the gene (subsection 3.2.1). The only transmissible deletion was one affecting the splice junction between exon 1 and intron 1 which was then further investigated. The other deletions could probably be lethal/untolerated and therefore were not transmitted to the next generation.

We found that *apobec2a*$^{ka98/ka98}$ and *apobec2b*$^{ka99/ka99}$ single mutants do not show any visible muscle defect. Also, there was no lethality observed. Therefore, a double knockout line was established (*apobec2a*$^{ka98/ka98}$; *apobec2b*$^{ka99/ka99}$). To rule out the possibility of maternal contribution, we further investigated the maternal-zygotic (MZ) *apobec* mutants. The MZ mutants also do not recapitulate the morphant phenotype. A detailed examination of these mutants did not show any obvious defects in muscle architecture, as shown by the immunohistochemistry. Since it was also reported that loss of APOBEC2 led to defective satellite cell self-renewability in mice (Ohtsubo et al., 2018), I also checked the profile of satellite cells in double mutants by immunostaining using an antibody against Pax7, a marker for quiescent satellite cells. The loss of Apobec2 in our mutants had no effect on the number and location of satellite cells. Since in mice the phenotype progresses with age, we raised the MZ mutants to adulthood and did not find any signs of lethargy or muscle weakness. However, there is a need for performing in-depth analysis of mutants by subjecting them to stress in order to check their overall muscle strength.

Investigating the effect of the mutations on the mRNA of *apobec2a* and *2b* by RT-PCR shows a complete loss of PCR products in mutant samples for both the genes. This complete absence of PCR product indicates early mRNA degradation. To confirm the PCR results, in situ hybridization using probes against *apobec2a* and *2b* genes was performed. Interestingly, we found that *apobec 2b* shows transient upregulation in *apobec2a* mutants at 24 hpf which

completely disappears by 48 hpf. This might suggest compensation by the paralogous gene, which is frequently seen.

The phenotypic discrepancy between morphant and mutant could have several reasons, morpholino off target effects being one of them. Morpholinos can prevent translation of both maternal and zygotic transcripts and recent studies have shown that over 80% of morphant phenotypes could not be confirmed by genetic knockouts (Kok et al., 2015). This disparity thus encourages us not to completely rely on morpholino based results.

For this project, in order to assess the specificity of morpholino and to evaluate the effectiveness of our *apobec2a* MO, I injected it into *apobec2b*$^{ka99/ka99}$, into *apobec2a*$^{ka98/ka98}$; *apobec2b*$^{ka99/ka99}$ double mutants and into wild-type as a control. Since an appropriate dose of the morpholino had already been chosen in previous work and all controls had been thoroughly performed (Etard et al., 2010), I used the same concentration for my experiments. After injection, the embryos were analyzed and at 24 hpf about 80% of the embryos show a dystrophic phenotype. A significant number of these show smaller eyes and curved body. This might suggest a possible off-target effect of the MO or the possibility of a mutant transcript being targeted, which would imply that the mutants are not null. Several different PCRs did not support any such possibility but it cannot be completely ruled out.

The mechanisms underlying compensation in mutants are very complex and a non-deleterious genomic lesion is not sufficient to trigger a genetic compensatory response (Rossi et al., 2015). Since the mutants I developed have deleterious lesions, it might indicate an early trigger for the machinery to cope with the loss by upregulating completely unrelated gene in zebrafish. This could only be tested by looking at the transcriptomic profile of the mutants.

Another possibility of transcriptional adaptation is highly likely to occur in these mutants if there is a mutant transcript being produced, as it has been recently reported that RNA decay activates this process. It was seen that this is a dominant phenomenon as heterozygous animals also display this kind of adaptation, just a little less pronounced to that of the homozygotes (El-Brolosy et al., 2019). It was shown that only specific DNA lesions regulate this adaptation as it was not seen in all mutant alleles of a gene. Pre-mRNA levels were not affected and mutant transcripts exhibited shorter half- lives, clearly indicating mutant mRNA decay. Alleles that fail to transcribe the mutated gene should not display such an adaptation which points out that transcribed mRNA triggers this adaptation.

Transcriptomic profiling of many knockout models has indicated a consistent correlation between sequence similarity and transcriptional adaptation (El-Brolosy et al., 2019). To our surprise the mutated *apobec2b* mRNA was found to be upregulated in which was unexpected since the genetic manipulation is supposed to generate premature stop codon. This upregulation of *apobec 2b* mRNA therefore indicate a possible transcript being generated.

This study thus indicates a need for further experiments comparing *apobec2* mutants and morphants to investigate whether the degradation of mutant mRNA is causing transcriptional adaptation that suppresses the phenotype. It also indicates that the type of mutation induced, plays a major role in triggering gene compensatory pathways.
Many of the human genetic diseases are caused by missense or in-frame insertions or deletions (indels). The missense and indel mutations are unlikely to lead to mutant mRNA degradation. Nonsense mutations on the other hand are less common and might lead to mRNA decay and upregulation of related genes thus, suppressing the phenotype. This clearly suggests that there is a need to generate missense mutations or indels in model organisms and study them with a view of better understanding disease pathology in humans.

4.3 Forward genetics: a window to novelty?

Forward genetics begins with a heritable trait of interest and strives to discover the alleles accounting for the observed defect using genetic mapping. It is one of the most powerful methods to enable understanding of the genetic basis of various human diseases (Moresco et al., 2013). Phenotypic driven research has led to various novel and unexpected discoveries. In zebrafish, two large-scale random mutagenesis screens performed in the 1990s identified thousands of mutants and established zebrafish as a mainstream model for development biology research (Driever et al., 1996; Haffter et al., 1996a).

Tübingen Ist and IIIrd ENU mutagenesis screens produced together over 2000 mutants and many of these alleles were stored as frozen sperm samples due to limited space, resources and phenotypic variability of the isolated mutants. These mutant lines are not yet analyzed and therefore serve as a great tool for identifying novel developmentally relevant genes. In this study we revived mutant lines showcasing mobility defects. We found out that the revivability of sperm samples varies quite a lot between different Tübingen screen (TU) samples. We revived a total of 10 lines and found that the revivability rate of samples from the Ist and IIIrd TU screens is about 66% and 40% respectively. As an additional difficulty, we noticed the Tübingen background to be behaviorally quite aggressive. Therefore, while crossing we either resorted to separating the fishes quickly after mating or we kept a small fiber ball in the mating box to provide hiding space. Once the mutant couples were identified, to detect the gene linked to phenotype remained a bottleneck for such studies over the years.

Traditionally, mapping the underlying mutations was a labor-intensive task which took several months and occasionally even years. However, the methods of mapping have evolved with the technological advancements and next generation sequencing based approaches, which has enabled fast and accurate mapping. Whole genome sequencing thus is a promising approach for discovering genetic perturbations. Massively parallel sequencing technology supports multiplexing the samples but the abundance of data that is generated requires

resources for data storage along with computational expertise for further analysis (Clark et al., 2011).

Recent advances in single nucleotide polymorphism algorithms have enabled fast mapping and cloning of recessive ENU mutations (Bowen et al., 2012; Leshchiner et al., 2012; Voz et al., 2012). Therefore, in this research work a robust bioinformatic pipeline, *`Zyg-score'* was developed which can consistently and accurately map the mutations, independent to the different experimental strategies (sequencing wild-type and mutant pools or sequencing only mutant pools obtained from different couples). The novel strategy of sequencing only mutants is cost-efficient and allows one to buy increased sequencing coverage (S. Virdi, 2019; manuscript in preparation). The six revived mutant lines were successfully mapped (Table 9), *slm*^{tt208} using novel mutant only strategy. Curiously, most of them were alleles of already known genes which might indicate that the identified genes are mutational 'hot spots', and more effort is needed to saturate the genome. Screening for unique phenotypes can be another way to identify novel genes.

However, some pitfalls have been realized that limit the use of these random mutagenesis approaches. One of the major disadvantages of this approach is that it relies completely on the zebrafish genome assembly. To annotate the variants, it becomes a necessity to have an accurate genome assembly to prevent missing of the candidate gene. Apart from that, the depth and integrity of such screens is also limited because it is impossible to incapacitate every gene in the genome by random mutagenesis as these screens rely on measurable phenotypes which can be missing in case of redundant loci or early compensation.

4.4 Postmeiotic mutagenesis: deletion in *t30064*

N-ethyl-N-nitrosourea (ENU), the DNA alkylating agent is the most widely used chemical mutagen for introducing point mutations. In zebrafish, the mutations are induced in the spermatogonia stem cells which is achieved by repeated treatment of adult males at weekly intervals followed by a brief gap before mating (Mullins et al., 1994b; Solnica-Krezel et al., 1994). This waiting period is extremely important to eliminate the affected post-meiotic germ cells which fixes the mutations and leads to non-mosaic off springs in the next generation. A great majority of the pre-meiotic mutations are point mutations suitable for functional analysis of the genes.

Post meiotic ENU mutagenesis on the other hand, is accomplished by quick mating (~2 weeks) after a single treatment (Alexander et al., 1998; Appel et al., 1999). The range of mutations induced in this way has not been extensively analyzed. Such a mutagenesis approach leads to mosaic progeny and non-Mendelian transmission which makes the

screening difficult. In the early 2000s it was reported that postmeiotic mutagenesis using ENU can cause wide spectrum of lesions including big deletions (Imai et al., 2000). Among a total of five alleles that were found in their screen, four were deletions ranging from < 3cM to ≥ 20 cM. The reason for the observed difference in lesion type in pre and postmeiotic treatments could be due one of the several reasons: due to the chromatin conformation, ploidy of sperm cells and spermatogonia or different DNA repair pathways. Similar effects were seen in mice as well as in medaka suggesting that the sperm stage determines the type of mutation induced (Russell et al., 1989; Shimada and Shima, 1998).

To our surprise, one of the revived mutants from the 3rd Tübingen screen, *t30064*, was found to have a large deletion on the telomere of LG1. Although the screen primarily was based on mutagenizing premeiotic sperm cells, this rare case highlights the heterogeneity that one should expect while dealing with mutants from such screens.

The deleted locus consists of a tightly packed cluster of about 17 genes which were found to be completely absent in our qPCR data. Several different BACs covering genes in this region were injected into the progeny of heterozygous parents, but none of them could rescue the muscle defect. Our search for the right candidate brought us to search in older genome assemblies for a gene in this area that might be a possible candidate for such a phenotype. As we anticipated, a gene called *dual specificity phosphatase 27 (dusp27)* was missing in this region in the current assembly. This gene was included in an unplaced scaffold whereas in older assemblies, it was in the telomeric region of chromosome 1. Loss of this gene is known to lead to massive disruption of myofibrils causing compromised motility in zebrafish (Fero et al., 2013). Due to the humungous size of this gene, cloning for rescue purposes was not possible and apart from that, a BAC containing this gene was also not available. However, a *dusp27* mutant line was imported from ZIRC. It has been revived and will be used for complementation testing.

4.5 Modeling human diseases in zebrafish

A myriad of mutants with disruption of conserved genes analogous to human disease loci were identified in chemical mutagenesis screens (Amsterdam and Hopkins, 2006; Haffter et al., 1996b; Santoriello and Zon, 2012). Genomic approaches have helped in identifying several gene variants in disease pathology and have been proofread in zebrafish.

Muscle mutants emerged from these screens that serve as excellent models for many of the diseases. *sapje* (dystrophin) for Duchenne muscular dystrophy and Becker muscular dystrophy (Bassett and Currie, 2003; Berger et al., 2010; Guyon et al., 2009), *laminin α2* (candyfloss) for congenital muscular dystrophy type 1A (MDC1A) and (LGMD) Limb-girdle muscular dystrophy (Hall et al., 2007), *dystroglycan 1* (*dag1*, also named *patchytail*) also for

LGMD (Gupta et al., 2011). In our screening, we have found another allele for *ryr1b* gene which has been reported to be a model for a myotonic muscular dystrophy (MmD), central core disease (CCD) (Hirata et al., 2007) NOTCH1 mutations in humans causes either Adams-Oliver syndrome or cardiovascular defects (Kerstjens-Frederikse et al., 2016; Stittrich et al., 2014).

Another zebrafish mutant allele of *notch1a* was identified in our study which shows a similar phenotype to that of other already reported alleles (Therapontos and Vargesson, 2010). Titin is a huge protein and plays developmental, regulatory, structural and mechanical roles in cardiac and skeletal muscles (Ferreiro, 2016). Due to its gigantic size and complexity the spectrum of diseases caused by mutations in this gene was initially underestimated. Mutations in this gene in humans are linked to cardiomyopathies, titinopathy, limb-girdle muscular dystrophy type 2J (LGMD2J), congenital centronuclear myopathy (CNM) and many more (Gigli et al., 2016; LeWinter and Granzier, 2013). Homozygous mutant mice for this gene exhibit progressive muscle degeneration (Charton et al., 2010; Garvey et al., 2001). Zebrafish mutant models like *runzel* and *pickwick* showcase myofibrillar disorganization and cardiomyopathy respectively. (Steffen et al., 2007; Xu et al., 2002b). We have reported another allele of this gene showing none of the phenotypes researched earlier. The mutant exhibits a motility defect but no obvious muscle or heart defects are seen. Due to the presence of extensive genetic variability, it is rather a challenge to determine disease causing mutations.

These disease models can serve as a great platform for assessing drug efficacies since zebrafish showcases comparable effects with the drugs that are used to treat human diseases (Lin, 2012).

Another gene, CHAT, has been associated with congenital myasthenic syndrome associated with episodic apnea (CMS-EA) (Ohno et al., 2001). We have reported a new allele of this gene which is conserved in humans. The CHAT gene in humans has also been recently associated with an increased risk of Alzheimer's disease (Hálová et al., 2018; Poirel et al., 2018) and therefore, it is rather important to report novel alleles which might add information to better understand the pathology of human diseases. Another zebrafish ChAT mutant, *baj*^{tf247c} *(bajan)* was reported to have a splice site mutation creating an early stop codon upstream of the catalytic site. Thus, the entire protein is eliminated. In contrast *chata*^{tk64} is a missense mutation in the catalytic domain of the enzyme. This mutation is situated close to the catalytic tunnel and identifies thus an important amino acid for proper functioning of the enzyme. Since no other mutant alleles are reported and zebrafish ChAT morphants are lethal, it is therefore a better model for human presynaptic CMS and might help in discovering therapeutic compounds for this disease.

5 Future perspectives

This thesis has utilized both reverse and forward genetic approaches to understand muscle development and function. In order to understand the molecular function and putative deaminase activity of the *apobec2a/b* genes in zebrafish, I created genetic knockouts. Contrary to our previous finding with morpholinos, *apobec2*a/b maternal-zygotic double mutants did not show any defects. Neither the muscle architecture nor stem cells were affected in the mutants which diverges from the recent findings in mice (Ohtsubo et al., 2017; Sato et al., 2018).

Due to the type of mutation which was introduced in these genes, i.e., deletion of splice junctions, it becomes extremely important to check the mRNA splicing in order to understand clearly if there any cryptic splice site is utilized; giving rise to transcripts that might still be functional. For this purpose, RNA sequencing will not only reveal alternately spliced products but also throw a light on differentially regulated genes. Any transcriptional adaptation would be clearly represented in such a data.

Apobec2 deficient mice exhibit a mild phenotype only in older stages and therefore, it becomes necessary to check the muscle sections of adult zebrafish mutants. Apart from histological studies, muscle integrity of the adults can be assessed by a swim tunnel assay (Mwaffo et al., 2017; Palstra et al., 2011).

Since the double mutants show transient upregulation of *apobec2* mRNA; it will be extremely informative to check the profile of these genes in single mutants. We have seen that apobec2a morpholino injections in both *apobec2b*$^{ka99/ka99}$ and *apobec2a*$^{ka98/ka98}$*; apobec2b*$^{ka99/ka99}$ could replicate the original morphant phenotype and to determine whether this is due to MO off-target effects, mutants lacking MO binding site can be created and assessed for a phenotype upon injections. Since the double mutants still contain the *apobec2a* morphant binding site, this cannot clearly invalidate the morpholino effect.

We have utilized the Tübingen screens as a valuable resource for studying developmentally relevant genes and have come across an uncommon deletion case. We have hypothesized that the *dusp27* gene is responsible for the muscle phenotype in *t30064* mutant. This will be confirmed by complementation testing with a *dusp27* line imported from ZIRC. *froto27c* and *t30064* share a similar muscle and ear phenotype but are linked to different chromosomes. The unconventional myosin, *myo18b*, mutated in *froto27c* has not been reported to play a role in inner ear development. Therefore, deciphering its role in otolith development and function might be another direction to explore.

6 References

Alexander, J., Stainier, D. Y. R. and Yelon, D. (1998). Screening mosaic F1 females for mutations affecting zebrafish heart induction and patterning. *Dev. Genet.*

Amack, J. D. and Yost, H. J. (2004). The T box transcription factor no tail in ciliated cells controls zebrafish left-right asymmetry. *Curr. Biol.*

Amsterdam, A. and Hopkins, N. (2006). Mutagenesis strategies in zebrafish for identifying genes involved in development and disease. *Trends Genet.*

Appel, B., Fritz, A., Westerfield, M., Grunwald, D. J., Eisen, J. S. and Riley, B. B. (1999). Delta-mediated specification of midline cell fates in zebrafish embryos. *Curr. Biol.*

Barrangou, R., Fremaux, C., Deveau, H., Richards, M., Boyaval, P., Moineau, S., Romero, D. A. and Horvath, P. (2007). CRISPR provides acquired resistance against viruses in prokaryotes. *Science (80-.).*

Bassett, D. I. and Currie, P. D. (2003). The zebrafish as a model for muscular dystrophy and congenital myopathy. *Hum. Mol. Genet.* **12**, R265–R270.

Berger, J., Berger, S., Hall, T. E., Lieschke, G. J. and Currie, P. D. (2010). Dystrophin-deficient zebrafish feature aspects of the Duchenne muscular dystrophy pathology. *Neuromuscul. Disord.*

Berger, J., Sztal, T. and Currie, P. D. (2012). Quantification of birefringence readily measures the level of muscle damage in zebrafish. *Biochem. Biophys. Res. Commun.*

Berger, J., Berger, S., Li, M. and Currie, P. D. (2017). Myo18b is essential for sarcomere assembly in fast skeletal muscle. *Hum. Mol. Genet.*

Bernhardt, R. R., Chitnis, A. B., Lindamer, L. and Kuwada, J. Y. (1990). Identification of spinal neurons in the embryonic and larval zebrafish. *J. Comp. Neurol.*

Bhattacharya, M. R. C., Bautista, D. M., Wu, K., Haeberle, H., Lumpkin, E. A. and Julius, D. (2008). Radial stretch reveals distinct populations of mechanosensitive mammalian somatosensory neurons. *Proc. Natl. Acad. Sci.* **105**, 20015 LP – 20020.

Blagden, C. S., Currie, P. D., Ingham, P. W. and Hughes, S. M. (1997). Notochord induction of zebrafish slow muscle mediated by sonic hedgehog. *Genes Dev.*

Boch, J., Scholze, H., Schornack, S., Landgraf, A., Hahn, S., Kay, S., Lahaye, T., Nickstadt, A. and Bonas, U. (2009). Breaking the code of DNA binding specificity of TAL-type III effectors. *Science (80-.).*

Bowen, M. E., Henke, K., Siegfried, K. R., Warman, M. L. and Harris, M. P. (2012). Efficient

mapping and cloning of mutations in zebrafish by low-coverage whole-genome sequencing. *Genetics*.

Briggs, A. W., Rios, X., Chari, R., Yang, L., Zhang, F., Mali, P. and Church, G. M. (2012). Iterative capped assembly: Rapid and scalable synthesis of repeat-module DNA such as TAL effectors from individual monomers. *Nucleic Acids Res.*

Brinkman, E. K., Chen, T., Amendola, M. and Van Steensel, B. (2014). Easy quantitative assessment of genome editing by sequence trace decomposition. *Nucleic Acids Res.*

Cermak, T., Doyle, E. L., Christian, M., Wang, L., Zhang, Y., Schmidt, C., Baller, J. A., Somia, N. V., Bogdanove, A. J. and Voytas, D. F. (2011). Efficient design and assembly of custom TALEN and other TAL effector-based constructs for DNA targeting. *Nucleic Acids Res.*

Chakrabarti, S., Streisinger, G., Singer, F. and Walker, C. (1983). Frequency of γ-ray induced specific locus and recessive lethal mutations in mature germ cells of the zebrafish, brachydanio rerio. *Genetics* **103**, 109–123.

Chal, J. and Pourquié, O. (2017). Making muscle: skeletal myogenesis in vivo and in vitro *Development* **144**, 2104 LP – 2122.

Charton, K., Danièle, N., Vihola, A., Roudaut, C., Gicquel, E., Monjaret, F., Tarrade, A., Sarparanta, J., Udd, B. and Richard, I. (2010). Removal of the calpain 3 protease reverses the myopathology in a mouse model for titinopathies. *Hum. Mol. Genet.*

Chemello, F., Bean, C., Cancellara, P., Laveder, P., Reggiani, C. and Lanfranchi, G. (2011). Microgenomic Analysis in Skeletal Muscle: Expression Signatures of Individual Fast and Slow Myofibers. *PLoS One* **6**, e16807.

Clark, M. D., Guryev, V., Bruijn, E. de, Nijman, I. J., Tada, M., Wilson, C., Deloukas, P., Postlethwait, J. H., Cuppen, E. and Stemple, D. L. (2011). Single nucleotide polymorphism (SNP) panels for rapid positional cloning in zebrafish. In *Methods in Cell Biology*, .

Comyn, S. A. and Pilgrim, D. (2012). Lack of Developmental Redundancy between Unc45 Proteins in Zebrafish Muscle Development. *PLoS One*.

Cong, L., Ran, F. A., Cox, D., Lin, S., Barretto, R., Habib, N., Hsu, P. D., Wu, X., Jiang, W., Marraffini, L. A., et al. (2013). Multiplex genome engineering using CRISPR/Cas systems. *Science* **339**, 819–823.

Conticello, S. G. (2008). The AID/APOBEC family of nucleic acid mutators. *Genome Biol.* **9**, 229.

Coste, B., Mathur, J., Schmidt, M., Earley, T. J., Ranade, S., Petrus, M. J., Dubin, A. E. and Patapoutian, A. (2010). Piezo1 and Piezo2 are essential components of distinct mechanically activated cation channels. *Science (80-.).*

Daggett, D. F., Domingo, C. R., Currie, P. D. and Amacher, S. L. (2007). Control of morphogenetic cell movements in the early zebrafish myotome. *Dev. Biol.*

Demarest, S. T. and Brooks-Kayal, A. (2018). From molecules to medicines: the dawn of targeted therapies for genetic epilepsies. *Nat. Rev. Neurol.*

Devoto, S. H., Melançon, E., Eisen, J. S. and Westerfield, M. (1996). Identification of separate slow and fast muscle precursor cells in vivo, prior to somite formation. *Development*.

DiFrancesco, D. and Noble, D. (1985). A model of cardiac electrical activity incorporating ionic pumps and concentration changes. *Philos. Trans. R. Soc. Lond. B. Biol. Sci.*

Doyon, Y., McCammon, J. M., Miller, J. C., Faraji, F., Ngo, C., Katibah, G. E., Amora, R., Hocking, T.

D., Zhang, L., Rebar, E. J., et al. (2008). Heritable targeted gene disruption in zebrafish using designed zinc-finger nucleases. *Nat. Biotechnol.*

Drapeau, P., Saint-Amant, L., Buss, R. R., Chong, M., McDearmid, J. R. and Brustein, E. (2002). Development of the locomotor network in zebrafish. *Prog. Neurobiol.*

Driever, W., Solnica-Krezel, L., Schier, A. F., Neuhauss, S. C., Malicki, J., Stemple, D. L., Stainier, D. Y., Zwartkruis, F., Abdelilah, S., Rangini, Z., et al. (1996). A genetic screen for mutations affecting embryogenesis in zebrafish. *Development* **123**, 37–46.

Eisen, J. S. and Smith, J. C. (2008). Controlling morpholino experiments: don't stop making antisense. *Development*.

El-Brolosy, M. A. and Stainier, D. Y. R. (2017). Genetic compensation: A phenomenon in search of mechanisms. *PLoS Genet.*

El-Brolosy, M. A., Kontarakis, Z., Rossi, A., Kuenne, C., Günther, S., Fukuda, N., Kikhi, K., Boezio, G. L. M., Takacs, C. M., Lai, S. L., et al. (2019). Genetic compensation triggered by mutant mRNA degradation. *Nature*.

Etard, C., Behra, M., Fischer, N., Hutcheson, D., Geisler, R. and Strähle, U. (2007). The UCS factor Steif/Unc-45b interacts with the heat shock protein Hsp90a during myofibrillogenesis. *Dev. Biol.* **308**, 133–143.

Etard, C., Roostalu, U. and Strähle, U. (2010). Lack of Apobec2-related proteins causes a dystrophic muscle phenotype in zebrafish embryos. *J. Cell Biol.* **189**, 527–539.

Etard, C., Joshi, S., Stegmaier, J., Mikut, R. and Strahle, U. (2017). Tracking of Indels by DEcomposition is a Simple and Effective Method to Assess Efficiency of Guide RNAs in Zebrafish. *Zebrafish* **14**, 586–588.

Faucherre, A., Nargeot, J., Mangoni, M. E. and Jopling, C. (2013). piezo2b Regulates Vertebrate Light Touch Response . *J. Neurosci.*

Fero, K., Bergeron, S. A., Horstick, E. J., Codore, H., Li, G. H., Ono, F., Dowling, J. J. and Burgess, H. A. (2013). Impaired embryonic motility in dusp27 mutants reveals a developmental defect in myofibril structure. *Dis. Model. Mech.*

Fero, K., Bergeron, S. a, Horstick, E. J., Codore, H., Li, G. H., Ono, F., Dowling, J. J. and Burgess, H. a (2014). Impaired embryonic motility in dusp27 mutants reveals a developmental defect in myofibril structure. *Dis. Model. Mech.*

Ferreiro, A. (2016). Titin-related myopathies: An emerging and growing group of striated muscle diseases. *Neuromuscul. Disord.*

Frontera, W. R. and Ochala, J. (2015). Skeletal Muscle: A Brief Review of Structure and Function. *Behav. Genet.*

Gagnon, J. A., Valen, E., Thyme, S. B., Huang, P., Ahkmetova, L., Pauli, A., Montague, T. G., Zimmerman, S., Richter, C. and Schier, A. F. (2014). Efficient Mutagenesis by Cas9 Protein-Mediated Oligonucleotide Insertion and Large-Scale Assessment of Single-Guide RNAs. *PLoS One* **9**, e98186.

Galpin, A. J., Raue, U., Jemiolo, B., Trappe, T. A., Harber, M. P., Minchev, K. and Trappe, S. (2012). Human skeletal muscle fiber type specific protein content. *Anal. Biochem.* **425**, 175–182.

Garvey, S. M., Rajan, C., Lerner, A. P., Frankel, W. N. and Cox, G. A. (2001). The muscular dystrophy with myositis (mdm) mouse mutation disrupts a skeletal muscle-specific

domain of titin. *Genomics*.

Gigli, M., Begay, R. L., Morea, G., Graw, S. L., Sinagra, G., Taylor, M. R. G., Granzier, H. and Mestroni, L. (2016). A Review of the Giant Protein Titin in Clinical Molecular Diagnostics of Cardiomyopathies . *Front. Cardiovasc. Med.* **3**, 21.

Goody, M. F., Carter, E. V, Kilroy, E. A., Maves, L. and Henry, C. A. (2017). "Muscling" Throughout Life: Integrating Studies of Muscle Development, Homeostasis, and Disease in Zebrafish. *Curr. Top. Dev. Biol.* **124**, 197–234.

Granato, M., van Eeden, F. J., Schach, U., Trowe, T., Brand, M., Furutani-Seiki, M., Haffter, P., Hammerschmidt, M., Heisenberg, C. P., Jiang, Y. J., et al. (1996). Genes controlling and mediating locomotion behavior of the zebrafish embryo and larva. *Development* **123**, 399–413.

Gray, M., Moens, C. B., Amacher, S. L., Eisen, J. S. and Beattie, C. E. (2001). Zebrafish deadly seven Functions in Neurogenesis. *Dev. Biol.* **237**, 306–323.

Gridley, T., Soriano, P. and Jaenisch, R. (1987). Insertional mutagenesis in mice. *Trends Genet.* **3**, 162–166.

Gupta, V., Kawahara, G., Gundry, S. R., Chen, A. T., Lencer, W. I., Zhou, Y., Zon, L. I., Kunkel, L. M. and Beggs, A. H. (2011). The zebrafish dag1 mutant: A novel genetic model for dystroglycanopathies. *Hum. Mol. Genet.*

Gurung, R., Ono, Y., Baxendale, S., Lee, S. L. C., Moore, S., Calvert, M. and Ingham, P. W. (2017). A Zebrafish Model for a Human Myopathy Associated with Mutation of the Unconventional Myosin MYO18B. *Genetics* **205**, 725 LP – 735.

Guyon, J. R., Goswami, J., Jun, S. J., Thorne, M., Howell, M., Pusack, T., Kawahara, G., Steffen, L. S., Galdzicki, M. and Kunkel, L. M. (2009). Genetic isolation and characterization of a splicing mutant of zebrafish dystrophin. *Hum. Mol. Genet.*

Haffter, P., Granato, M., Brand, M., Mullins, M. C., Hammerschmidt, M., Kane, D. a, Odenthal, J., van Eeden, F. J., Jiang, Y. J., Heisenberg, C. P., et al. (1996a). The identification of genes with unique and essential functions in the development of the zebrafish, Danio rerio. *Development* **123**, 1–36.

Haffter, P., Granato, M., Brand, M., Mullins, M. C., Hammerschmidt, M., Kane, D. A., Odenthal, J., van Eeden, F. J., Jiang, Y. J., Heisenberg, C. P., et al. (1996b). The identification of genes with unique and essential functions in the development of the zebrafish, Danio rerio. *Development*.

Hall, T. E., Bryson-Richardson, R. J., Berger, S., Jacoby, A. S., Cole, N. J., Hollway, G. E., Berger, J. and Currie, P. D. (2007). The zebrafish candyfloss mutant implicates extracellular matrix adhesion failure in laminin 2-deficient congenital muscular dystrophy. *Proc. Natl. Acad. Sci.*

Hálová, A., Janoutová, J., Ewerlingová, L., Janout, V., Bonczek, O., Zeman, T., Gerguri, T., Balcar, V. J. and Šerý, O. (2018). CHAT gene polymorphism rs3810950 is associated with the risk of Alzheimer's disease in the Czech population. *J. Biomed. Sci.* **25**, 41.

Hawkins, T. A., Haramis, A.-P., Etard, C., Prodromou, C., Vaughan, C. K., Ashworth, R., Ray, S., Behra, M., Holder, N., Talbot, W. S., et al. (2008). The ATPase-dependent chaperoning activity of Hsp90a regulates thick filament formation and integration during skeletal muscle myofibrillogenesis. *Development*.

Hirata, H., Watanabe, T., Hatakeyama, J., Sprague, S. M., Saint-Amant, L., Nagashima, A., Cui, W. W., Zhou, W. and Kuwada, J. Y. (2007). Zebrafish relatively relaxed mutants have a ryanodine receptor defect, show slow swimming and provide a model of multi-minicore disease. *Development*.

Holley, S. A., Geisler, R. and Nüsslein-Volhard, C. (2000). Control of her1 expression during zebrafish somitogenesis by a Delta- dependent oscillator and an independent wave-front activity. *Genes Dev.*

Holley, S. A., Julich, D., Rauch, G. J., Geisler, R. and Nüssleinvolhard, C. (2002). her1 and the notch pathway function within the oscillator mechanism that regulates zebrafish somitogenesis. *Development*.

Hoshijima, K., Jurynec, M. J. and Grunwald, D. J. (2016). Precise genome editing by homologous recombination. *Methods Cell Biol.*

Hruscha, A., Krawitz, P., Rechenberg, A., Heinrich, V., Hecht, J., Haass, C. and Schmid, B. (2013). Efficient CRISPR/Cas9 genome editing with low off-target effects in zebrafish. *Development* 140, 4982–7.

Hwang, W. Y., Fu, Y., Reyon, D., Maeder, M. L., Tsai, S. Q., Sander, J. D., Peterson, R. T., Yeh, J.-R. J. and Joung, J. K. (2013). Efficient genome editing in zebrafish using a CRISPR-Cas system. *Nat. Biotechnol.*

Hyde, D. R., Godwin, A. R. and Thummel, R. (2012). In vivo Electroporation of Morpholinos into the Regenerating Adult Zebrafish Tail Fin. *J. Vis. Exp.*

Imai, Y., Feldman, B., Schier, A. F. and Talbot, W. S. (2000). Analysis of chromosomal rearrangements induced by postmeiotic mutagenesis with ethylnitrosourea in zebrafish. *Genetics*.

Ingham, P. W. (2009). The power of the zebrafish for disease analysis. *Hum. Mol. Genet.* 18, R107–R112.

Jackson, H. E. and Ingham, P. W. (2013). Control of muscle fibre-type diversity during embryonic development: The zebrafish paradigm. *Mech. Dev.* 130, 447–457.

Jao, L.-E., Wente, S. R. and Chen, W. (2013). Efficient multiplex biallelic zebrafish genome editing using a CRISPR nuclease system. *Proc. Natl. Acad. Sci.*

Jayasinghe, I. D. and Launikonis, B. S. (2013). Three-dimensional reconstruction and analysis of the tubular system of vertebrate skeletal muscle. *J. Cell Sci.*

Joshi, S., Virdi, S., Etard, C., Geisler, R. and Strähle, U. (2018). Mutation of a serine near the catalytic site of the choline acetyltransferase a gene almost completely abolishes motility of the zebrafish embryo. *PLoS One*.

Jülich, D., Hwee Lim, C., Round, J., Nicolaije, C., Schroeder, J., Davies, A., Geisler, R., Lewis, J., Jiang, Y.-J. and Holley, S. A. (2005). beamter/deltaC and the role of Notch ligands in the zebrafish somite segmentation, hindbrain neurogenesis and hypochord differentiation. *Dev. Biol.* 286, 391–404.

Kelley, L. A., Mezulis, S., Yates, C. M., Wass, M. N. and Sternberg, M. J. E. (2015). The Phyre2 web portal for protein modeling, prediction and analysis. *Nat. Protoc.* 10, 845.

Kerstjens-Frederikse, W. S., van de Laar, I. M. B. H., Vos, Y. J., Verhagen, J. M. A., Berger, R. M. F., Lichtenbelt, K. D., Klein Wassink-Ruiter, J. S., van der Zwaag, P. A., du Marchie Sarvaas, G. J., Bergman, K. A., et al. (2016). Cardiovascular malformations caused by NOTCH1 mutations

do not keep left: data on 428 probands with left-sided CHD and their families. *Genet. Med.* **18**, 914.

Khodabukus, A., Prabhu, N., Wang, J. and Bursac, N. (2018). In Vitro Tissue-Engineered Skeletal Muscle Models for Studying Muscle Physiology and Disease. *Adv. Healthc. Mater.*

Kimmel, C. B., Ballard, W. W., Kimmel, S. R., Ullmann, B. and Schilling, T. F. (1995). Stages of embryonic development of the zebrafish. *Dev. Dyn.*

Kisia, S. M. and Onyango, D. W. (2005). *Muscular System of Vertebrates*. Science Publishers.

Kleinstiver, B. P., Prew, M. S., Tsai, S. Q., Topkar, V. V, Nguyen, N. T., Zheng, Z., Gonzales, A. P. W., Li, Z., Peterson, R. T., Yeh, J.-R. J., et al. (2015). Engineered CRISPR-Cas9 nucleases with altered PAM specificities. *Nature* **523**, 481.

Kok, F. O., Shin, M., Ni, C.-W., Gupta, A., Grosse, A. S., van Impel, A., Kirchmaier, B. C., Peterson-Maduro, J., Kourkoulis, G., Male, I., et al. (2015). Reverse genetic screening reveals poor correlation between morpholino-induced and mutant phenotypes in zebrafish. *Dev. Cell* **32**, 97–108.

Lamboley, C. R., Murphy, R. M., Mckenna, M. J. and Lamb, G. D. (2014). Sarcoplasmic reticulum Ca2+ uptake and leak properties, and SERCA isoform expression, in type I and type II fibres of human skeletal muscle. *J. Physiol.*

Lawson, N. D. and Wolfe, S. A. (2011). Forward and Reverse Genetic Approaches for the Analysis of Vertebrate Development in the Zebrafish. *Dev. Cell* **21**, 48–64.

Lee, H. J., Kim, E. and Kim, J. S. (2010). Targeted chromosomal deletions in human cells using zinc finger nucleases. *Genome Res.*

Lee, P. Y., Costumbrado, J., Hsu, C.-Y. and Kim, Y. H. (2012). Agarose Gel Electrophoresis for the Separation of DNA Fragments. *J. Vis. Exp.*

Leshchiner, I., Alexa, K., Kelsey, P., Adzhubei, I., Austin-Tse, C. A., Cooney, J. D., Anderson, H., King, M. J., Stottmann, R. W., Garnaas, M. K., et al. (2012). Mutation mapping and identification by whole-genome sequencing. *Genome Res.*

LeWinter, M. M. and Granzier, H. L. (2013). Titin Is a Major Human Disease Gene. *Circulation*.

Li, M., Zhao, L., Page-McCaw, P. S. and Chen, W. (2016). Zebrafish Genome Engineering Using the CRISPR–Cas9 System. *Trends Genet.*

Liao, W., Hong, S. H., Chan, B. H., Rudolph, F. B., Clark, S. C. and Chan, L. (1999). APOBEC-2, a cardiac- and skeletal muscle-specific member of the cytidine deaminase supergene family. *Biochem. Biophys. Res. Commun.* **260**, 398–404.

Lim, C. X., Ricos, M. G., Dibbens, L. M. and Heron, S. E. (2016). KCNT1 mutations in seizure disorders: The phenotypic spectrum and functional effects. *J. Med. Genet.*

Lin, Y. Y. (2012). Muscle diseases in the zebrafish. *Neuromuscul. Disord.*

Liu, Y. (2005). Central and Peripheral Axon Branches from One Neuron Are Guided Differentially by Semaphorin3D and Transient Axonal Glycoprotein-1. *J. Neurosci.*

Liu, Q., Segal, D. J., Ghiara, J. B., Barbas Iii, C. F. and Lerner, R. A. (1997). Design of polydactyl zinc-finger proteins for unique addressing within complex genomes (molecule designzinc-finger proteinsgenome addressingtranscriptional regulationgene therapy). *Biochemistry*.

Liu, J., Zhou, Y., Qi, X., Chen, J., Chen, W., Qiu, G., Wu, Z. and Wu, N. (2017). CRISPR/Cas9 in zebrafish: an efficient combination for human genetic diseases modeling. *Hum. Genet.*

MacIntosh, B. R., Gardiner, P. F. and McComas, A. J. (2006). Skeletal muscle : form and function.

Mali, P., Yang, L., Esvelt, K. M., Aach, J., Guell, M., DiCarlo, J. E., Norville, J. E. and Church, G. M. (2013). RNA-guided human genome engineering via Cas9. *Science (80-.).*

Manabe, Y. and Fujii, N. L. (2016). Experimental research models for skeletal muscle contraction. *J. Phys. Fit. Sport. Med.* 5, 373–377.

Maurya, A. K., Tan, H., Souren, M., Wang, X., Wittbrodt, J. and Ingham, P. W. (2012). Integration of Hedgehog and BMP signalling by the engrailed2a gene in the zebrafish myotome. *Development*.

Meeker, N. D., Hutchinson, S. A., Ho, L. and Trede, N. S. (2007). Method for isolation of PCR-ready genomic DNA from zebrafish tissues. *Biotechniques*.

Metcalfe, W. K., Myers, P. Z., Trevarrow, B., Bass, M. B. and Kimmel, C. B. (1990). Primary neurons that express the L2/HNK-1 carbohydrate during early development in the zebrafish. *Development* 110, 491 LP – 504.

Mikl, M. C., Watt, I. N., Lu, M., Reik, W., Davies, S. L., Neuberger, M. S. and Rada, C. (2005a). Mice deficient in APOBEC2 and APOBEC3. *Mol. Cell. Biol.* 25, 7270–7277.

Mikl, M. C., Watt, I. N., Lu, M., Reik, W., Davies, S. L., Neuberger, M. S. and Rada, C. (2005b). Mice deficient in APOBEC2 and APOBEC3. *Mol. Cell. Biol.* 25, 7270–7277.

Montague, T. G., Cruz, J. M., Gagnon, J. A., Church, G. M. and Valen, E. (2014). CHOPCHOP: a CRISPR/Cas9 and TALEN web tool for genome editing. *Nucleic Acids Res.* 42, W401–W407.

Moreno-Mateos, M. A., Vejnar, C. E., Beaudoin, J.-D., Fernandez, J. P., Mis, E. K., Khokha, M. K. and Giraldez, A. J. (2015). CRISPRscan: designing highly efficient sgRNAs for CRISPR-Cas9 targeting in vivo. *Nat. Methods* 12, 982.

Moresco, E. M. Y., Li, X. and Beutler, B. (2013). Going Forward with Genetics. *Am. J. Pathol.*

Moscou, M. J. and Bogdanove, A. J. (2009). A simple cipher governs DNA recognition by TAL effectors. *Science (80-.).*

Müller, F., Chang, B., Albert, S., Fischer, N., Tora, L. and Strähle, U. (1999). Intronic enhancers control expression of zebrafish sonic hedgehog in floor plate and notochord. *Development*.

Mullins, M. C., Hammerschmidt, M., Haffter, P. and Nüsslein-Volhard, C. (1994a). Large-scale mutagenesis in the zebrafish: in search of genes controlling development in a vertebrate. *Curr. Biol.*

Mullins, M. C., Hammerschmidt, M., Haffter, P. and Nüsslein-Volhard, C. (1994b). Large-scale mutagenesis in the zebrafish: in search of genes controlling development in a vertebrate. *Curr. Biol.* 4, 189–202.

Mwaffo, V., Zhang, P., Romero Cruz, S. and Porfiri, M. (2017). Zebrafish swimming in the flow: a particle image velocimetry study. *PeerJ* 5, e4041–e4041.

Myhre, J. L., Hills, J. A., Prill, K., Wohlgemuth, S. L. and Pilgrim, D. B. (2014). The titin A-band rod domain is dispensable for initial thick filament assembly in zebrafish. *Dev. Biol.*

Nguyen-Chi, M. E., Bryson-Richardson, R., Sonntag, C., Hall, T. E., Gibson, A., Sztal, T., Chua, W., Schilling, T. F. and Currie, P. D. (2012). Morphogenesis and Cell Fate Determination within the Adaxial Cell Equivalence Group of the Zebrafish Myotome. *PLoS Genet.*

Nikaido, M., Kawakami, A., Sawada, A., Furutani-Seiki, M., Takeda, H. and Araki, K. (2002). Tbx24,

encoding a T-box protein, is mutated in the zebrafish somite-segmentation mutant fused somites. *Nat. Genet.*

Noveroske, J. K., Weber, J. S. and Justice, M. J. (2000). The mutagenic action of N-ethyl-N-nitrosourea in the mouse. *Mamm. Genome*.

Nüsslein-Volhard, C. (2012). The zebrafish issue of Development *Development* 139, 4099 LP – 4103.

Ochi, H. and Westerfield, M. (2007). Signaling networks that regulate muscle development: Lessons from zebrafish. *Dev. Growth Differ.* 49, 1–11.

Ogino K., H. H. (2018) (2018). Rohon-Beard Neuron in Zebrafish. In *Zebrafish, Medaka, and Other Small Fishes. Springer, Singapore*, .

Ohno, K., Tsujino, A., Brengman, J. M., Harper, C. M., Bajzer, Z., Udd, B., Beyring, R., Robb, S., Kirkham, F. J. and Engel, A. G. (2001). Choline acetyltransferase mutations cause myasthenic syndrome associated with episodic apnea in humans. *Proc. Natl. Acad. Sci.* 98, 2017–2022.

Ohtsubo, H., Sato, Y., Suzuki, T., Mizunoya, W., Nakamura, M., Tatsumi, R. and Ikeuchi, Y. (2017). Data supporting possible implication of APOBEC2 in self-renewal functions of myogenic stem satellite cells: Toward understanding the negative regulation of myoblast differentiation. *Data Br.* 12, 269–273.

Ohtsubo, H., Sato, Y., Matsuyoshi, Y., Suzuki, T., Mizunoya, W., Nakamura, M., Tatsumi, R. and Ikeuchi, Y. (2018). Fluorescence microscopy data on expression of Paired Box Transcription Factor 7 in skeletal muscle of APOBEC2 knockout mice. *Data Br.* 17, 1348–1351.

Oxtoby, E. and Jowett, T. (1993). Cloning of the zebrafish krox-20 gene (krx-20) and its expression during hindbrain development. *Nucleic Acids Res.*

Palstra, A. P., Tudorache, C., Rovira, M., Brittijn, S. A., Burgerhout, E., van den Thillart, G. E. E. J. M., Spaink, H. P. and Planas, J. V (2011). Establishing Zebrafish as a Novel Exercise Model: Swimming Economy, Swimming-Enhanced Growth and Muscle Growth Marker Gene Expression. *PLoS One* 5, e14483.

Parant, J. M., George, S. A., Pryor, R., Wittwer, C. T. and Yost, H. J. (2009). A rapid and efficient method of genotyping zebrafish mutants. *Dev. Dyn.* 238, 3168–3174.

Pette, D. and Staron, R. S. (1997). Mammalian skeletal muscle fiber type transitions. *Int. Rev. Cytol.*

Pietri, T., Manalo, E., Ryan, J., Saint-Amant, L. and Washbourne, P. (2009). Glutamate drives the touch response through a rostral loop in the spinal cord of zebrafish embryos. *Dev. Neurobiol.*

Pires, D. E. V, Ascher, D. B. and Blundell, T. L. (2014). mCSM: predicting the effects of mutations in proteins using graph-based signatures. *Bioinformatics* 30, 335–42.

Poirel, O., Mella, S., Videau, C., Ramet, L., Davoli, M. A., Herzog, E., Katsel, P., Mechawar, N., Haroutunian, V., Epelbaum, J., et al. (2018). Moderate decline in select synaptic markers in the prefrontal cortex (BA9) of patients with Alzheimer's disease at various cognitive stages. *Sci. Rep.* 8, 938.

Powell, C., Elsaeidi, F. and Goldman, D. (2012). Injury-Dependent Muller Glia and Ganglion Cell Reprogramming during Tissue Regeneration Requires Apobec2a and Apobec2b. *J. Neurosci.*

Powell, C., Cornblath, E. and Goldman, D. (2014). Zinc-binding domain-dependent, deaminase-independent actions of apolipoprotein B mRNA-editing enzyme, catalytic polypeptide 2 (apobec2), mediate its effect on zebrafish retina regeneration. *J. Biol. Chem.*

Qiu, P., Shandilya, H., D'Alessio, J. M., O'Connor, K., Durocher, J. and Gerard, G. F. (2004). Mutation detection using Surveyor™ nuclease. *Biotechniques*.

Reyes, R., Haendel, M., Grant, D., Melancon, E. and Eisen, J. S. (2004). Slow degeneration of zebrafish Rohon-Beard neurons during programmed cell death. *Dev. Dyn.* **229**, 30–41.

Reyon, D., Tsai, S. Q., Khgayter, C., Foden, J. A., Sander, J. D. and Joung, J. K. (2012). FLASH assembly of TALENs for high-throughput genome editing. *Nat. Biotechnol.*

Rosen, J. N. and Baylies, M. K. (2017). Myofibrils put the squeeze on nuclei. *Nat. Cell Biol.* **19**, 1148–1150.

Rossi, A., Kontarakis, Z., Gerri, C., Nolte, H., Hölper, S., Krüger, M. and Stainier, D. Y. R. (2015). Genetic compensation induced by deleterious mutations but not gene knockdowns. *Nature*.

Russell, L. B., Russell, W. L., Rinchik, E. M. and Hunsicker, P. R. (1989). Factors affecting the nature of induced mutations.p. United States.

Samarut, É., Lissouba, A. and Drapeau, P. (2016). A simplified method for identifying early CRISPR-induced indels in zebrafish embryos using High Resolution Melting analysis. *BMC Genomics* **17**, 547.

Santoriello, C. and Zon, L. I. (2012). Hooked! Modeling human disease in zebrafish. *J. Clin. Invest.* **122**, 2337–2343.

Santos, D., Monteiro, S. M. and Luzio, A. (2018). General whole-mount immunohistochemistry of zebrafish (Danio rerio) embryos and larvae protocol. In *Methods in Molecular Biology*, .

Sato, Y., Probst, H. C., Tatsumi, R., Ikeuchi, Y., Neuberger, M. S. and Rada, C. (2010a). Deficiency in APOBEC2 leads to a shift in muscle fiber type, diminished body mass, and myopathy. *J. Biol. Chem.*

Sato, Y., Probst, H. C., Tatsumi, R., Ikeuchi, Y., Neuberger, M. S. and Rada, C. (2010b). Deficiency in APOBEC2 leads to a shift in muscle fiber type, diminished body mass, and myopathy. *J. Biol. Chem.*

Sato, Y., Ohtsubo, H., Nihei, N., Kaneko, T., Sato, Y., Adachi, S. I., Kondo, S., Nakamura, M., Mizunoya, W., Iida, H., et al. (2018). Apobec2 deficiency causes mitochondrial defects and mitophagy in skeletal muscle. *FASEB J.*

Schiaffino, S. and Reggiani, C. (2011). Fiber Types in Mammalian Skeletal Muscles. *Physiol. Rev.* **91**, 1447–1531.

Schmid-Burgk, J. L., Schmidt, T., Kaiser, V., Höning, K. and Hornung, V. (2013). A ligation-independent cloning technique for high-throughput assembly of transcription activator-like effector genes. *Nat. Biotechnol.*

Sevy, A., Cerino, M., Gorokhova, S., Dionnet, E., Mathieu, Y., Verschueren, A., Franques, J., Maues de Paula, A., Figarella-Branger, D., Lagarde, A., et al. (2016). Improving molecular diagnosis of distal myopathies by targeted next-generation sequencing. *J. Neurol. Neurosurg. & Psychiatry* **87**, 340 LP – 342.

Shestopalov, I. A., Pitt, C. L. W. and Chen, J. K. (2012). Spatiotemporal resolution of the Ntla

transcriptome in axial mesoderm development. *Nat. Chem. Biol.*

Shimada, A. and Shima, A. (1998). Combination of genomic DNA fingerprinting into the medaka specific-locus test system for studying environmental germ-line mutagenesis. *Mutat. Res. Mol. Mech. Mutagen.* 399, 149–165.

Shin, J., Chen, J. and Solnica-Krezel, L. (2014). Efficient homologous recombination-mediated genome engineering in zebrafish using TALE nucleases. *Development*.

Siriwardena, S. U., Chen, K. and Bhagwat, A. S. (2016). Functions and Malfunctions of Mammalian DNA-Cytosine Deaminases. *Chem. Rev.* 116, 12688–12710.

Smith, S. J., Horstick, E. J., Davidson, A. E. and Dowling, J. (2015). Analysis of Zebrafish Larvae Skeletal Muscle Integrity with Evans Blue Dye. *J. Vis. Exp.*

Solnica-Krezel, L., Schier, A. F. and Driever, W. (1994). Efficient recovery of ENU-induced mutations from the zebrafish germline. *Genetics* 136, 1401–1420.

Stainier, D. Y. R. and Schulte-Merker, S. (2014). Out with the old, in with the new: reassessing morpholino knockdowns in light of genome editing technology. *Development*.

Steffen, L. S., Guyon, J. R., Vogel, E. D., Howell, M. H., Zhou, Y., Weber, G. J., Zon, L. I. and Kunkel, L. M. (2007). The zebrafish runzel muscular dystrophy is linked to the titin gene. *Dev. Biol.*

Stellabotte, F., Dobbs-McAuliffe, B., Fernandez, D. A., Feng, X. and Devoto, S. H. (2007). Dynamic somite cell rearrangements lead to distinct waves of myotome growth. *Development*.

Stickney, H. L., Barresi, M. J. F. and Devoto, S. H. (2000). Somite development in zebrafish. *Dev. Dyn.* 219, 287–303.

Stittrich, A. B., Lehman, A., Bodian, D. L., Ashworth, J., Zong, Z., Li, H., Lam, P., Khromykh, A., Iyer, R. K., Vockley, J. G., et al. (2014). Mutations in NOTCH1 Cause Adams-Oliver Syndrome. *Am. J. Hum. Genet.*

Summerton, J. (1999). Morpholino antisense oligomers: The case for an RNase H-independent structural type. *Biochim. Biophys. Acta - Gene Struct. Expr.*

Summerton, J. and Weller, D. (1997). Morpholino antisense oligomers: design, preparation, and properties. *Antisense Nucleic Acid Drug Dev.*

Tallafuss, A., Gibson, D., Morcos, P., Li, Y., Seredick, S., Eisen, J. and Washbourne, P. (2012). Turning gene function ON and OFF using sense and antisense photo-morpholinos in zebrafish. *J. Cell Sci.*

Tang, H. and Thomas, P. D. (2016). PANTHER-PSEP: predicting disease-causing genetic variants using position-specific evolutionary preservation. *Bioinformatics* 32, 2230–2232.

Tao, S., Witte, M., Bryson-Richardson, R. J., Currie, P. D., Hogan, B. M. and Schulte-Merker, S. (2011). Zebrafish prox1b mutants develop a lymphatic vasculature, and prox1b does not specifically mark lymphatic endothelial cells. *PLoS One*.

Tautz, D. (1992). Redundancies, development and the flow of information. *BioEssays*.

Therapontos, C. and Vargesson, N. (2010). Zebrafish notch signalling pathway mutants exhibit trunk vessel patterning anomalies that are secondary to somite misregulation. *Dev. Dyn.*

Thummel, R., Bai, S., Sarras, M. P., Song, P., McDermott, J., Brewer, J., Perry, M., Zhang, X., Hyde, D. R. and Godwin, A. R. (2006). Inhibition of zebrafish fin regeneration using in vivo electroporation of morpholinos against fgfr1 and msxb. *Dev. Dyn.*

Ting, C. N., Rosenberg, M. P., Snow, C. M., Samuelson, L. C. and Meisler, M. H. (1992). Endogenous retroviral sequences are required for tissue-specific expression of a human salivary amylase gene. *Genes Dev.*

Umeda, K., Ishizuka, T., Yawo, H. and Shoji, W. (2016). Position- and quantity-dependent responses in zebrafish turning behavior. *Sci. Rep.* **6**, 27888.

Urnov, F. D., Rebar, E. J., Holmes, M. C., Zhang, H. S. and Gregory, P. D. (2010). Genome editing with engineered zinc finger nucleases. *Nat. Rev. Genet.*

van Eeden, F. J. M., Granato, M., Schach, U., Brand†, M., Furutani-Seiki, M., Haffter, P., Hammerschmidt, M., Heisenberg, C.-P., Jiang, Y.-J., Kane, D. A., et al. (1996). Mutations affecting somite formation and patterning in the zebrafish, Danio. *Development*.

Varshney, G. K., Pei, W., Lafave, M. C., Idol, J., Xu, L., Gallardo, V., Carrington, B., Bishop, K., Jones, M., Li, M., et al. (2015a). High-throughput gene targeting and phenotyping in zebrafish using CRISPR/Cas9. *Genome Res.*

Varshney, G. K., Sood, R. and Burgess, S. M. (2015b). Understanding and Editing the Zebrafish Genome. *Adv. Genet.* **92**, 1–52.

Varshney, G. K., Sood, R. and Burgess, S. M. (2015c). Understanding and Editing the Zebrafish Genome. *Adv. Genet.*

Voz, M. L., Coppieters, W., Manfroid, I., Baudhuin, A., von Berg, V., Charlier, C., Meyer, D., Driever, W., Martial, J. A. and Peers, B. (2012). Fast homozygosity mapping and identification of a zebrafish enu-induced mutation by whole-genome sequencing. *PLoS One*.

Wang, M., Wen, H. and Brehm, P. (2008). Function of Neuromuscular Synapses in the Zebrafish Choline-Acetyltransferase Mutant *bajan*. *J. Neurophysiol.* **100**, 1995–2004.

Wang, L., Geist, J., Grogan, A., Hu, L.-Y. R. and Kontrogianni-Konstantopoulos, A. (2018). Thick Filament Protein Network, Functions, and Disease Association. *Compr. Physiol.* 631–709.

Wedekind, J. E., Dance, G. S. C., Sowden, M. P. and Smith, H. C. (2003). Messenger RNA editing in mammals: new members of the APOBEC family seeking roles in the family business. *Trends Genet.* **19**, 207–216.

Westerfield, M. (2007). *The Zebrafish Book: A guide for the laboratory use of zebrafish (Danio rerio)*.

Whitfield, T. T., Riley, B. B., Chiang, M. Y. and Phillips, B. (2002). Development of the zebrafish inner ear. *Dev. Dyn.*

Wolff, C., Roy, S. and Ingham, P. W. (2003). Multiple muscle cell identities induced by distinct levels and timing of Hedgehog activity in the zebrafish embryo. *Curr. Biol.*

Wu, H. H., Brennan, C. and Ashworth, R. (2011). Ryanodine receptors, a family of intracellular calcium ion channels, are expressed throughout early vertebrate development. *BMC Res. Notes* **4**, 541.

Xu, X., Meiler, S. E., Zhong, T. P., Mohideen, M., Crossley, D. A., Warren, W. and Fishman, M. C. (2002a). Cardiomyopathy in zebrafish due to mutation in an alternatively spliced exon of titin. **30**, 205–209.

Xu, X., Meiler, S. E., Zhong, T. P., Mohideen, M., Crossley, D. A., Burggren, W. W. and Fishman, M. C. (2002b). Cardiomyopathy in zebrafish due to mutation in an alternatively spliced exon of titin. *Nat. Genet.*

Yen, H. J., Tayeh, M. K., Mullins, R. F., Stone, E. M., Sheffield, V. C. and Slusarski, D. C. (2006). Bardet-Biedl syndrome genes are important in retrograde intracellular trafficking and Kupffer's vesicle cilia function. *Hum. Mol. Genet.*

Zhou, Y., Kunkel, L. M., Zon, L. I., Steffen, L. S., Howell, M. H., Guyon, J. R., Vogel, E. D. and Weber, G. J. (2007). The zebrafish runzel muscular dystrophy is linked to the titin gene. *Dev. Biol.*

Zou, C., Li, J., Luo, W., Li, L., Hu, A., Fu, Y., Hou, Y. and Li, C. (2017). Transcriptome analysis reveals long intergenic non-coding RNAs involved in skeletal muscle growth and development in pig. *Sci. Rep.*

Appendix

A1 Supplementary figures

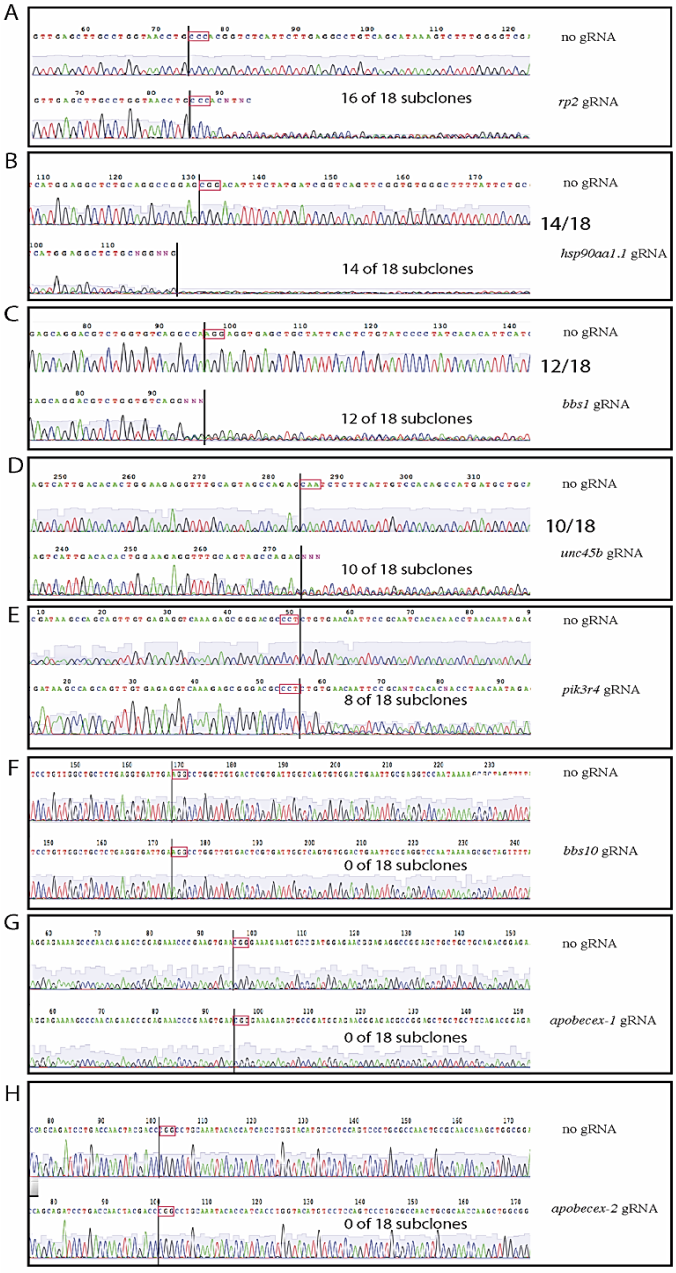

Figure S 1. (A-H) Examples of sequencing profiles obtained from sequencing the PCR fragments from pools of F0 embryos injected with gRNAs directed against *rp2* (A), *hsp90a* (B), *bbs1* (C), *unc45b* (D), *pik3r4* (E), *bbs10* (F), *apobec2a-exon1* (G), *apobec2a-exon2* (H). The upper sequence in each case corresponds to the sequencing profile obtained from sequencing the PCR fragment of uninjected embryos. The proportion of the number of mutant subclones relative to the total number of subclones is indicated for each gRNA. A total of 18 subclones was sequenced for each gRNA.

A

Number of seq	yellow = PAM, red = differs from WT
	***smyd1b* (reverse sequence)**
Wt = 2	TGTGTG TCGGCCAGAACATTCTCCTGTTTCTCCACACACTC
2	TGTGTG TCGGCCAGA ATTCTCCTGTTTCTCCACACACTC
1	TGTGTG TCGGCCAG TTCTCCTGTTTCTCCACACACTC
3	TGTGTG TCGGCCA TTCACCTGTTTCTCCACACACTC
1	TGTGTG TCGGCCAGCCCATTCTCCTGTTTCTCCACACACTC
1	TGTGTG TCTCCTGTTTCTCCACACACTC
1	TGTGTG TCGGCCAGAACACAACGTCCTCCTGTTTCTCCACACACTC
1	TGTGTG TCGGCCA TTCTCCTGTTTCTCCACACACTC
1	TGTGTG TCGGCCAGAACATGTGGTGTCTCCATGTGTGTGTCTCCTGTTTCTCCACACACTC
1	TGTGTG TCAGCCAGAACACACCCACATTCTCCTGTTTCTCCACACACTC
1	TGTGTG TCGGCCA- TTCTCCTGTTTCTCCACACACTC
1	TGTGTG TCAGCCAGAACACACCCACATTCTCCTGTTTCTCCACACACTC
	hsp90a
Wt = 4	CAAAGGCCTTCATGGAGGCTCTGCAGGCCGGAGCGGACATTTCTATGATCGGTCAGTTCGGTGTGGGCT
1	CAAAGGCCTTCATGGAGGCTCTGCAGGC-GG ACATTTCTATGATCGGTCAGTTCGGTGTGGGCT
2	CAAAGGCCTTCATGGAGGCTCTGCAGGC-GG GACATTTCTATGATCGGTCAGTTCGGTGTGGGCT
1	CAAAGGCCTTCATGGAGGCCTGCAGGC ATTTCTATGATCGGTCAGTTCGGTGTGGGCT
1	CAAAGGCCTTCATGGAGGCTCTGCAGGCCTGCAGGCAGAGCGGACATTTCTATGATCGGTCAGTTCGGT
1	CAAAGGCCTTCATGGAGGCTCTGCAG GACATTTCTATGATCGGTCAGTTCGGTGTGGGCT
1	CAAAGGCCTTCATGGAGGCTCAGC ACATTTCTATGATCGGTCAGTTCGGTGTGGGCT
1	CAAAGGCCTTCATGGAGGCTTT GTGGGCT
1	CAAAGGCCTTCATGGAGGCTCTGCAGACATTTCTATGATCTGCTCTGCWGAGCGGACATTTCTATGATCGGTCAGT
1	CAAAGGCCTTCATGGAGGCACTGCAGCG GACATTTCTATGATCGGTCAGTTCGGTGTGGGCT
1	CAAAGGCCTTCATGGAGGCTCTGCAGG CCATTTCTATGATCGGTCAGTTCGGTGTGGGCT
1	CAAAGGCCTTCATGGAGGCTCTGCAGGCGG ACATTTCTATGATCGGTCAGTTCGGTGTGGGCT
1	CAAAGGCCTTCATGGAGGCTCTGCAGGCATTTCTAGAGCGGACATTTCTATGATCGGTCAGTTCGGTGTGGGCT
1	CAAAGGCCTTCATGGAGGCTCTGCAGGCGGACATTTCTCTGAGCGGACATTTCTATGATCGGTCAGTTCGGTGTGGG
	bbs1
Wt = 6	GAGCAGGACGTCTGGTGTCAGGCCA AGGAGGTGAGCTGCTA
1	GAGCAGGACGTCTGGTGTCGTGAGCTGCTA AGGAGGTGAGCTGCTA
1	GAGCAGGACGTCTGGTGTCAGGAGGTGCCA AGGAGGTGAGCTGCTA
1	GAGCAGGACGTCTGGT GTGAGCTGCTA
1	GAGCAGGAG GTGAGCTGCTA
1	GAGCAGGACGTCTGGTGTCAA AGGAGGTGAGCTGCTA
1	GAGCAGGACGTCTGGTGTC AGGAGGTGAGCTGCTA
1	GAGCAGGACGTCTGGTGTCAGGCAAACCTTAATAGCAGGTGAGCTGCTA
1	GAGCAGGACGTCTGGTGTCAGG GAGGTGAGCTGCTA
1	GAGCAGGACGTCTGGTGTCAGGACCTGACACCAAGGAGGTGAGCTGCTA
1	GAGCAGGACGTCTGGTGTCAGGAGGAGCCA AGGAGGTGAGCTGCTA
1	GAGCAGGACGTCTGGTGTCAGG GGAGGTGAGCTGCTA
2	GAGCAGGACGTCTGGTGTCAAG GAGGTGAGCTGCTA
	unc45b
Wt = 8	CATGGCTGTGGACAATGAAGAGATTGCTC TGGCTACTGCAAACCTCTT
1	AGATCTGGCTACTGGCTAATGAAGAGATC TGGCTACTGCAAACCTCTT
1	CATGGCTGTGGACAATGAAGAGAT-ACTC TGGCTACTGCAAACCTCTT
1	CATGGCTGTGGACAATGAAGAGACTGCACAGCSTC TGGCTACTGCAAACCTCTT
1	CATGGCTGTGGACGATGAAGAGAT TGGCTACTGCAAACCTCTT
1	CATGGCTGTGGACAATGAAGAGATATCCTC TGGCTACTGCAAACCTCTT
1	CATGGCTGTGGACAATGAAGAGATGGTGTCTC TGGCTACTGCAAACCTCTT
1	CATGGCTATGGACAATGAAGAGAT TACTGCAAACCTCTT
1	CATGGCTGTGGACAATGAAGAGA TGGCTACTGCAAACCTCTT
1	CATGGCTGTGGACAATGAAGAG GTACTGCAAACCTCTT
1	CATGGCTGTGGACAATGAAGAGAT TGGCTACTGCAAACCTCTT
	***rp2* (seq reverse)**
Wt = 2	GAGCTTGCCTGGTAACCTGCCCACGGTCTCA TTCTTGAGGCCTGTCAG
1	GAGCTTGCCTGGTAACCAGCCCAC-AGG CA TTCTTGAGGCCTGTCAG
1	GAGCTTGCCTGGTARCCTGCCCACTAACCTGTCTCA TTCTTGAGGCCTGTCAG
3	GAGCTTGCCTGGTAACCTGCCCTCA TTCTTGAGGCCTGTCAG
1	GAGCTTGCCTGGTAACCTGCCC ACGGCCTGTCAG
2	GAGCTTGCCTGGTAACCTGCCCACGTCTCA TTCTTGAGGCCTGTCAG
1	GAGCTTGCCTGGTAACCTGCCCAGGCCTCTCA TTCTTGAGGCCTGTCAG
1	GAGCTTGCCTGGTAACCTGCCCACCTGCCTGTCTCA TTCTTGAGGCCTGTCAG
1	GAGCTTGC CTCA TTCTTGAGGCCTGTCAG
1	GAGCTTGCCTGGTAACCTGAGGCCTCATTCTTGAGGCCTCA TTCTTGAGGCCTGTCAG
1	GAGCTTGCCTGGTAACCTGCCC-CGTTACCA TTCTTGAGGCCTGTCAG
1	GAGCTTGCCTGGTAACCTGCCCACCAGATTACTTGAATATCTCTGACAGGCCTCATATCTCTGACAGGCCTCA TTCTTGAGGCCTGTCAG
1	GAGCTTGCCTGGTAACCTGCCCTGGTCTCA TTCTTGAGGCCTGTCAG
1	GAGCTTGCCTGGTAACCTGCCC CA TTCTTGAGGCCTGTCAG
	bbs10
Wt = 18	GACTTCCTGTTGGCTGCTCTGAGGTGATTGAAGGCCT GGTTGTGACTCGTGATTGGTCAGTGTGGACTGA
	apobec2aexon1
Wt = 18	GGCAGAAAATGATGCCAAGAAAGAGGAGAAAAGCCCAACAGAAGCGGAGAAACCCGAAGTGA
	apobec2aexon2
Wt = 18	CTGCGCTCCAGGAAGAACATCCGGCTGGCCATCTTTTCGTCGCGGCTGTTCGAGT

B

	forward	reverse	Guide + PAM	Expected size (bp)
smyd1b	GTGGTGAAGATCTGCCGTG	GGTATCCGTCCACCATCTTG	GGAGAAACAGGAGAATGTTCTGG	163
hsp90a	GACAGATCCGAGCAAACTGG	CGAAGTCTGGCTTGACAGTG	GGAGGCTCTGCAGGCCGGAGCGG	338
bbs1	ATGGACCTGCACGAGCC	CGTAGTGATCTGACAGACAGTGG	GGACGTCTGGTGTCAGGCCAAGG	428
unc45b	GTTTGCGTCCCAAAGGCAAC	CAATGGTGAAAAGGCACTTGG	GGACAATGAAGAGATTGCTCTGG	427
rp2	AGGAAGCCAGAGAGCAAAGA	GACCGGACCTAACACAATGC	GGCCTCAAGAATGAGACCGTGGG	284
bbs110	CCATAGCGACAAACTGGAGC	CAGGTGAATGTGGTGCTGTC	GGCTGCTCTGAGGTGATTGAAGG	435
apobecexon1	GTGTTTAGTTTCAGAGATGGCCGAT	ATGGCGGCAGCTCTATAGGTTC	GGAGAAAAGCCCAACAGAAGCGG	278
apobecexon2	GAACGTGGAGTACTCGTCCGG	CAGGGTGTGAACTGCTGTTCG	GGCTGGCCATCTTTTCGTCGCGG	423

Figure S 2. (A) Sequence alignment of the area around the PAM sequence of 18 subclones of PCR fragment pools from each gRNA injection. "Number of seq" indicates the number of mutant and wild-type clones for each sequence. The PAM is indicated in yellow. The black sequence represents the nucleotides identical to wild-type and the bases in red the sequence that diverged is highlighted. Note that for *bbs10* and for *apobec2a exon1* and *2,* no fragments with mutations were found. (B) Primers used to amplify the sequences flanking the target area of the different gRNAs along with the expected product size. Primers used for sequencing are indicated in red.

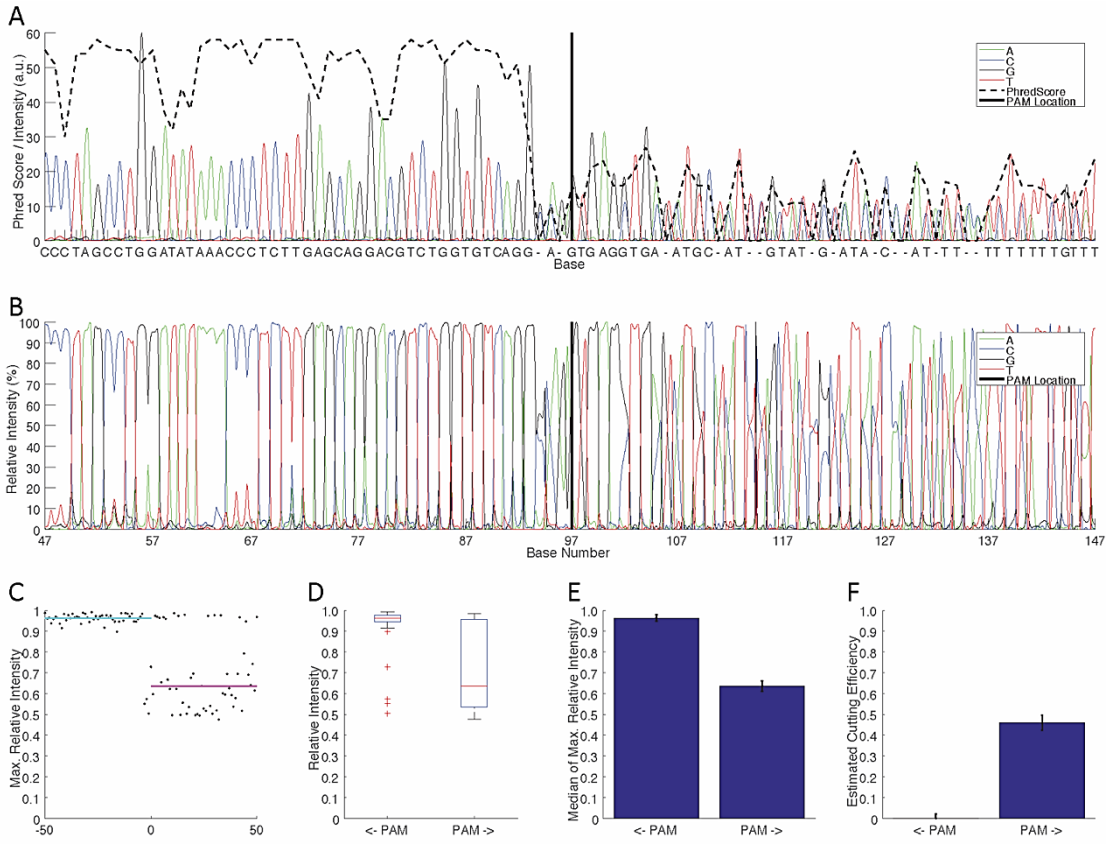

Figure S 3. Illustration of the processing steps involved in quantifying mutagenesis efficiency from sequencing profiles in PCR-F-Seq.

The DNA flanking the region targeted by the gRNA was amplified and the fragment pool consisting of wild-type and mutant fragments was subjected to Sanger sequencing. To demonstrate that the method can be used for genotyping of indel mutant carriers, the fragment pool was amplified from a *bbs1* heterozygous zebrafish embryo, thus consisting only of wild-type and a single mutant sequence (see Fig. S4B) with a 5 bp deletion (unpublished).

(A) Raw electropherogram of the intensity values for the four nucleotides A, C, G, T and the associated phred score. Intensity values of the bases were scaled to match the value range of the phred score. (B) Relative signal intensities obtained by converting the raw signal intensities to percentages at each location. Clear peaks are observed left of the black bar (PAM location or user-defined location of interest) and ambiguous peaks are observed on the right-hand side. (C) Maximum relative intensity values of 50 bases before and 50 bases after the specified location of interest. Colored bars indicate the median values of the relative intensity values before and after the location of interest, respectively. (D) Box plots of the relative intensity value distributions before and after the location of interest. (E) Bar plots of the median values with error bars indicating the standard error of the mean. (F) Derived estimate for the gRNA mutagenesis efficiency, calculated as described in the main text. The estimated frequency of about 46% is close to the expected 50% for a *bbs1* heterozygous zebrafish embryo.

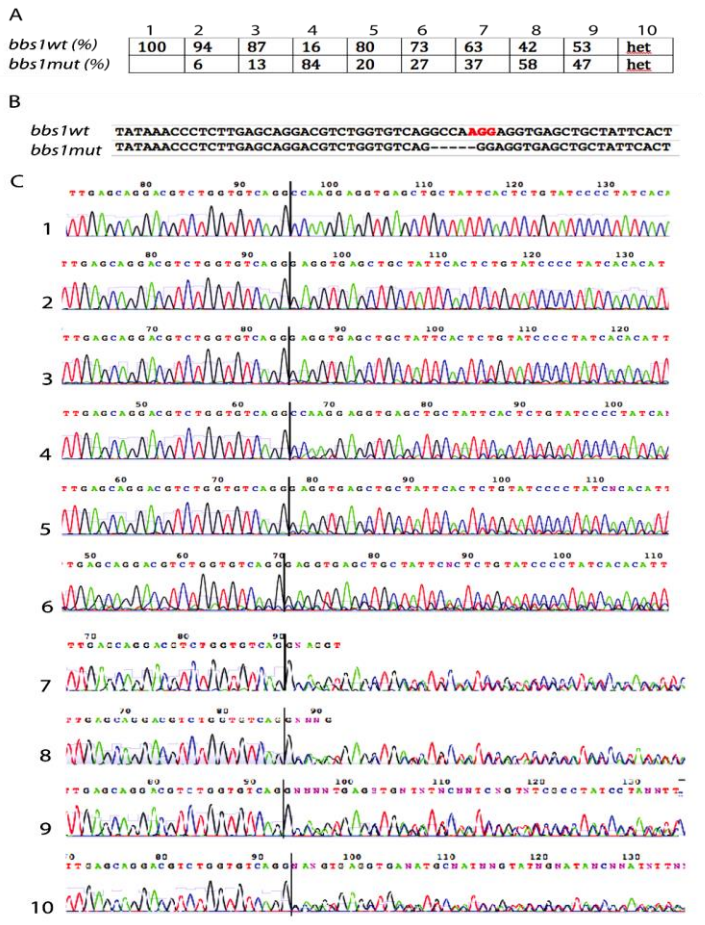

Figure S 4. (A) Mixture of two different PCR fragments *(*obtained from wild type and *bbs1* homozygous mutant, respectively) in different proportions (in %). The number above each mix refers to the original sequencing data (see File S1). (B) Sequence comparison of the two clones used for mixing. The PAM is indicated in red. (C) Sequence visualization of the PAM area for each mixture. The number refers to the original sequence data (see (A), and File S1).

A

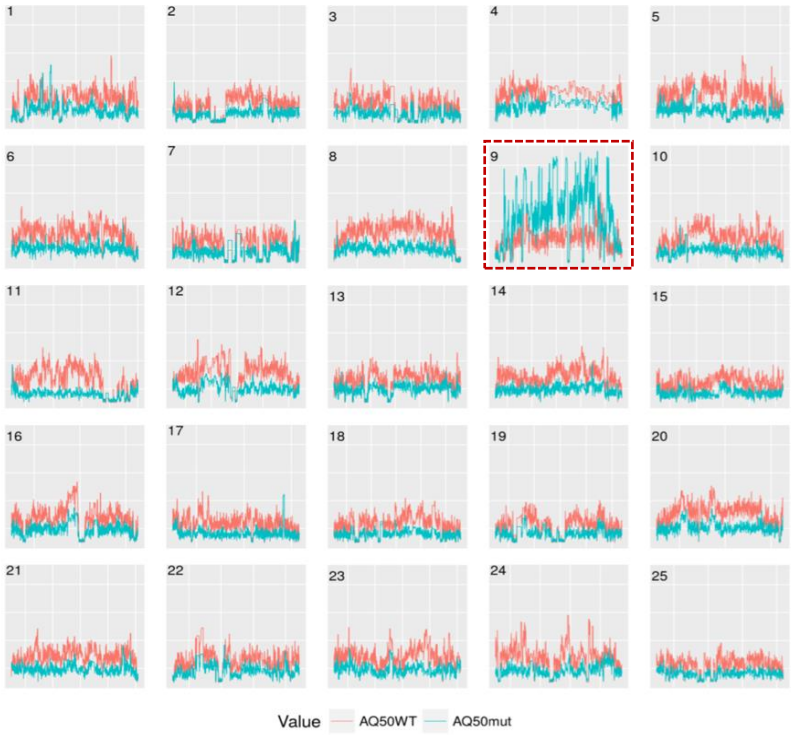

B

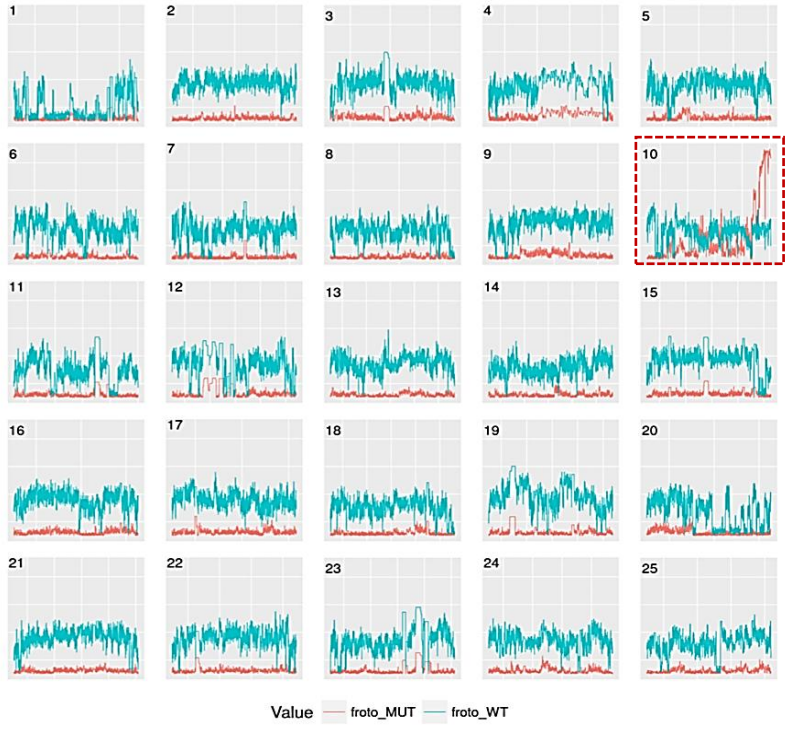

Figure S 5. Homozygosity score plotted over all of the chromosomes.
(A) Homozygosity score in mutant (blue) and wild-type (orange) samples, elevated homozygosity seen in the telomeric region of chromosome 9 in *dus*^{tq250} *(AQ50) and* (B) In mutant (orange) and wild-type (blue) samples of *fro*^{to27c}, elevated homozygosity seen in the telomeric region of chromosome 10; both highlighted by the red box.

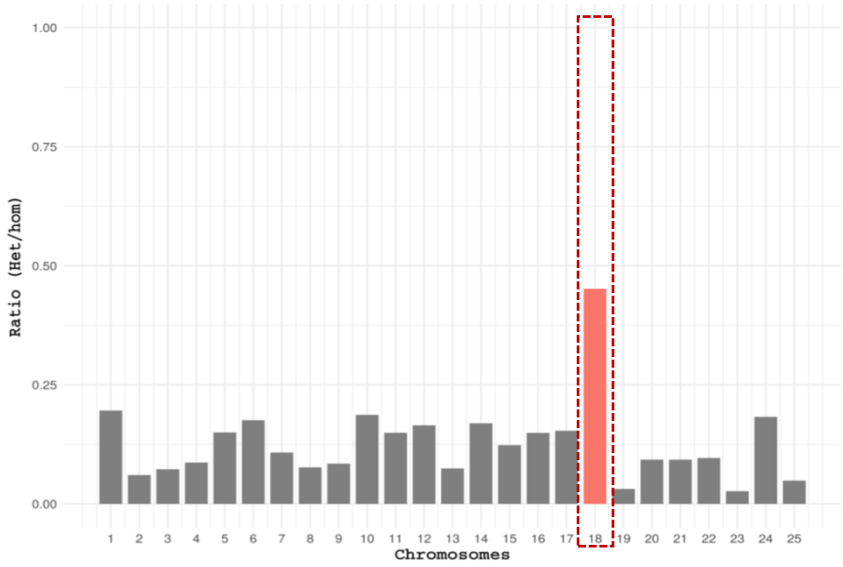

Figure S 6. Homozygosity score plotted over all of the chromosomes. Elevated homozygosity was seen in chromosome 18 of *slm*^{tt208}, highlighted by the red box.

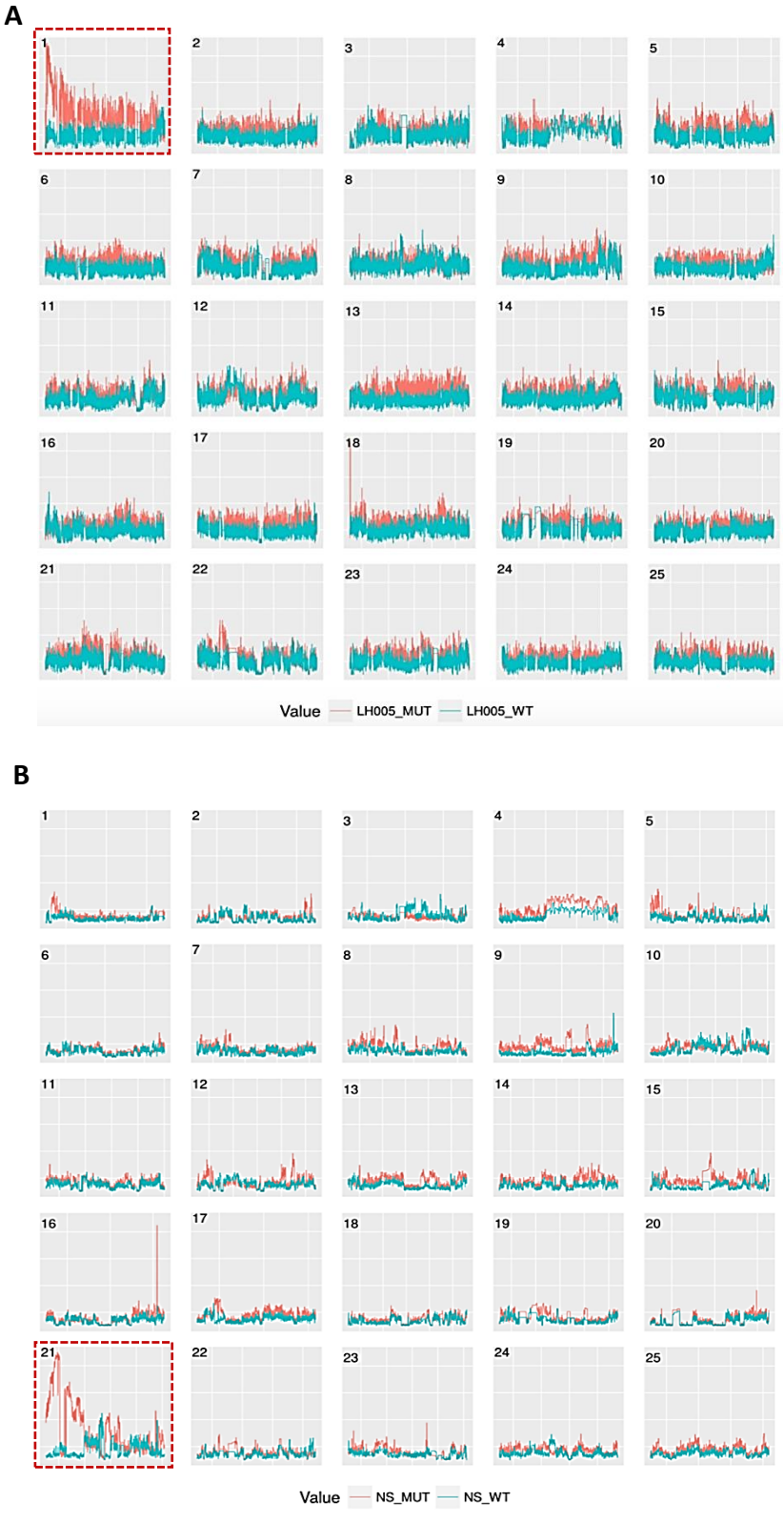

Figure S 7. Homozygosity score plotted over of all chromosomes. Homozygosity score in mutant (orange) and wild-type (blue) samples, (A) elevated homozygosity seen in the telomeric region of chromosome 1 in *t30064 (LH005),* (B) elevated homozygosity was seen on chromosome 21 in *t31198 (NS078)*; both highlighted by the red box.

A2 Materials

Laboratory equipment

The laboratory equipment used in the study is listed below with the details on their manufacturer.

Name	Company
Bacterial incubators	Heraeus, Hanau, Germany
Cool centrifuge J2-HS	Beckman, Stuttgart, Germany
Dissection forceps	Fine Tip No. 5, Dumont
Eppendorf microcentrifuge tubes	Eppendorf, Hamburg, Germany
Falkon tubes	Greiner, Nürtingen, Germany
FemtoJet microinjector	Eppendorf, Hamburg, Germany
Flaming-Brown needle puller	Sutter Instruments, USA
Gas microinjector	Tritech research Inc., L.A., USA
Glass capillaries, 1.0mm outer diameter, 0.58mm inner diameter with filament (TW100)	WPI Inc., USA
Incubator for fish embryos	Heraeus, Hanau, Germany
Magnetic thermomixer	Heidolph, Rosenfeld, Germany
MicroAmpTM 96-Well Full Plate Cover	Applied Biosystems, Foster city, USA
Microcentrifuge 5417 R and C	Eppendorf, Hamburg, Germany
Microloader tips	Eppendorf, Hamburg, Germany
Confocal microscope TCS SP2, fluorescent microscope DMI6000 SD, fluorescent stereomicroscope MZ FLI-II	Leica Microsystems, Wetzlar, Germany
Stereomicroscope SMZ645	Nikon, Japan
Multitank recirculation system	Schwarz GmbH, Germany
NanoDrop ND-1000	Peqlab, Erlangen, Germany
Neubauer chamber	Roth, Karlsruhe, Germany
Omnifix® RF 0.01R 1ml syringe	Braun, Melsungen AG, Germany
PCR-Thermocycler	Peqlab, Erlangen, Germany; Eppendorf, Hamburg, Germany
Petri dishes	Greiner, Nürtingen, Germany
Pipette tips	Corning, UK
qPCR 96-well FrameStar Fastplate	Steinbrenner Laborsysteme, Germany
qPCR Clear Seal Klebe-Folie	Steinbrenner Laborsysteme, Germany
Thermomixer	Eppendorf, Hamburg, Germany
Vortex	Bender & Hobein, Karlsruhe
Water bath	diverse

Chemicals

All the chemicals used in this thesis with their corresponding sources are mentioned in the table below.

Name	Source
1-phenyl-2-tricaine	Sigma-Aldrich, Taufkirchen, Germany
4',6-diamidino-2-phenylindole (DAPI)	Sigma-Aldrich, Taufkirchen, Germany
Acetic acid	Merck, Darmstadt, Germany
Agarose	Peqlab, Erlangen, Germany
Ammoniumacetate	Merck, Darmstadt, Germany
Ampicillin	Roth, Karlsruhe, Germany
Bacto Agar	Roth, Karlsruhe, Germany
Calcium acetate	Roth, Karlsruhe, Germany
Calciumchloride	Sigma-Aldrich, Taufkirchen, Germany
Chloroform	Sigma-Aldrich, Taufkirchen, Germany
Citric acid	Roth, Karlsruhe, Germany
Dimethylsulfoxide (DMSO)	Fluka, Neu-Ulm, Germany
Disodiumhydrogen phosphate	Roth, Karlsruhe, Germany
Dithiothreitol (DTT)	Roth, Karlsruhe, Germany
DNA-Ladder GeneRuler (Mix-1kb)	Thermo Fisher Scientific, Waltham, USA
DNA-Ladder GeneRuler 50bp	Thermo Fisher Scientific, Waltham, USA
DNAseI	Ambion Ltd, Warrington, UK
dNTPs	Promega, Mannheim, Germany
Ethanol (EtOH)	Roth, Karlsruhe, Germany
Ethidiumbromide	Roth, Karlsruhe, Germany
Ethylene diaminetetra acetic acid (EDTA)	Roth, Karlsruhe, Germany
Formaldehyde	Merck, Darmstadt, Germany
GeneArtTM PlatinumTM Cas9 nuclease (3 µg/µL)	Invitrogen, Carlsbad, USA
Glycerol	Roth, Karlsruhe, Germany
GoTaq DNA polymerase	Promega, Mannheim, Germany
GoTaq qPCR Master Mix	Promega, Mannheim, Germany
Hydrochloric acid (HCl)	Merck, Darmstadt, Germany
Isoamyl alcohol	Roth, Karlsruhe, Germany
Isopropanol	Roth, Karlsruhe, Germany
Potassium chloride	Sigma-Aldrich, Taufkirchen, Germany
Kanamycin	Sigma-Aldrich, Taufkirchen, Germany
Low melting agarose	Roth, Karlsruhe, Germany
Magnesium sulphate ($MgSO_4$)	Sigma-Aldrich, Taufkirchen, Germany
Maxi script T7 Kit	Life Technologies GmbH, Darmstadt, Germany

Maxima First strand cDNA Synthesis Kit for RT-qPCR	Thermo Fisher Scientific, Waltham, USA
Methanol (MeOH)	Roth, Karlsruhe, Germany
Methylene blue	Interpret, Germany
mMESSAGEmMACHINE T3 Transcription Kit	Ambion, Darmstadt, Germany
Megashortscript T7 Kit	Ambion, Darmstadt, Germany
NucleoBond BAC 100	Macherey-Nagel, Düren, Germany
Nucleospin purification Kits	Macherey-Nagel, Düren, Germany
Oligonucleotides	Metabion, Planegg, Germany
Paraformaldehyde	Merck, Darmstadt, Germany
pCS2+ vector	
Phosphate Buffered Saline (PBS)	Life Technologies GmbH, Darmstadt, Germany
pGEMT-easy	Promega, Mannheim, Germany
Phenol	Roth, Karlsruhe, Germany
Phenol Red	Roth, Karlsruhe, Germany
Proteinase K	Sigma-Aldrich, Taufkirchen, Germany
Q5 Hifi DNA Polymerase	New England Biolabs, Frankfurt a.M, Germany
QIAGEN Plasmid Midi purification kit	Qiagen, Hilden, Germany
QIAGEN Plasmid Maxi Kit	Qiagen, Hilden, Germany
Restriction enzymes	New England Biolabs, Frankfurt a.M, Germany
Sodium acetate (NaAc)	Roth, Karlsruhe, Germany
Sodium chloride (NaCl)	Roth, Karlsruhe, Germany
Sodium hydrogen carbonate ($NaHCO_3$)	Roth, Karlsruhe, Germany
Sodium hydroxide (NaOH)	Roth, Karlsruhe, Germany
Sodiumdodecylsulphate (SDS)	Roth, Karlsruhe, Germany
Sp6/T3/T7 RNA polymerase	Life Technologies GmbH, Darmstadt, Germany
T4 DNA Ligase	New England Biolabs, Frankfurt a.M, Germany
T4 DNA Polymerase	New England Biolabs, Frankfurt a.M, Germany
Tricaine methane sulphonate	Von Pharmaq Ltd., Hampshire, United Kingdom
Tris-base	Roth, Karlsruhe, Germany
Tris-HCl	Roth, Karlsruhe, Germany
Triton-X-100	Roth, Karlsruhe, Germany
Tween20	Roth, Karlsruhe, Germany

Solution and buffers

All solutions were prepared using autoclaved deionized water in sterile vessels and, if necessary, were autoclaved again before use. Below is the detailed recipe for each reagent used in this thesis.

Name	Recipe
20x SSC-Buffer	3 M NaCl, 0.3 M sodium citrate
Blocking buffer	1x PBS, 0.1% v/v Tween20, 0.2% w/v BSA, 1% v/v DMSO; stored at 4°C
Blocking buffer ISH	1% BSA, 1% DMSO in 1X PBS
BSMIS solution	75 mM NaCl, 70 mM KCl, 2 mM CaCl2, 1 mM MgSO4, 20 mM Tris pH8 filled upto 1L; stored at 4°C
BT-fix	4% w/v PFA, 4% w/v sucrose, 0.12 mM CaCl2, 0.2 M Na2HPO4, 0.2 M NaH2PO4; stored at -20°C
E3 medium (60x)	5 mM NaCl, 0.17 mM KCl, 10 mM HEPES, 0.33 mM MgSO4, 0.33 mM CaCl2
Extraction buffer (whole genome sequencing)	80 mM Tris-HCl pH 8.5, 200 mM NaCl, 0.5% SDS, 5 mM EDTA
Fructose solution	0.5% Fructose in egg water; can be stored at 4°C for two weeks
Hybridization (HYB) buffer	50% v/v formamide, 5x SSC, 500 µg/ml yeast RNA, 50 µg/ml heparin, 0.1% v/v Tween20, 9 mM citric acid; stored at -20°C
KOH solution (50x)	1.25 M KOH, 10 mM EDTA; stored at 4°C
Neutralization buffer (50x)	315.2g Tris-Hcl in 1l water; stored at 4°C
Pronase solution	0.01 g/ml Pronase in E3 medium; stored at -20°C
Proteinase K solution	10 µg/ml proteinase K in PTW; stored at -20°C
PTW	1x PBS, 0.1% v/v Tween20
PTU solution	0.0003% w/v phenylthiourea, 1x E3 medium
Staining buffer	100 mM Tris-HCl pH 9.5, 50 mM MgCl2, 100 mM NaCl, 0.5% v/v Tween20
TE buffer	10 mM Tris-HCl pH 8.0, 1 mM EDTA
Wash buffer 1	50% formamide, 50% 2x SSC; 0.1% v/v Tween20
Wash buffer 2	2x SSC, 0.1% v/v Tween20
Wash buffer 3	0.2% SSC, 0.1% v/v Tween20
Wash buffer 4	50% PTW, 0.5% v/v 20x SSC, 0.05% v/v Tween20

Softwares

The softwares used in this thesis were mostly open source and available on the mentioned websites. Adobe Illustrator however were provided by KIT.

Name	Usage	Source
Adobe illustrator CS6	Used for figure configuration	Adobe
ApE	Plasmid editor	Wayne Davis from the University of Utah

ChopChop	Online tool to design guide RNAs	http://chopchop.cbu.uib.no/
Clustal Omega	Online tool for multiple sequence alignment	https://www.ebi.ac.uk/Tools/msa/clusta lo/
ExPASy translate tool	Online tool to predict protein sequences	https://web.expasy.org/translate/
Ensembl	Gene sequence database, genome browser	https://www.ensembl.org/index.html
Ligation calculator	Online tool to calculate ligation mixes	http://2011.igem.org/Team:UT_Dallas/li gation
Primer3 version 4.1.0	Online tool to design PCR primers	http://primer3.ut.ee/
Punnett Square Calculator	Online tool for assessing genotypes derived from mendelian principles	http://scienceprimer.com/punnett- square-calculator

Antibodies

The primary antibodies used in this thesis were stored at 4°C post thawing but the original vials were stored at -20°C. The secondary antibodies however were always stored at 4°C away from light. The antibody solutions are made just before the final incubation step and primary antibodies were reused.

Primary Antibodies			
Name	**Species of origin**	**Target**	**Source**
α-actinin (1:300)	Mouse	α- skeletal and cardiac muscle actinin (Z line)	Sigma
F59 (1:500)	Mouse	Slow muscle myosin	Developmental Studies Hybridoma Bank [DSHB], University of Iowa
A1025 (1:100)	Mouse	All muscle myosin	Developmental Studies Hybridoma Bank [DSHB], University of Iowa
Laminin (1:100)	Rabbit	Basement membrane (horizontal myosepta)	Sigma
Titin (1:250)	Mouse	Titin localized around A-I junction (skeletal and cardiac muscle)	Sigma

β-sarcoglycan (1:100)	Mouse	Component of sarcoglycan complex, link between F-actin and extracellular matrix	Novocastra, Leica
Pax7 (1:50)	Mouse	Courtesy: Dr. Olivier Kassel	In house at KIT
Acetylated α −tubulin (1:500)	Mouse	microtubules	Sigma
Secondary Antibodies			
α-bungarotoxin Alexa Four 488 (1:1000)	Venom from *Bungarus multicinctus*	Acetylcholine receptors in skeletal muscle (neuromuscular junction)	Molecular probes
Alexa Flour 488 or 546 Phalloidin (1:1000)	Toxin from *Amanita phalloides* (death cap mushrooms)	Filamentous actin	Thermo fisher scientific
Alexa flour 546 (1:1000)	Donkey anti-mouse	Red fluorescence	Invitrogen
Alexa flour 488 (1:1000)	Donkey anti-mouse	Green fluorescence	Invitrogen
DRAQ5 (1:2000)	Nuclear staining	From blue to red fluorescence	Thermo fisher scientific